UiT
THE ARCTIC
UNIVERSITY
OF NORWAY

FACULTY OF SCIENCE AND TECHNOLOGY

Department of Geology

Focused fluid flow through the gas-hydrate stability zone on the Vestnesa Ridge, offshore W-svalbard

—

Cecilie Aas

EOM-3901 Master's Thesis in Energy, Climate and Environment

July 2014

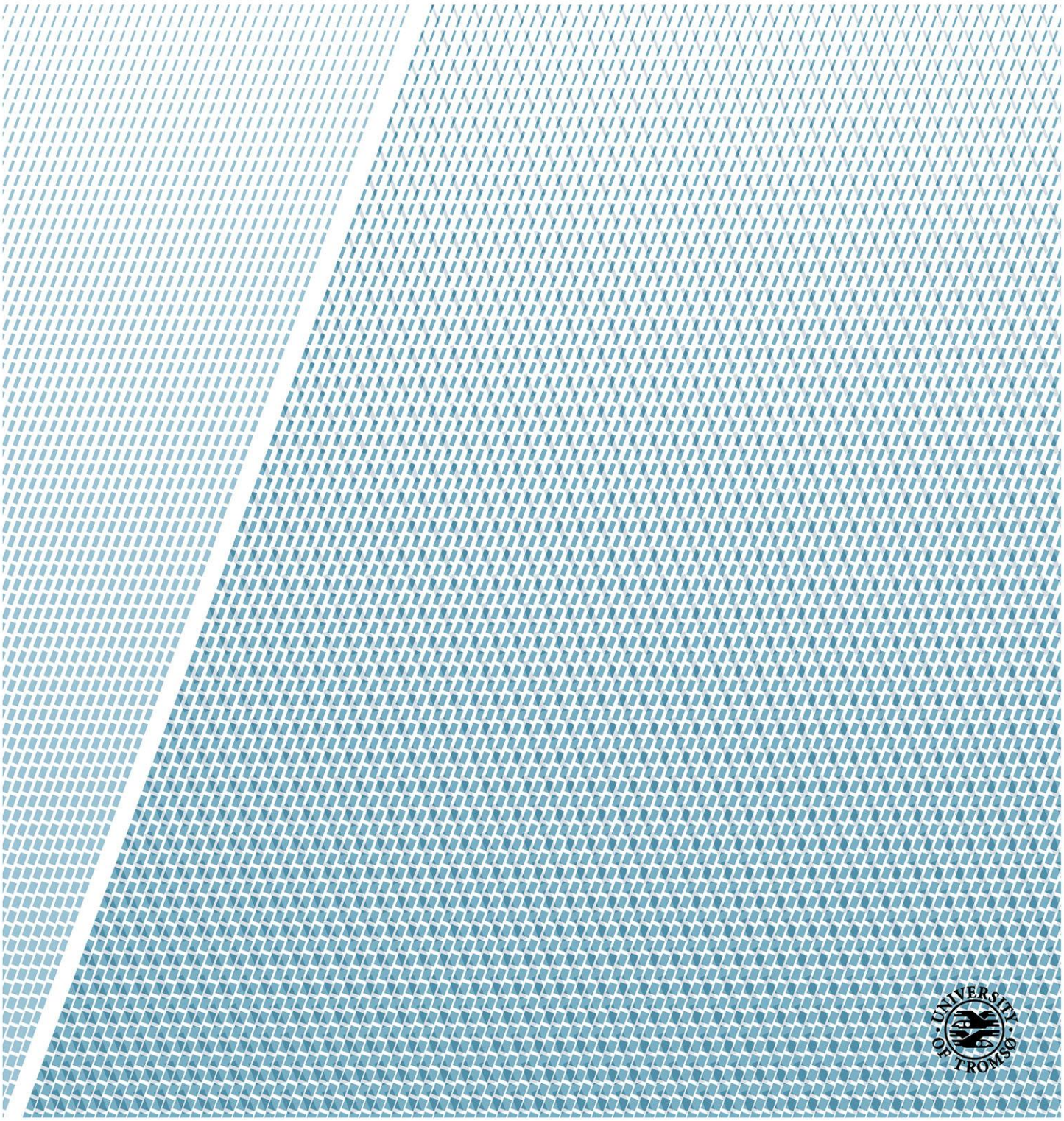

EOM-3901
MASTER'S THESIS IN ENERGY, CLIMATE AND ENVIRONMENT

Focused fluid flow through the gas-hydrate stability zone on the Vestnesa Ridge, offshore W-svalbard

Cecilie Aas

July, 2014

Abstract

Numerous unburied seafloor pockmarks are related to current methane-leakage at Vestnesa Ridge (~79° N), west of Svalbard. About 50 km long and 1-3 km wide, Vestnesa Ridge is a 1-2 km thick sediment drift to the north of the active Molloy transform – on the eastern spreading segment. With its crest at 1200-1300 m depth, the ridge is located on young (<19.6 Ma) oceanic crust.

The entire length of the crest is dominated by more than 100 pockmarks that are up to 700 m in diameter. The depressions in the seabed are caused by the vertical migration of gas through leakage structures; chimneys and pipes. The study area for this project is at the eastern end of Vestnesa Ridge, where the pockmarks are predominantly of a larger scale than those at the western end of the ridge.

The distribution of pockmarks is associated to a wide-spread Bottom-Simulating-Reflector (BSR), which indicates the possible occurrence of gas hydrates by representing the base of the Gas-Hydrate-Stability-Zone (GHSZ). Gas hydrates act as a permeability barrier regarding fluid flow. Presumably, their occurrence in this area is controlling the distribution of gas-leakage. Beneath the GHSZ, free gas is shown by strongly negative reflections in the seismic – confirming this assumption.

Chimneys are leakage-structures connecting the pockmarks to the BSR. The chimneys and their internal fluid flow are related to several faults spreading through the ridge. Faults are well known conduits for fluid flow. Mechanisms for fluid flow through chimney-structures, is however uncertain. Results from RMS-amplitude mapping in this project, indicate that the chimneys internal fluid flow is also strongly influenced by faults.

Acknowledgements

Endelig skal skyggelappene av, og jeg kan kjenne på den befriende følelsen av å endelig være ferdig med 5 års utdannelse. Hurra! Med kroppen full av stress-hormoner, forstyrret nattesøvn og et svekket immunforsvar – har det ikke alltid vært like enkelt å holde motivasjonen oppe i innspurten. Heldigvis for meg, har jeg hatt mange å støtte meg på i denne tiden.

Først vil jeg takke min veileder Stefan Bünz for å ha gitt meg en oppgave etter mine ønsker, og for den veiledning jeg har fått. Takk også til Andreia Plaza Faverola for dine engasjerte innspill, og hjelp til oppgaven.

Jeg vil takke mine nærmeste kolleger som jeg har hatt mange trivelige vakter sammen med. Takk til mine medstudenter fra blå-brakka og fra EOM. En særlig takk går til jentene mine på EOM-kull-09 for ei fin studietid sammen. Takk til gutta på kontoret for deres tekniske support og tips. En spesiell takk går til Kirsti; en fin diskusjonspartner for masteroppgaven, GOT og livets opp- og nedturer. Takk for all oppgiring for å peisa på!

Takk til dere som har gledet min hverdag. Takk til alle som heiet på meg.

Kjære Aleksander, min klippe i livet. Min største takk går definitivt til deg. Du har alltid vært støttende og oppmuntrende, og dette hadde jeg ikke klart uten deg. Nå ser jeg frem til vår nye tilværelse og fremtidige planer og eventyr. Endelig kan vi komme oss videre i livet, etter alt vårt harde arbeid. Takk for alle gode ord, alle klemmer og alle de herlige middagene =)

Cecilie Aas
Tromsø, Juli 2014

Now I'm ready to start
My mind is open wide
-Arcade Fire-

Contents

1 INTRODUCTION

This chapter covers the essentials of gas hydrates, free gas and fluid flow. An overview is given on the generation, migration and accumulation of gas, and also the means by which it can flow out of the subsurface. Gas hydrates are reviewed regarding occurrence, governing formation-factors and stability.

1.1 Objectives

The primary objectives of the thesis are to identify and map fluid flow structures and possibly gas hydrate occurrence in the subsurface sediments of the Vestnesa Ridge on the West-Svalbard margin (**fig. 1.1.1**), where methane-gas is actively leaking into the water column. It is desired to achieve a better understanding of the occurrence of fluid flow and gas hydrates, their origin and their governing mechanism. The thesis includes analysis of high-resolution P-Cable 3D seismic data.

However, the means by which gas can by-pass the hydrate-stability zone, is an inadequately explored matter. The secondary objective is to achieve a more detailed insight in the internal architecture of the fluid flow structures that are actively leaking gas. This could lead to a better understanding of the passage of gas through the hydrate-stability zone without the formation of hydrates. Emphasis lies on identification and mapping of fluid flow structures and potentially existing gas hydrates in the subsurface sediments. These structures are only poorly understood at this location and it is required to establish baseline information for future time-lapse and seismic modeling studies.

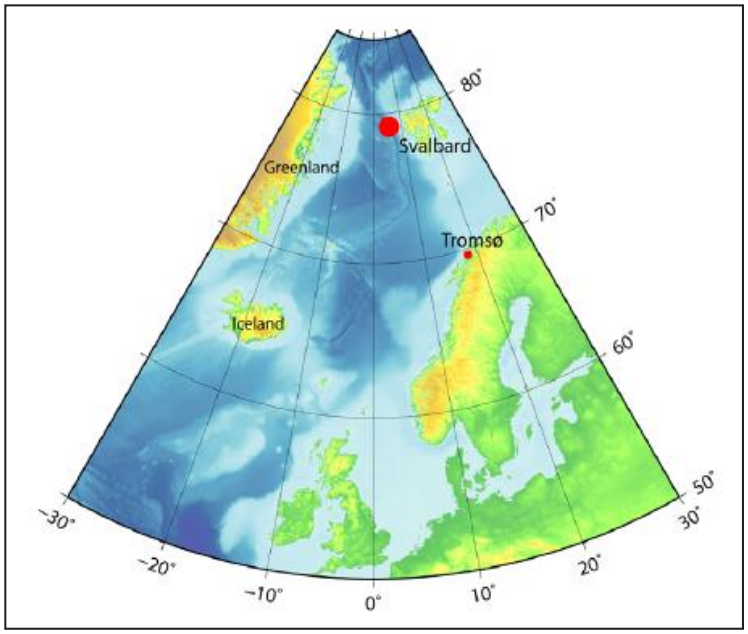

Fig. 1.1.1: The investigation area is located west of Svalbard. (From *Petersen et al,. 2008*)

1.2 Motivation

The seabed (SB) at Vestnesa Ridge shows several large-scale depressions, aka pockmarks, which are indicative of fluid flow. Recordings have proved that methane-release through several of these is more or less continuously ongoing in our day (*Smith et al., 2014*). Methane is responsible for 21% of the enhanced greenhouse effect, and the effect caused by a singular molecule of methane is about eight times as high as that of a molecule of carbon dioxide. Ice-core data has proved that the concentration of methane in the atmosphere has more than doubled over the past 200 years, and today it has reached a level that is higher than ever over the past 650 000 years (*Houghton, 2009*).

The subsurface at Vestnesa ridge displays a BSR (Bottom-Simulating Reflector) indicative of gas hydrates. Gas hydrates are of importance in that they may possibly discharge large amounts of greenhouse gas, mainly methane, which affects the global climate. They act as a geo-hazard considering their ability to cause submarine land sliding, and also they represent a potential future energy resource (*Andreassen, 2009*). There is a possibility that gas hydrates have greatly affected the climate both recently, and at the end of the Paleocene when the temperature increased rapidly. Enormous quantities of methane were caged into hydrates within permafrost and submarine sediments during glacial maxima. Climate warming to a critical temperature caused the destabilization of gas hydrates, and the release of methane gas in tremendous amounts. This extensive increase in greenhouse gas in the atmosphere may have caused the sudden global temperature increase that is established at the end of the glacial maxima (*Selley, 1998*).

Global warming is a relevant issue and an expediting factor in the reduction of the GHSZ (Gas Hydrate Stability Zone), and the subsequent dissolution of gas-hydrates. This effect will be noticed first at the Polar Regions, where the impact probably also will be greater than elsewhere (*Bünz et al., 2012*). In the Arctic, the warming-rate is ~2 times faster than at lower latitudes (*Graversen et al., 2008*). It is unlikely that the gas hydrates are to dissolve in the near future due to continuous global warming, as they are situated at a depth that will take long time (100 – 1000 years) to be affected by the changes in temperature (*Reagan and Moridis, 2007).* However, if the warming continues for many decades, temperatures will increase in the hydrate-reservoirs and cause severe methane-release into the atmosphere (*Houghton, 2009*).

1.3 Methane-Gas in the Subsurface

1.3.1 Generation

The natural gas methane (CH_4) is included in the hydrocarbon-gases. As the most abundant of them, it is commonly registered during well-drilling. Methane is classified as a dry gas; it has less than 0.1 gal/1000 ft^3 of condensate. The chemically nonreactive gas is sparingly soluble in water, and it has a relative density of 0.554 – making it lighter than air.

There are three manners of which methane can be generated;

- Mantle-derived (Thermal)
- Thermal maturation of buried organic matter
- Biogenic by bacterial degradation of organic matter at shallow depths

It is possible to use geochemical and isotope analysis to establish the source of methane in a reservoir (*Selley, 1998*).

1.3.2 Migration

There are two aspects of migration;

- Primary migration from the source rock in which it was formed, into a permeable carrier bed.
- Secondary migration refers to the movements within the permeable carrier bed, through the sedimentary strata (**fig 1.3.1**) and through other conduits, e.g. faults, fractures, pipes and chimneys. Secondary migration occurs by buoyancy, and thus impacts until the fluids are accumulated within a form of sealed trap or are released at the surface.

Depending on the permeability and buoyancy; the fluids are able of vertical and lateral flow (*Selley, 1998*).

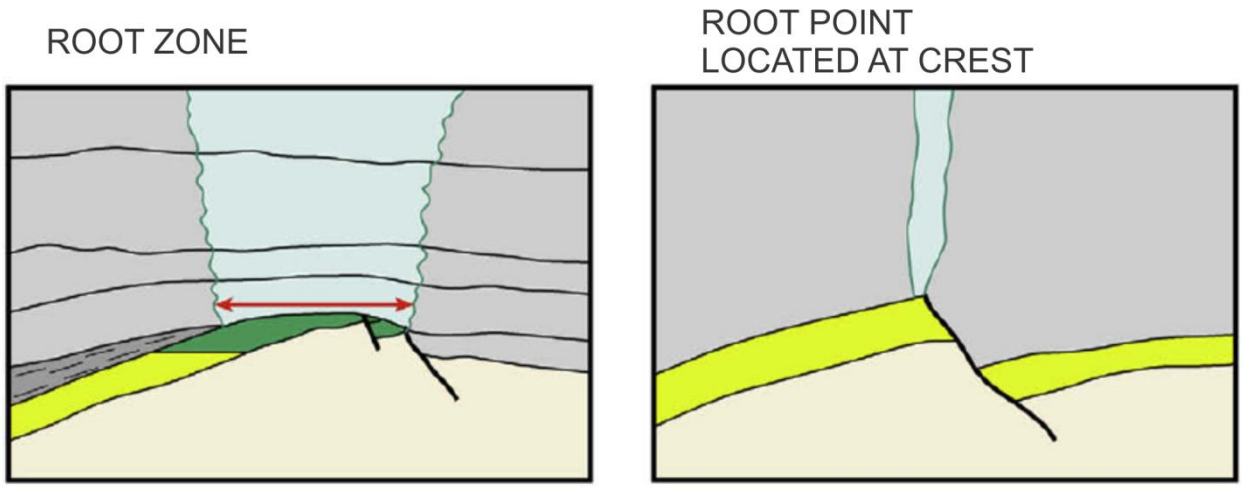

Fig. 1.3.1: Schematic illustration of different roots of leakage zones at a crest. The leakage zone can be wide or narrow like a "point" (From *Løseth et al., 2009*).

1.3.3 Accumulation

Free gas may end its migration in a trap; an impermeable structure that prohibits the fluids from further movements. There are several types of traps;

- Structural traps formed by post-depositional tectonic processes. Compression and compaction are forces that cause folding and anticlinal traps. Faults may act both as seals and as conduits regarding fluid flow depending on how they have affected the stratigraphy.
- Stratigraphic traps are made by depositional or post-depositional changes in the lithology. These changes are associated with unconformities, diagenetic effects or smaller depositions that separate from the general sedimentation.
- Diapiric traps are less common. They form by the diapirical upward movement of salt or overpressure clay.

A combination of these types may also occur, although at the present there are mostly found structural traps. Additionally, fluids may be trapped by counteracting water-flow down through the permeable sedimentary layer, so-called hydrodynamic traps (*Selley, 1998*).

1.4 Gas Hydrates

1.4.1 Definition and Occurrence

Gas hydrates are an ice-like matter made of natural gas captured in a rigid cage of water-molecules. Physically, they look like white and powdery snow. Conditions of high pressure and low temperature are required for the formation of gas hydrates within the pore space of sediments. This constrains the gas hydrate stability zone (GHSZ) to an interval within the uppermost few hundred meters of sediments (*Hustoft et al., 2009*). Gas hydrates are mostly found in large reservoirs at high latitudes (*Houghton, 2009*), however they occur naturally in many parts of the world (**fig.1.4.1**) (*Birchwood et al., 2010*). They generally occur in ocean floor sediments at water depths from and beneath 500 m. In Polar Regions however, they are found both in offshore and onshore sediments due to permafrost (*Andreassen, K., 2009*). Due to low permeability, they form a seal under which free gas may accumulate. The presence of gas-hydrates can be indicated from the interpretation of seismic data nevertheless can only be proved by engineering data, e.g. pressure core barrels and log responses (*Selley, 1998*).

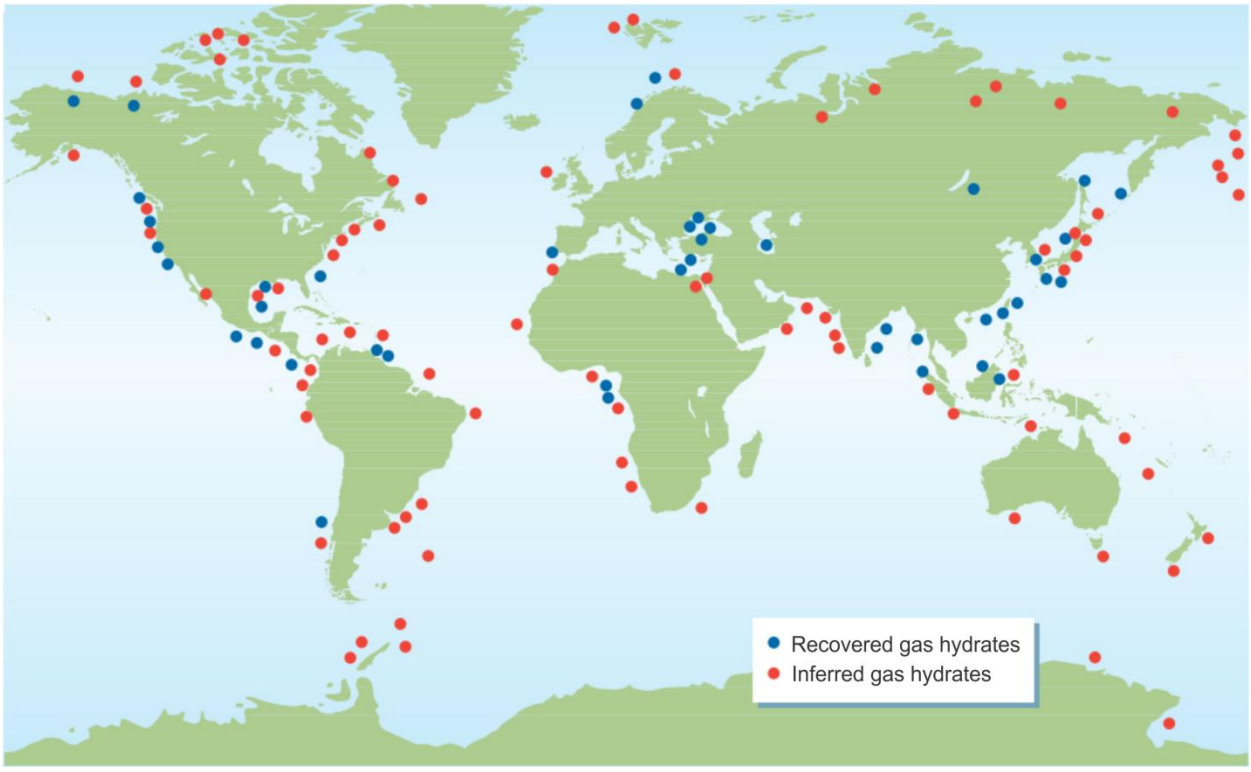

Fig. 1.4.1: Marine and onshore hydrate locations; recovered gas hydrates in blue, and inferred from seismic interpretation in red (from *Birchwood et al., 2010*).

1.4.2 Formation

The molecule of natural gas within crystalline structure of water molecules act as a stabilizer to the matter (**fig. 1.4.2, fig. 1.4.3**). The guest molecule in most of the recovered natural marine gas hydrates is methane (*Andreassen, K. 2009*). The single ice-molecules of gas-hydrates are referred to as clathrathes (*Sloan, 1990*). There are two types of unit structure in the formation of gas-hydrates;

- The structure of 12 Å is the smallest, and contains up to 8 methane molecules within 46 water-molecules. It may also contain some other gases in addition to the methane; ethane, hydrogen sulfide and carbon dioxide.
- The structure of 17.4 Å is larger, and consists of unit cells with 136 water-molecules that are able to hold the larger hydrocarbon molecules of the pentanes and n-butanes.

Clathrates can hold up to six times the amount of gas that an open gas-filled pore-system is able to. Hence, gas hydrates are significantly perceived as potential sources of energy. However, these involve comprehensive difficulties regarding production and are still not commercialized (*Selley, 1998*).

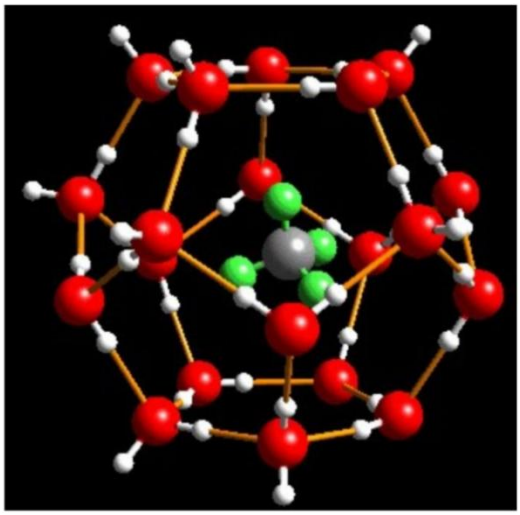

Fig. 1.4.2: Example of a gas hydrate molecule; a methane molecule of hydrogen (green) and carbon (grey) is imbedded in a water molecule of hydrogen (white) and oksygen (red) (From http://peer.tamu.edu/curriculum_modules/ecosystems/ module_3/ whatweknow2.htm).

Fig. 1.4.3: The typical occurrence of natural submarine gas hydrates; A) Lamina, B) Hydrate veins and C) Hydrate nodules (From *Andreassen, 2009*).

1.4.3 Stability and Dissociation

Gas hydrates are stable at high pressures and low temperatures. The geothermal gradient is a measurement of the temperature-increase from the earth's surface towards its center, a rate that is ~26°C per km depth in global average. For a linear geothermal gradient, the required pressure increases logarithmically (*Selley, 1998*). Heat flow of the earths' crust is related to the geothermal gradient and the thermal conductivity of the various sediments;

Heat flow = geothermal gradient × thermal conductivity of rock

Heat flow shows great regional variations. At convergent plate boundaries, the heat flow is especially low. Whilst at divergent plate boundaries (e.g. mid-ocean ridges) the crust is thin and magma can reach the surface, resulting in high heat flow (*Selley, 1998*).

Pressure is the force per unit area acting on a surface, and total pressure is caused by several factors in the subsurface;

- Lithostatic pressure encompasses the pressure of rock that is conveyed by grain-to-grain contacts. It is affected by the pressure of fluids in between the grains, from the density of overburden rock and depth.
- Fluid pressure is caused by the fluids within the pore spaces. Fluid pressure has two aspects; hydrostatic caused by the overlying fluid-column, and hydrodynamic that is caused by fluid flow through the sediment (*Selley, 1998*).

The relation between these governing factors is illustrated in **Fig. 1.4.4**, which shows a stability diagram for methane-hydrates at oceanic deposits.

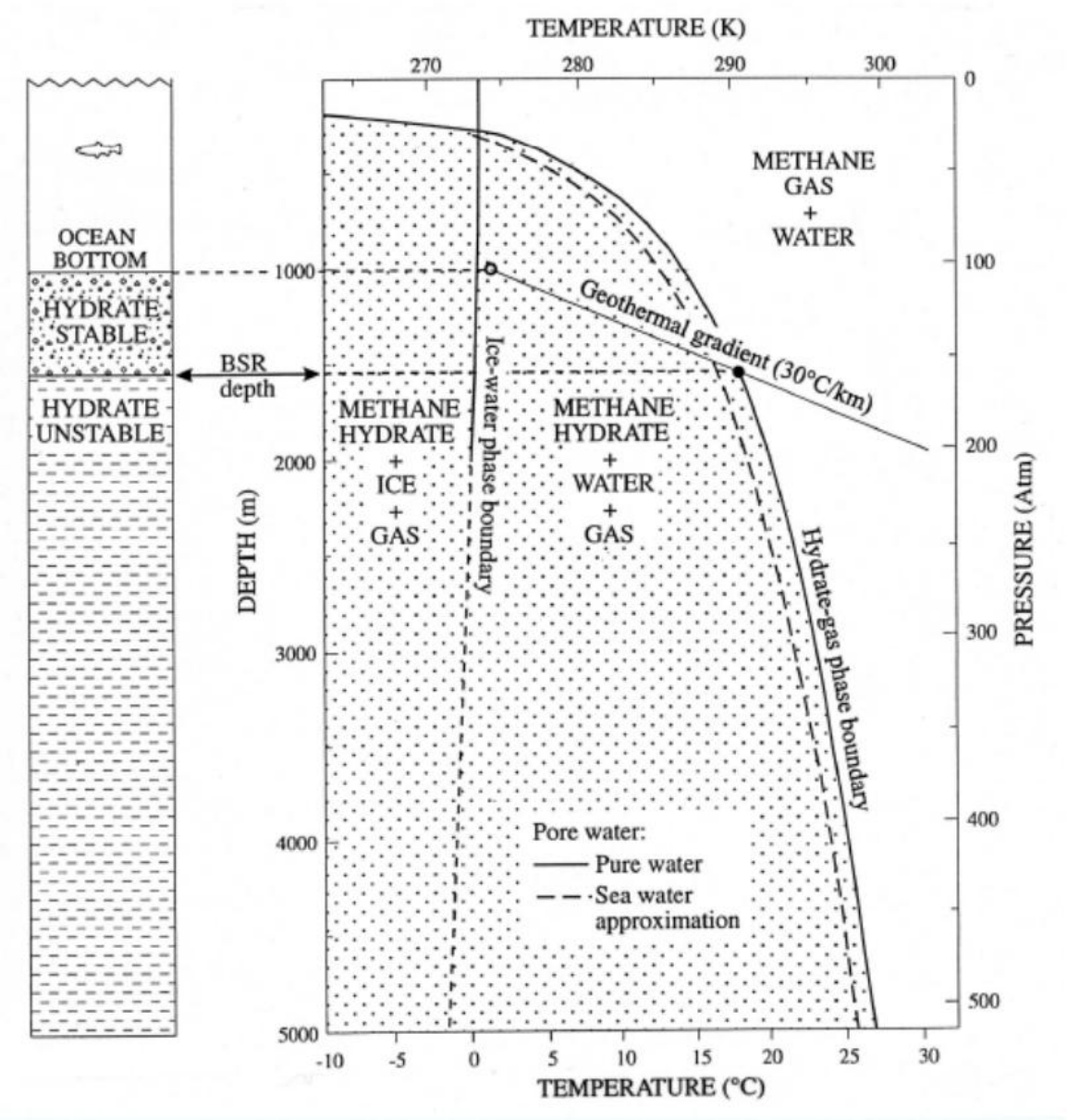

Fig. 1.4.4: Stability diagram for methane hydrate to the right. The sediment column to the left illustrates where methane hydrates will be stable within the sediments (From *Andreassen K., 2009*).

2 STUDY AREA

2.1 Localization and Bathymetry

The study area is located on the eastern segment of the Vestnesa Ridge at 79° N, located NE of the Molloy Transform Fault, N of the Knipovich Ridge and S of the Yermak Plateau, on the continental slope off the W-Svalbard margin (**fig. 2.1.1**). The area covers ~15.5 km^2 of the Vestnesa Ridges' crest and subsurface, at ~1200 m water depth.

The sedimented Knipovich Ridge is the northernmost extending of the Mid-Atlantic Ridge system. This slow spreading ridge is N-S oriented and connects to the Molloy Ridge to its NW. The fault system further to the north argues that the Knipovich Ridge is further-extending and propagating in the underground, where it connects to the Gakkel Ridge in the Arctic Ocean (*Bünz et al., 2012*). The W Svalbard Margin is mainly formed by a western orogenic belt that is affected by a glaciated shelf and fjords e.g. Kongsfjorden and Krossfjorden. Within the orogenic belt, compression caused the Tertiary western Spitsbergen fold belt (Prins Karl Forlandet and the W coast of Svalbard) to be characterized by folds, thrusts and a strike slip basin (Forlandsundet Graben) (*Ritzmann et al., 2004; Sarkar et al., 2011*).

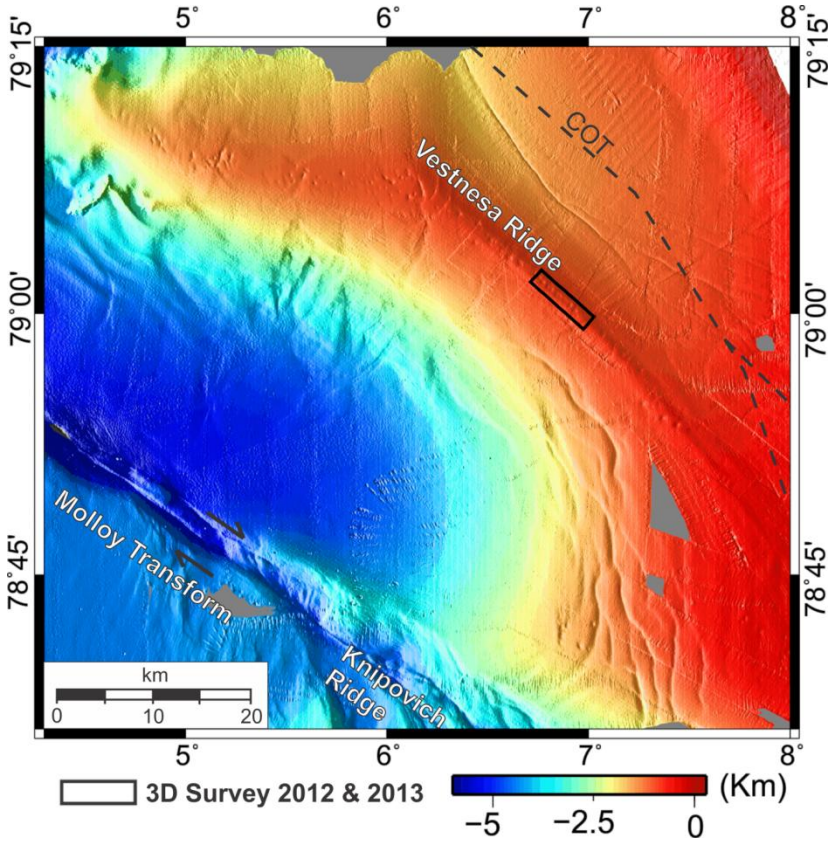

Fig. 2.1.1: Bathymetric overview map of the area containing the Vestnesa Ridge, Molloy Transform and the Knipovich Ridge. The box indicates the location of the 3D seismic data of which this study is interpreted on. COT denotes Continent-Ocean Transition.

2.2 Oceanography

The opening of the Fram Strait gave rise to the ocean currents that are presently dominating the oceanography off Svalbard (**fig. 2.2.1**) (*Sarkar et al., 2011*). The West Spitsbergen Current (WSC) provides warm and salt North Atlantic water northwards at the sea surface along the W Svalbard shelf edge, preventing the formation of ice. The current divides into two branches at the southern Yermak Plateau; one flows eastwards along the NW Svalbard shelf edge into the Arctic Ocean – the other flows along the western Yermak Plateau towards the north, and a part of this current supply the Fram Strait that is the single deep water connection to the Arctic Ocean (*Aagaard et al. 1987*). The WSC overlies the Norwegian Sea Deep Water flowing towards the S and the Yermak Slope Current (*Hansen and Osterhus, 2000; Howe et al., 2008*). The cold East-Greenland Current (EGC) brings polar water along the Greenland margin southwards and into the North Atlantic (*Howe et al., 2008*).

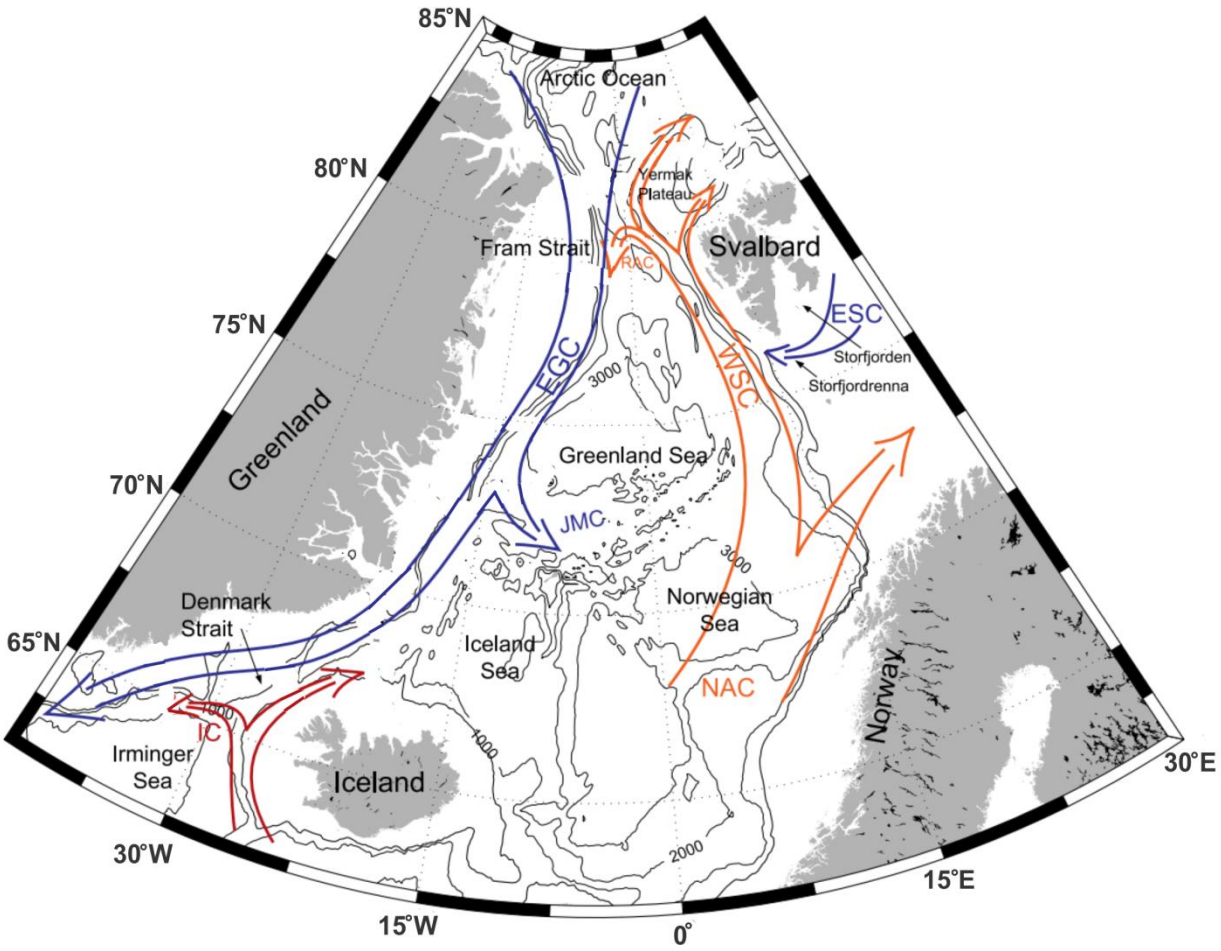

Fig. 2.2.1: Map of the ocean currents in the Nordic Seas, where the cold currents are displayed in blue and the warmer currents are displayed in red. EGC = East Greenland Current, ESC = East Spitsbergen Current, IC = Irminger Current, JMC = Jan Mayen Current, NAC = Norwegian Atlantic Current, RAC=Return Atlantic Current, WSC = West Spitsbergen Current (modified from *Rudels et al., 2004*).

2.3 Geologic Development

A late Paleocene strike-slip along ancient shear zones marked the transition from a transpressional to an oblique divergent regime at ~36 Ma between Svalbard and northern Greenland. The separation of Svalbard from NE Greenland was initiated by the spreading and strike slip movements of the Arctic Gakkel Ridge along the W Svalbard shear zone during the Early Eocene. In addition to being compressive, the W Svalbard Orogeny is a transpressive deformation with a dextral strike slip displacement between Greenland and Svalbard (*Harland et al., 1997*). The Fram Strait represents the final opening of the Atlantic-Arctic gateway, as a part of the non-glacial uplift and subsidence (*Knies et al., 2013*). An early shallow water connection existed through the Fram Strait during the late Oligocene (*Jokat et al., 2008; Hegewald and Jokat, 2013*).

During the Neogene, Fast flowing ice-streams discarded thick glacial wedges (TMFs) from the western part of the shelf margin at the mouth of the cross-shelf troughs, forming delta-like extensions. The wedges are found to consist of stacks of glacial debris flow (*Vorren and Laberg, 1997; Vorren et al., 1998*). In the Early Miocene, Sea floor spreading connected the North Atlantic MOR system (Mohns Ridge – Knipovich Ridge) with the Arctic Gakkel Ridge, causing the opening of the Fram Strait (*Ritzmann and Johat, 2003*). Through the late Miocene, the Greenland–Scotland Ridge subsided and led to an increased flow of North Atlantic Deep Water to the Atlantic Ocean. Prior to the middle Miocene, the ridge was probably partially and sub-aerially exposed (*Poore et al., 2006*). Between ~17.5 – 13.7 Ma, the Fram Strait passage developed to a depth of more than 2000 m (*Jakobson et al., 2007*). Until the Miocene, the Hovgård Ridge in the central Fram Strait acted partially as a barrier against the flow of both surface and deep-water masses. The ridge was sub-aerially exposed at ~25 – 6.7 Ma (*Myhre at al., 1995; Matthiessen et al., 2009b*). During the early Pliocene, the Barents Sea shelf was uplifted and the western passive margin subsided (*Ryseth et al., 2003*). Non-glacial, tectonic uplift in far-off Polar Regions during the early Pliocene may have been an exaggerating factor for the intensification of the Northern Hemisphere Glaciation (*Ruddiman, 2010*). Vågnes et al. (1992) estimated a post-glacial uplift of ~1000 m in the NW Barents Sea. The non-glacial uplift of Svalbard since the late Miocene is probably a result of thermal erosion of the mantle lithosphere under Svalbard (*Dörr et al., 2013*). During the early Pliocene uplifting and subsidence, the Hovgård Ridge subsided to a depth that enabled through-flow of both Arctic and Atlantic surface and deep-water masses (*Ryseth et al., 2003*). The initial exchange of deepwater between the Norwegian-Greenland Sea and the Arctic Ocean through the Fram Strait, is estimated to have occurred at between minimum 9.8 Ma and maximum 20-15 Ma (*Hustoft et al., 2009*). This timing is supported by Mattingsdal et al. (2013), who argued that this event took place during the middle Miocene.

The final expansion of the Fram Strait is proposed between 6.5 and 5 Ma, and is likely to have greatly affected the intensification of the Northern Atlantic thermohaline circulation (*Knies et al. 2013*).
The intensification of the Northern Hemisphere Glaciation (INHG) since the Mid-Pliocene, is proved by both Arctic and sub-Arctic terrestrial and marine records (*Matthiessen et al., 2009a*). The transition probably spanned over a time between 3.6 – 2.4 Ma, as a steady event (*Mudelsee and Raymo, 2005*). A stronger thermohaline circulation caused the warming of surface waters of the N Northern Atlantic between 2.95 – 2.92 Ma (*Bartoli et al., 2005*). The increase was a response to the closure of the Central American Seaways during the Pliocene (*Sarnthein et al., 2009; De Schepper et al., 2013*). All ice sheets in the Northern Hemisphere, including the ice sheet covering N to NW Svalbard, most likely reached the shelf break at 2.74 Ma as a response to the irreversible "climate crash" (*Bartoli et al., 2005; Mattingsdal et al., 2013*). Large prograding wedges along the margin of the Atlantic-Arctic gateway region developed at ~2.7 Ma, confirming the INHG (*Knies et al., 2013; Dahlgren et al., 2005*). Mattingsdal et al. (2013) confirmed this timing by progradation of glacial fans from the NW Svalbard onto the Yermak Plateau. At the W Barents Sea – Svalbard Margin this event occurred at a much later time; ~1.5 Ma (*Andreassen et al. 2007b*) when the Yermak Plateau was severely prone to glacial erosion. Together these events indicate an extensive glacial intensification of the Barents Sea – Svalbar region (*Mattingsdal et al., 2013*). A schematic overview of the Pliocene-events of the Arctic-Atlantic gateway region is given in **fig. 2.3.1**. At the present, contour currents along the slope lead erosional sediments from the Barents Shelf and Svalbard, along the slope and deposit them in sediment drifts e.g. Vestnesa Ridge (*Fohrmann et al., 2001*).

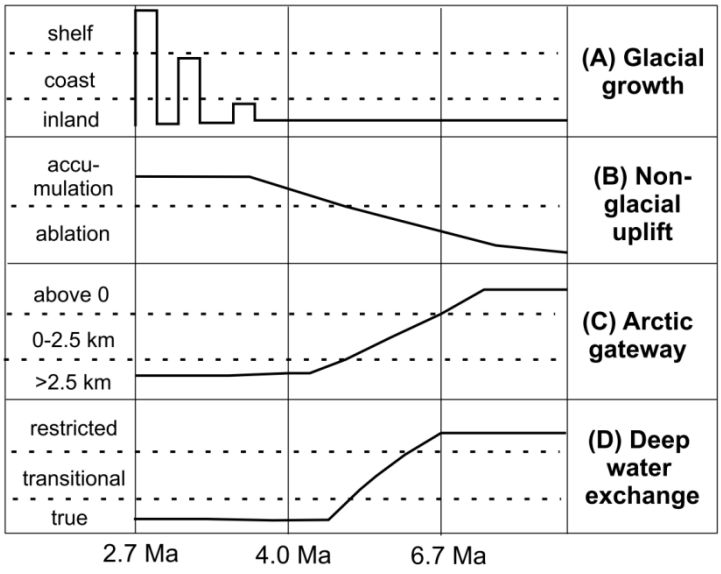

Fig. 2.3.1: Overview of the paleoclimatic and tectonic events during the Pliocene in the Arctic-Atlantic gateway region. A) Build-up of the northern Svalbard/Barents Sea ice sheet. B) Non-glacial uplift in the NW-Europe during the Late Miocene/Early Pliocene. C) Subsidence of the Hovgård Ridge and widening/deepening of the central Fram Strait. D) Inferred deep-water mass exchange throughthe Arctic-Atlantic gateway (From *Knies et al., 2013*).

2.4 Sedimentation and Stratigraphy

There are two dominating sets of sediments on the western Svalbard margin; glacigenic debris flows in through mouth fans beyond the shelf break - and turbiditic, glaciomarine and hemipelagic sediments which are to some extent reworked by contour currents (*Bünz et al., 2012*). The rough basement morphology includes graben-like structures that are covered by ~1-4 km thick layers of sediments (*Geissler and Jokat, 2004*) The sedimentary strata are continuous and show merely minor unconformities.

Eiken and Hinz (1993) established a three-sectioned sub-division of the eastern Vestnesa Ridge area; YP1, YP2 and YP3 (**fig. 2.5.1**). YP1 is the unit at the bottom consisting of syn and post-rift deposits. YP2 is the unit in-between, mainly characterized by contourites. Consisting of wedges thickening towards the west and down-lapping sequences in this direction, YP2 shows that the depocenter migrated to the west. Glaci-fluvial erosion during the latest Miocene – early Pliocene, deposited sandy sediments along the continental margin (*Knies et al., 2013; Dahlgren et al., 2005*). Plio-Pleistocene glaciations resulted in an unconformity between YP2 and the overlying YP3 unit. The boundary between the YP2 and YP3 units are dated to ~2.7 Ma by Knies et al. (2009), and represents the base of glacial deposits. By new results, Mattingsdal et al. (2013) propose that the entire YP2-unit is more than 11 Ma old, contradicting the estimates by earlier studies suggesting a timing of 6-7 Ma or mid-Miocene for the lower boundary. The upper slope of YP3 mainly consists of glacial sediments in the Kongsfjorden through mouth fan. Prior to 2.7 Ma, glaciofluvial environments controlled the transport of sandy sediments towards the shelf break off-Svalbard (*Forsberg et al., 1999; Butt et al., 2000; Laberg et al., 2010*). The YP3 sediments at Vestnesa Ridge contain silty turbidites and muddy-silty contourites of Weichselian and Holocene age (*Hustoft et al., 2009*).

The southern Yermak Plateau at the eastern flank of the Fram Strait in the marginal Arctic Ocean was dominated by contourites during the late Miocene-Pleistocene (*Mattingsdal et al., 2013*). ODP sites at the Yermak Plateau showed that a major increase in sedimentation-rate occurred at ~2.7 Ma, which was attributed to the increase in glacial erosion at that time. Continuous contourite depositions dominate the Yermak Plateau after 2.7 Ma (*Mattingsdal et al. 2013*). Sjubrebanken Fan is a glacial debris-flow S of the Yermak Plateau and NE of the Vestnesa Ridge, formed by sediments from an ice stream flowing out Kongsfjorden, between the Late to Early Pliocene glaciations (*Sarkar et al. 2011*). At ~1.5 Ma, a major erosional event affected the crest of the Yermak Plateu, and the sedimentation of the Sjubrebanken Fan decreased drastically while the Konsfjorden Fan was established (*Mattingsdal et al. 2013*). Mattingsdal et al. (2013) confirmed the timing of development between ~2.7 Ma and ~1.5 Ma by correlation of ODP sites.

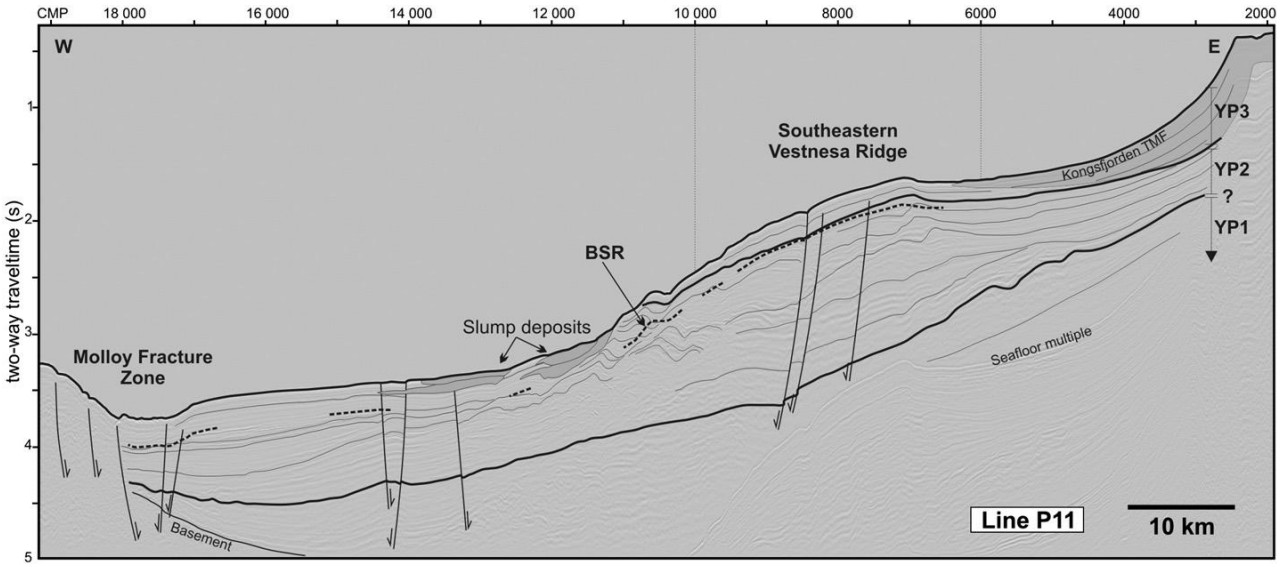

Fig. 2.5.1: Illustration of the three-sectioned sub-division into YP1, YP2 and YP3 of the eastern Vestnesa Ridge. Identified BSR across the margin is marked by a dashed line. (From *Hustoft et al., 2009*).

2.5 Vestnesa Ridge

On the eastern spreading segment of the Molloy Ridge lies the SE-NW to E-W bending Vestnesa Ridge, which is up to 120 m in height and ~5 km of lateral extension (*Howe et al., 2008*). The oceanic crust at this location is hot (>115 mW/m^2) and young of post late-Miocene age (<19.6 Ma) (*Hustoft et al., 2009*). Due to bottom-current, the ridge is a growing sediment drift that is being shaped by the W-Spitsbergen current which is directed towards the north (*Bünz et al., 2012*). Vestnesa Ridge is a classical sedimentary drift, mainly consisting of contouritic hemipelagic sediments (*Howe et al., 2008*).

Along the crest of Vestnesa Ridge there are numerous pockmarks, indicating the occurrence of focused fluid flow from the underground through the seabed (*Bünz et al, 2012*). Pockmarks are often observed in relationship with chimneys or pipes in the subsurface, vertical structures which serves as conduits for fluid flow (*Bünz et al, 2012*). The currently active hydrodynamic system is proved by the recent (yr 2006) discovery of gas flares at this location (*Hustoft et al., 2009*). Smith et al. (2014) recorded fluid leakage from several pockmarks at the study-area in 2010 and 2012 (**fig. 2.5.1**).

Vestnesa Ridge is one of the northernmost areas with occurring gas hydrates along the arctic continental margins. The occurrence of gas hydrate and free gas is inferred by seismic data on the area, by several studies (*Vanneste et al., 2005; Petersen et al., 2008; Bünz et al., 2012*). A striking BSR (Bottom-Simulating-Reflector) is found to be spreading throughout the W-Svalbard margin (*Petersen et al, 2008*). Vanneste et al. (2005) found the BSR in water depths between 750-2500 m, stretching from the upper Continental Slope to the Oceanic Ridge. The compiled results infer a gas-hydrate zone covering ~3000 km^2 on the NW-Svalbard margin, extending over the entire Vestnesa Ridge (*Hustoft et al., 2009*). The BSR is indicative of the base of the gas-hydrate stability zone (GHSZ), and is evident by the strong impedance contrast between sediments saturated by hydrates and possibly gas (*Bünz et al, 2012*). It is possible that methane is generated deeper in the subsurface adjacent to the Vestnesa Ridge, and that it migrates upwards until being prohibited by sealing gas hydrates. Further, the methane migrates laterally up under the hydrates until being accumulated in the anticlinal trap of hydrates beneath Vestnesa Ridge (*Vogt et al., 1994*). Biogenic origin is suggested as main source for the methane within the gas hydrates situated in this area (*Bünz et al, 2012*). Vanneste et al. (2005) identified several faults that stretch from the seafloor and down into the YP1-unit, thus cutting the BSR and possibly affecting the sealing-effect.

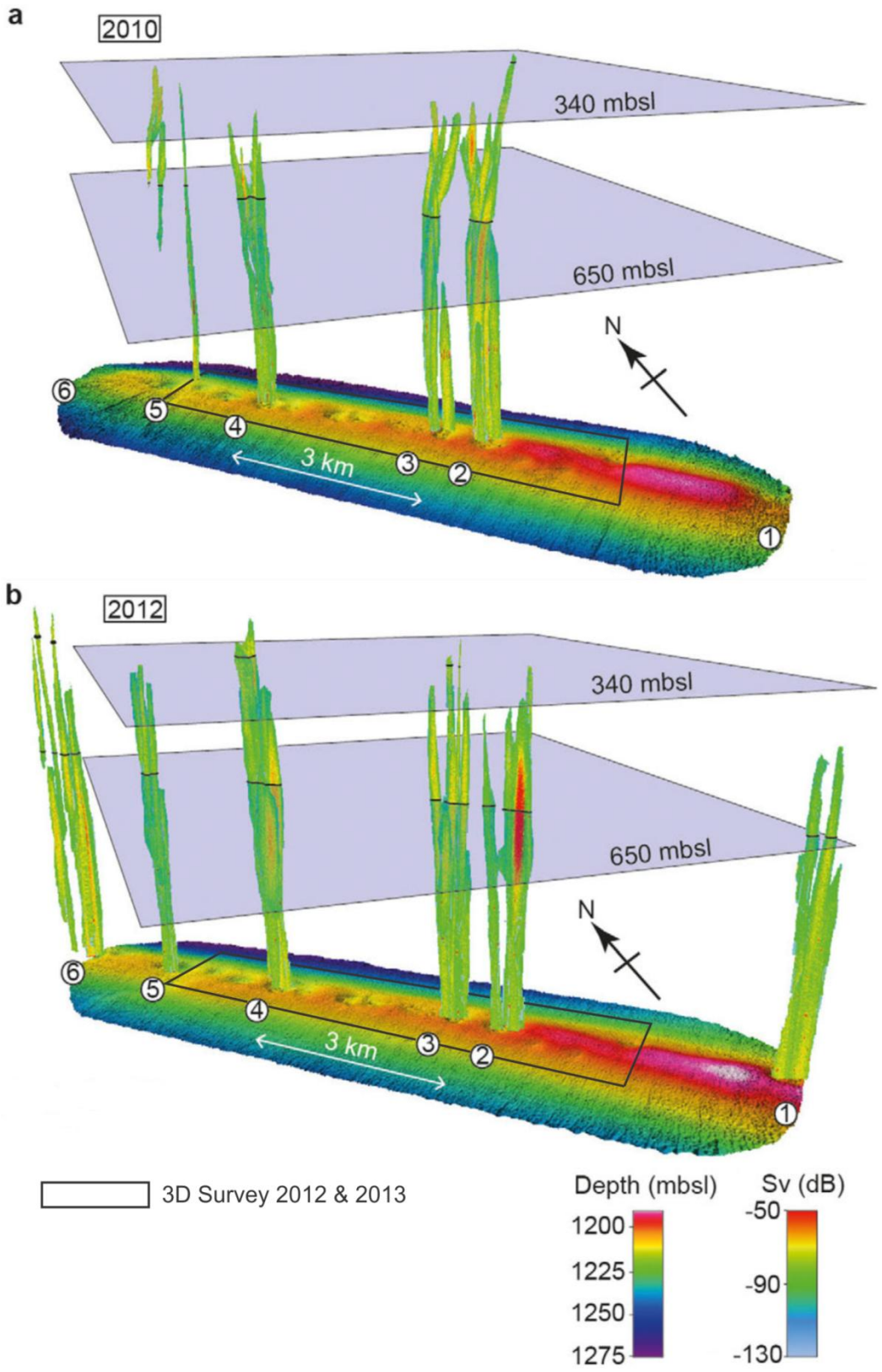

Fig. 2.5.1: Recorded fluid leakage from the pockmarks in the investigation area in 2010 and 2012. The location of the 3D-seismic dataset used in this project is indicated by a black rectangle. The investigation-area contains both recently leaking and non-leaking pockmarks. (Modified from *Smith et al. 2014*)

3 DATA AND METHODS

This project is based on the interpretation of 3D seismic data using Schlumberger's Interpretation and Visualization platform Petrel. Analysis has been performed on high-resolution P-Cable 3D seismic data acquired in 2012 and 2013, by UiT The Arctic University of Norway.

3.1 3D Seismic Data

The P-Cable 3D seismic system was used in the collecting of the datasets. The system consists of up to 24 streamers which are equidistantly towed. A cross cable is attached to the streamers with hydrophones; these are 25 m long and each containing 8 recording channels. Two large trawl doors ensures that the cross cable is spread (*Bünz et al, 2012*). An illustrative overview of this system is shown in **fig 3.1.1**, where the streamers are towed by a vessel.

Compared to conventional 3D seismic, the P-Cable 3D seismic system have the advantage of improved spatial resolution by about one order of magnitude and improved temporal resolution by 3-5 times. The increases in resolution enables simplified identification and improved imaging of shallow subsurface structures (*Bünz et al, 2012*).

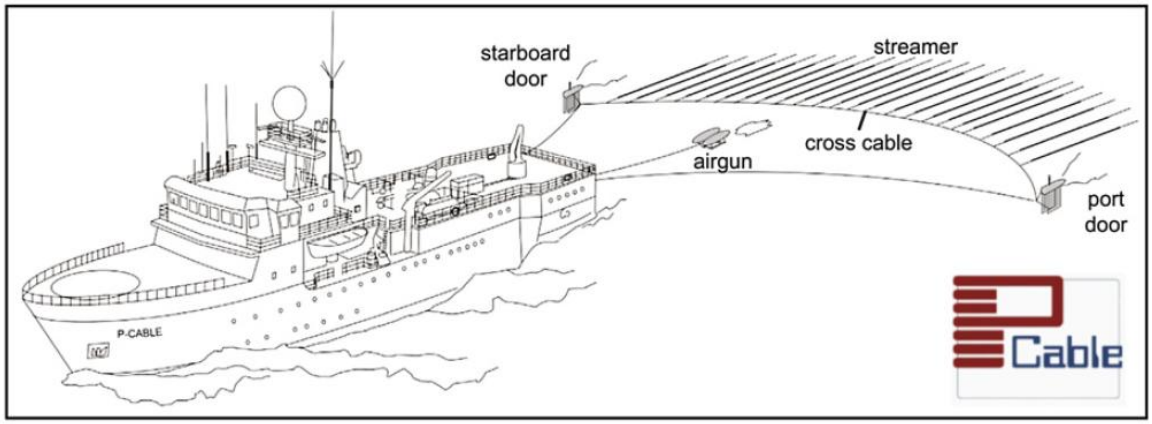

Fig. 3.1.1: Illustration of a P-Cable 3D seismic system (From *Petersen et al., 2010*).

3.1.1 The Seismic Reflection

Seismic data is acquired by sending- and measuring the strength of signals that are reflected by interfaces of acoustic impedance contrast. Seismic reflections typically arise from lithological boundaries or pore-fill characteristics, e.g. like the presence of gas within the sediments. The value of acoustic impedance (acoustic impedance = density × velocity) differs for the many seismic layers in the subsurface. The strength of the reflection is dependent of the magnitude of contrast between two interfacing reflectors, whereas a larger contrast generates a stronger reflection.

A positive reflection arises from an interface where the underlying layer has higher-valued impedance than the overlying layer. This is the most common polarity of reflections as the velocity and density within the rocks generally increases with depth. In the opposite case, the underlying layer has lower-valued impedance than the overlying layer, a negative reflection will be generated (*Andreassen, K. 2009*). **Fig. 3.1.2** displays the polarity convention for a zero phase wavelet, as a zero phased signal is used on the interpreted seismic in this thesis. However, a seismic signal can also be displayed in a minimum phase signal, which gives slightly different polarity-representations.

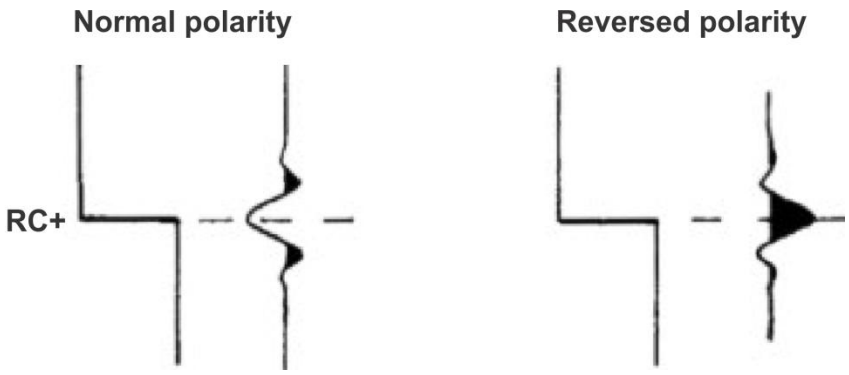

Fig. 3.1.2: The polarity convention for a zero phase signal, from *Badley 1985*. RC+ denotes an increase in reflection coefficient (Modified from *Andreassen, K., 2009*).

The reflections are collected by the CMP-method (Common-Mid-Point); the same point of the subsurface is repeatedly sampled by using various travel-paths of the wave-front (**fig. 3.1.3**). This is done by different intervals between the source and receivers, recording sequential reflections from a CMP. The method ensures improved seismic data by improving the signal to noise ratio (*Bacon et al., 2003*).

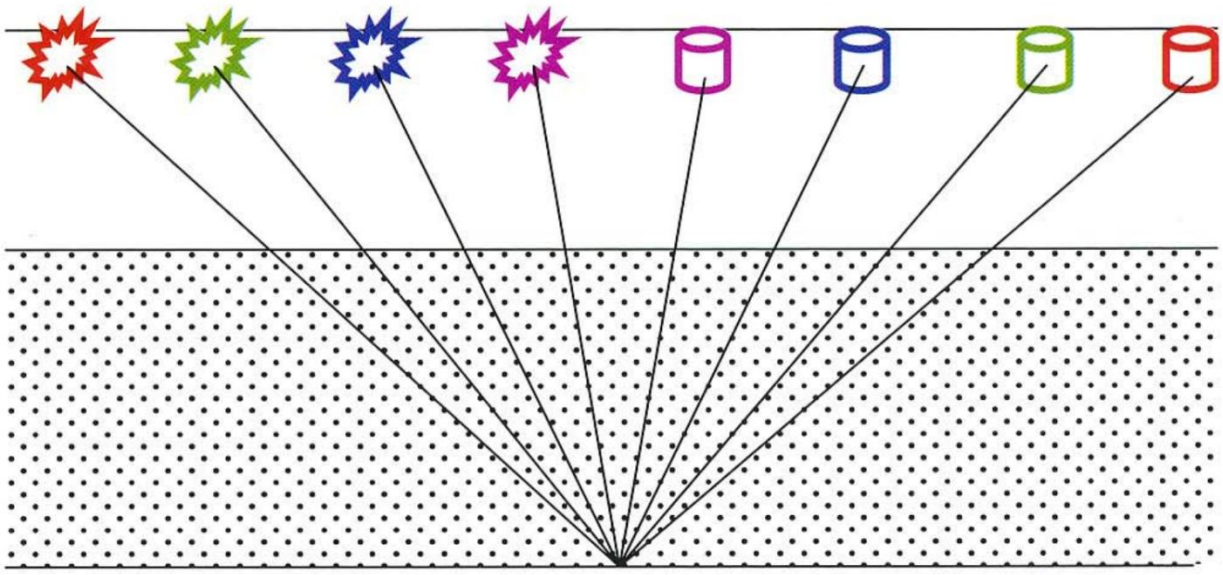

Fig. 3.1.3: Illustration of the CMP-method; Different combinations of shots and receivers are recording the same reflection point (From *Bacon et al., 2003*).

3.2 Seismic Resolution

Resolution is defined as the least separation between two features, such that they appear as individual identities on the collected data. In that way, the resolution determines the possibility of distinguishing two closely positioned features (*Sheriff 2006*). Seismic resolution is referred to in vertical and horizontal aspects.

3.2.1 Vertical Resolution

Vertical resolution mainly involves the ability to separate between reflectors. The distance between two neighboring reflectors must be at least λ/4, where λ is the dominant wavelength and wavelength = velocity/frequency, λ = V/f. Lesser thickness between two reflectors than the above will cause the two reflections to interfere with each other in a debilitative matter. Thus, a smaller wavelength will improve the resolution. The relation λ = V/f entails that resolution will be better for the more shallow lithologies, as the velocity of the sedimentary layers generally increases with depth (*Andreassen, K. 2009*).

3.2.2 Horizontal Resolution

Horizontal resolution involves the differentiation of lateral features. On un-migrated seismic data, this is determined by the Fresnel Zone; rf = V/2 (t/f)1/2, where; rf = radius of the Fresnel Zone, V = average velocity, t = two-way travel time in seconds, f = dominant frequency in hertz. The Fresnel Zone is the circular zone of the reflector, upon which the seismic reflection is produced (**fig. 3.2.1**). The absolute lower limit of the Fresnel Zone on migrated 3D seismic data is given by its diameter; Fd = λ \ 4. However, the horizontal resolution cannot be less than the bin spacing of the data-collecting system, typically 12.5 – 15 m. The horizontal resolution decreases as the Fresnel Zone increases with depth, increasing velocity, and lower frequency (*Cartwright & Huuse, 2005*).

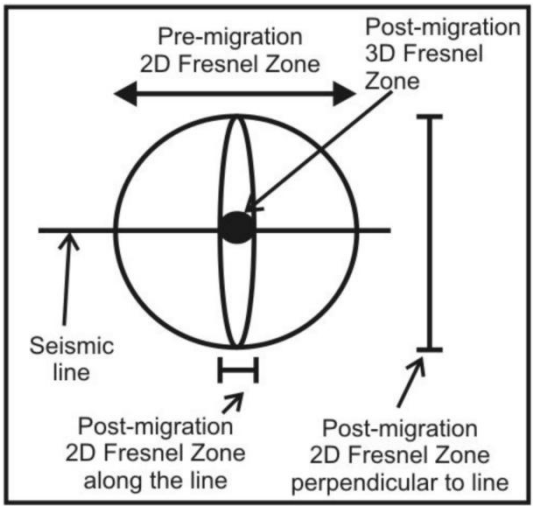

Fig. 3.2.1: Illustration of the Fresnel Zone before- and after migration for both 2D and 3D seismic data (From *Andreassen, K., 2009*).

3.2.3 Attenuation

The seismic energy is diminished with depth due to several aspects;

- The wave front of seismic energy is expanding as it spreads through the earth's crust. The increasing radius of the wave front-sphere causes a proportional decrease in seismic amplitude. This is known as spherical/geometrical divergence.
- Energy is absorbed due to various rock-properties like heat and elasticity. High frequencies are absorbed faster, than lower frequencies.
- Part of the energy is lost by reflections, refractions, mode-conversions and scattering/diffractions.

Additionally, increasing velocity causes the reduction of acoustic impedance contrast with depth. By these effects, the amplitude decreases as the wavelength increases with the seismic wave's propagation through the earth (*Andreassen, K., 2009*).

3.3 Petrel E&P Software Platform

Petrel is an interpretation and visualisation platform provided by Schlumberger. This thesis is based upon seismic interpretations and modelling conducted in the Petrel 2013 version. The software features several tools enabling interpretation, mapping and volume-calculations of seismic data. Petrel is utilized to obtain subsurface geological information.

The depth-scale is TWT (two way time); the surface-generated seismic signal's travel-time to reach a reflector and return to the surface. Consequently, TWT does not give an appropriate presentation considering depth of the stratigraphy in meters. Depth-conversion of the TWT is done by the relationship; Depth = 1/2 (TWT x V), where V denotes the velocity of the element through which the seismic reflection propagates.

3.3.1 Petrel Features

Faults and seismic horizons are interpreted by different tracking methods, in varying degrees between manual to automatic. Automatic tracking is used on the shallowest reflectors, including the SB, which appears as clear and strong reflections on the seismic data. Faults, BSR and deeper-lying reflectors are however preferably manually interpreted due to their weak responses in the seismic; these are easily misinterpreted by automatic tracking. From these interpretations, it is possible to generate surfaces; furthermore thickness maps can be calculated between surfaces based on their dip and azimuth. Color-scales can be manipulated and opacity can be used on the data, which is viewable in both 2D and 3D.

Several seismic attributes are used on the seismic data:

RMS Amplitude: Measures the reflectivity within a time window by calculating the square root of the sum of the squared amplitudes, divided by the number of samples. It is a classical attribute for bright spot detection.

Instantaneous Frequency: Presents the time derivative of the phase. Low frequency anomaly indicates hydrocarbons and occasionally fracture-zones.

Variance: Estimates inconsistencies of the seismic signal, trace to trace, without being affected by amplitude strengths. Stratigraphic terminations and structural lineaments are enhanced by the attribute. Variance values are high and continuous at faults. The values are also high at fracture-accumulations, which is helpful in gas chimney mapping.

Chaos: Maps the disorder of the local seismic signal, by a statistical analysis of dip/azimuth estimation. The attribute is used in detecting faults, fractures and gas chimneys.

Structural Smoothing: Enhances discontinuities and diminishes the noise of the seismic data. The attribute evens out the irregularities of the seismic data, by using Gaussian for confined averaging along flow surfaces following the local azimuth. Hence, layer continuity is increased without sacrificing vertical resolution. The attribute is used to optimize the seismic data prior to applying other attributes.

Envelope: Primarily represents the acoustic impedance contrast, and is therefore also known as reflection strength. It is useful in detecting bright spots. The attribute is used to optimize the seismic data prior to applying other attributes.

3.4 Seismic Interpretation Theory

3D seismic has allowed for a more advanced interpretation of seismic data, including the observations of geological features that were not recognized on 2D seismic (*Cartwright & Huuse, 2005*).
Seismic horizons are continuous reflections that are usually generated by geologic boundaries. These are sometimes affected by interfering features. The term noise covers all non-geologic phenomena that have to be ignored in the seismic interpretation. However, there are several geologic phenomena that must be recognized.

3.4.1 Indications of Gas

There are several indicators of gas-presence in the sediments. Gas within the sediments will reduce the velocity, and cause a strong reflection with reversed polarity. Gas saturations from 8-20% have shown to make the strongest velocity decrease. The velocity-decrease can cause an artifactual pull-down effect on underlying reflectors. Bright spots (**fig 3.4.1**) are high-amplitude reflections that are often caused by gas, and typically associated with porous sands. Bright spots can also result from carbonates, igneous intrusions, thinning beds and by tuning thickness - limitations of the seismic wave. High frequencies are occasionally lost underneath bright spots, as gas-bearing sediments are strongly absorbent of the seismic energy (*Andreassen, K. 2009*).

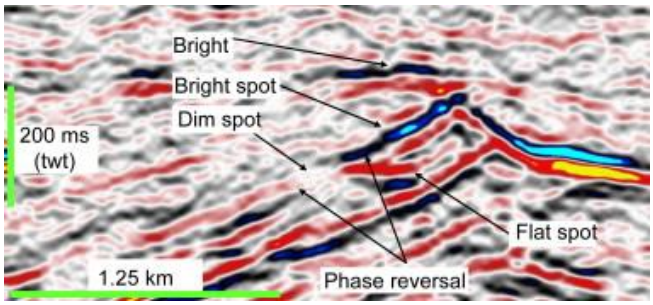

Fig. 3.4.1: Examples of bright spot, dim spot and flat spot on a seismic profile (From *Løseth et al., 2009*).

3.4.2 Indications of Gas Hydrates

Gas hydrates are able to form under specific conditions regarding temperature and pressure. The geothermal gradient limits the depth of which the temperature is still low enough for gas-hydrates to form. Combined with the physical properties of H_2O-phases, the "window" where gas-hydrates are able to form is narrow. Due to these limitations, the occurrences of gas-hydrates are restricted to the upper ~500 m of oceanic sediments. With an average velocity of 2000 m/s in the sediments, this corresponds to ~ -500 ms (TWT) bsf.

A strong BSR (Bottom-Simulating-Reflector) corresponding to the base of the gas-hydrate stability zone, is the common indicator of gas-hydrate bearing sediments. Considering the dependence on temperature, a BSR typically parallels to the Seabed – following iso-temperature lines (**fig 3.4.2**). The reflection is of negative polarity caused by;

-The high velocity of the gas-hydrate present above the BSR.

Or

-By the low velocity of free gas accumulated beneath the BSR, as gas-hydrates work as a permeability-barrier (*Andreassen, K. 2009*).

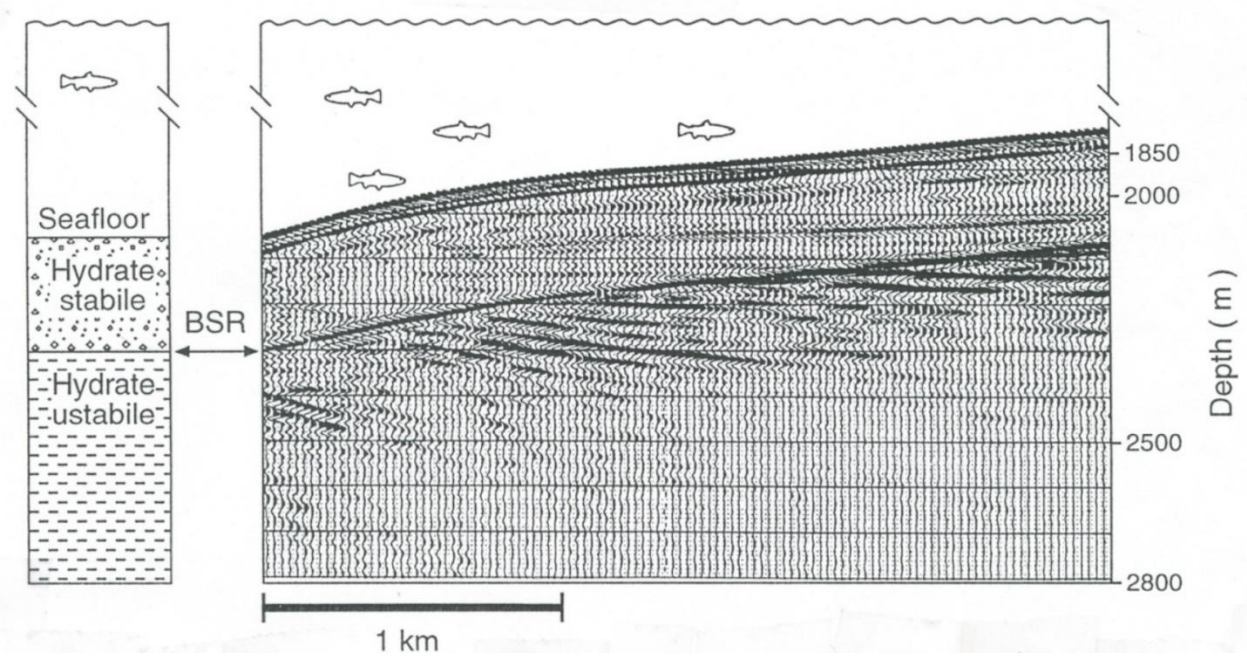

Fig. 3.4.2: A sedimentary column to the left illustrates the gas hydrate stability zone, and a BSR follows the base of the stability zone on a seismic profile (From *Andreassen, K., 2009*).

3.4.3 Indications of Fluid Flow

There are a few conduits for the migration of fluids.

i. Pipes and Chimneys

Acoustic masking is the wipe-out of seismic reflections, or deterioration of a seismic signal. Pipes and chimneys are circular zones of acoustic masking (**fig. 3.4.3**), which disrupts reflections over a longer vertical range (*Cartwright & Huuse, 2005*). Pipes are narrow and less than 200 m in diameter. Chimneys are larger and their diameters can be several hundreds of meters. A gas chimney can be identified by diffuse to well-defined acoustic masking. Pipes and chimneys represent leakage-structures of fractured cap rock, through which fluids have emerged (*Løseth et al. 2001*). Bright spots and dim anomalies are often closely related to these structures. Additionally, the low-velocity anomalies give rise to the artifact of pull-down (velocity sags) in the nearest surroundings (*Andreassen, K. 2009*). Pipes and chimneys are associated with surface- or subsurface pockmark craters (**fig. 3.4.4**), which have probably formed due to rapid discharge of gas-charged pore fluids (*Løseth et al. 2001*).

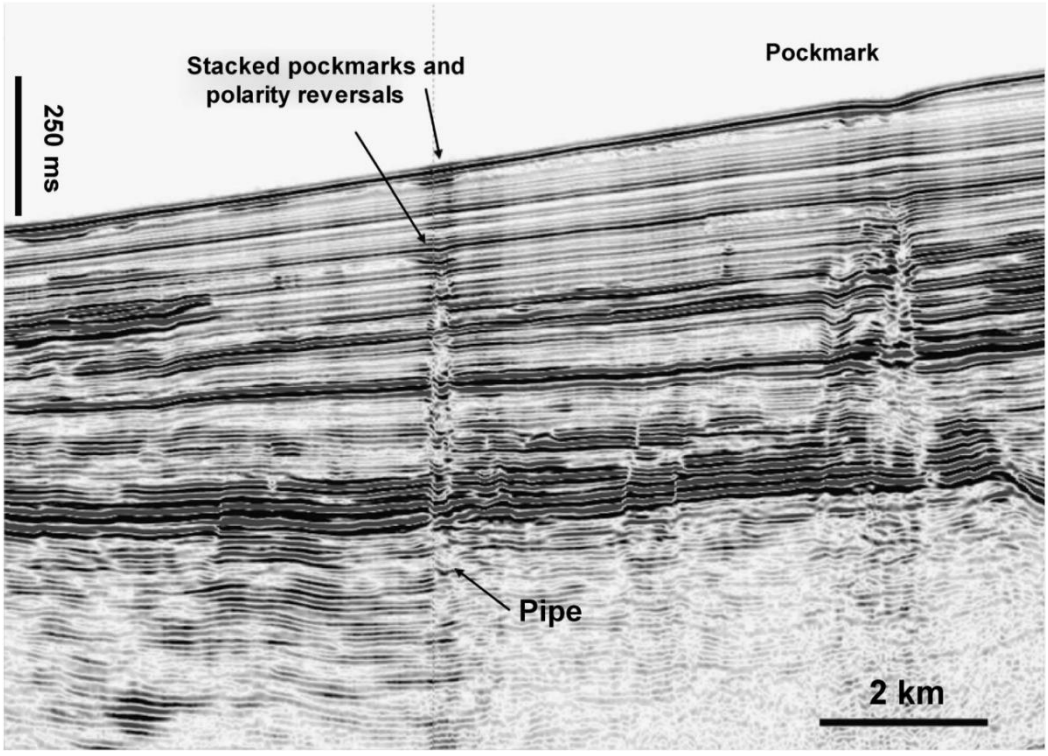

Fig. 3.4.3: Example of acoustic pipe and pockmarks at the surface and at the subsurface on a seismic profile (From *Cartwright et al., 2007*).

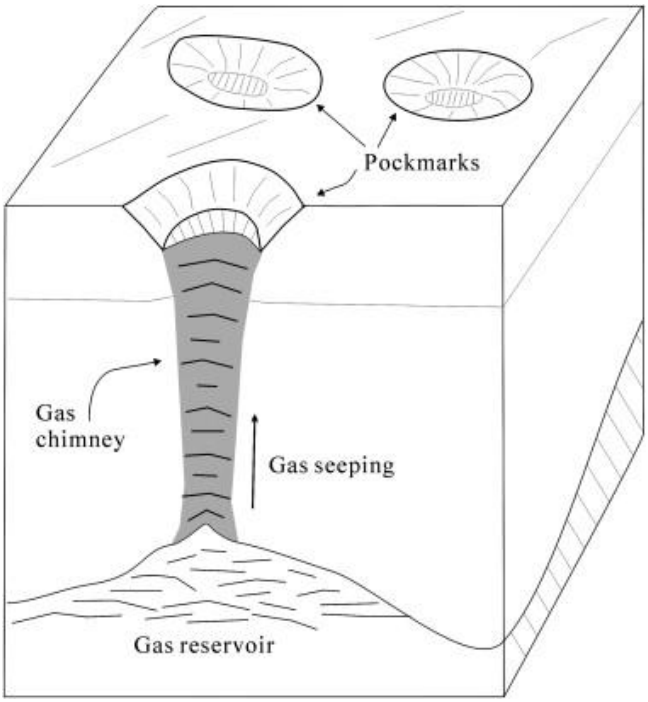

Fig. 3.4.4: Illustration of the relation between a subsurface gas-reservoir, chimney and pockmark at the SB (From *Cathles et al., 2010*; modified from *Hovland, 1989*).

ii. Faults

Faults appear as larger, thinner dim amplitude-surfaces that cut through the sedimentary strata (**fig. 3.4.5**). They are often obvious by causing the vertical throw of seismic horizons. Faults are best observed in seismic lines that are taken straight across them. These structures are often connected to each other, or numerous fractures. By physically cutting through the sedimentary strata, faults represent good conduits for fluid flow. Indications of hydrocarbons are often found in permeable layers on the sides of faults, by high-amplitude anomalies. This is observed where fluid flow has occurred vertically through the fault, until a point where it propagates laterally into easily-permeable sedimentary layers.

The amplitude of reflectors is often reduced in the boundary to a fault, because it is not produced by the entire Fresnel Zone. The seismic reflections of the up-thrown block are often seen as bending down towards the fault plane, termed rollover. This feature can be caused by;

- Actual rollover of the sedimentary layer, caused by the drag-movements of the faulting process.
- Artifact from insufficient migration of the seismic.
- Velocity artifact from lower-velocity rocks above the fault plane (*Andreassen, K. 2009*).

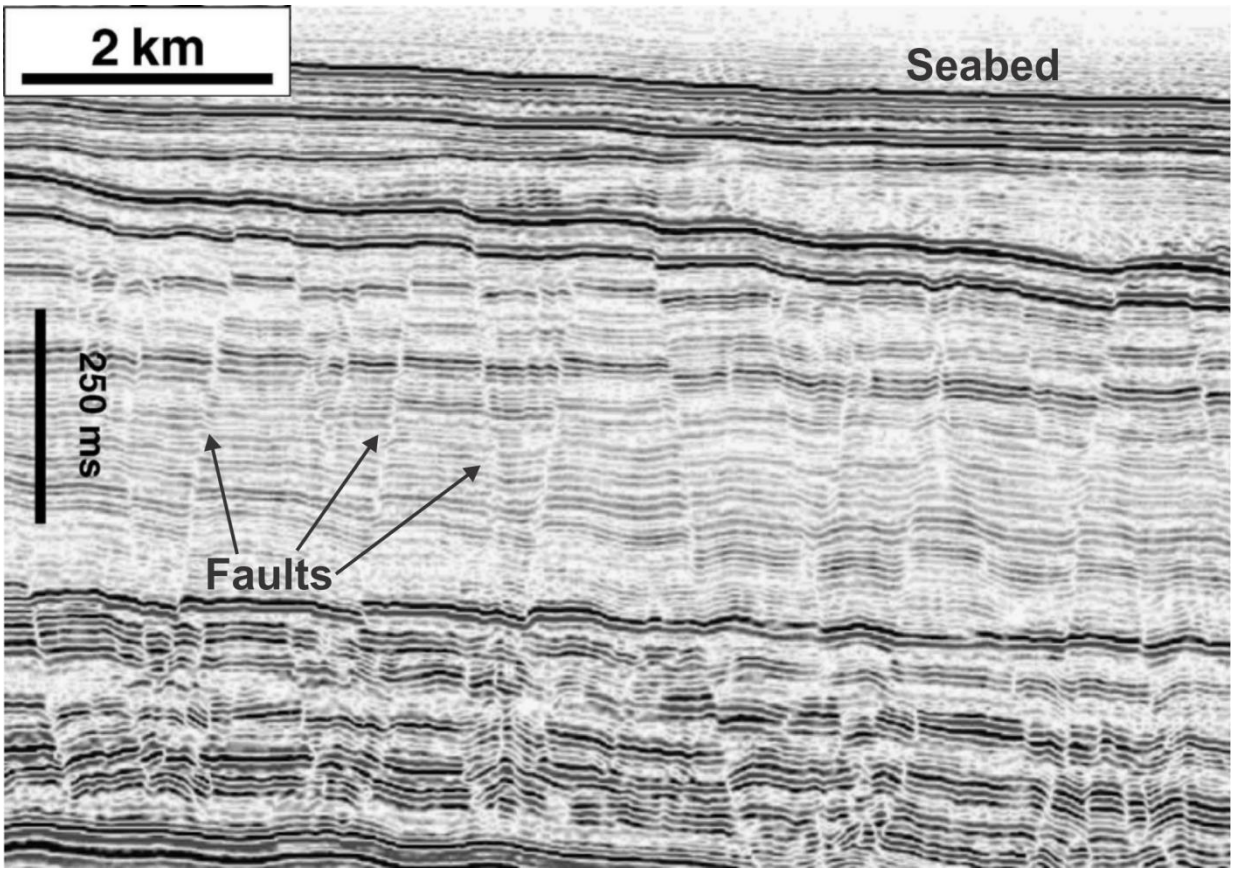

Fig. 3.4.5: Polygonal faults as observed on a seismic profile (Modified from *Cartwright et al., 2007*).

4. RESULTS AND OBSERVATIONS

This chapter covers the seismic observations, interpretations and models made from the 3D seismic data. Most of the work is done on the 2013 3D-seismic, and some results are found from the 2012 3D-seismic. (The figures made from the 2012 dataset is denoted, otherwise the results are made from the 2013 dataset).

The 3D seismic data is utilized for an attentive examination of the structures affecting the fluid flow, at the eastern Vestnesa Ridge crest. Mapping of several horizons enabled investigation of the sedimentation and axis-progradation at this study-area. A prominent BSR, several faults and chimneys are identified and mapped throughout the area. Within the chimneys there are found high amplitude anomalies indicating the presence of gas. Besides the crest of the ridge; the faults are found as strong influencers on the location of the chimneys, as well as affecting the fluid-flow within them. Emphasis lies on a detailed study of gas-migration within chimney-structures, by thoroughly investigating two currently leaking chimneys and one chimney which has not showed signs of recent leakage.

In the figures, an arrow pointing towards north is provided where necessary; it is green from above and red from beneath.

Hereinafter a description of the Vestnesa Ridge area and its features are given.

4.1 Morphology

In water depths of ~1200-1500 m, the ~100 km long Vestnesa Ridge is SE-NW oriented. The dipping ridge has a slope angle of ~0.1° from SE to the place where it bends towards the west. The angle increases to ~1° towards the western part of the ridge, where it increases more abruptly to ~6° - in direction of The Molloy Deep. The northern flank of the ridge has a slope angle from ~0.9° to ~1.5° from the SE- to the western part. The southern flank has a slope angle from ~2.5° to ~3.5° from the SE- to the western part (*Bünz et al, 2012*).

The seabed along the crest of the ridge is interspersed by several large pockmarks with depths up to 10 m, as shown on **Fig. 4.1.1**. Bünz et al. (2009) counted more than 100 pockmarks on the entire Vestnesa Ridge. At the study area, the pockmarks are of circular to oval shape and their diameters are up to 700 m. At this part of the ridge, the pockmarks are generally larger than at the western end of the ridge. The pockmarks are positioned along the top of the crest, and are not appearing on the flanks. At a couple of situations, some of the pockmarks are very closely sited, and they almost appear as one. The pockmarks are slightly buried at a varying degree, and may be indicative of current fluid flow activity (*Hustoft et al., 2009*).

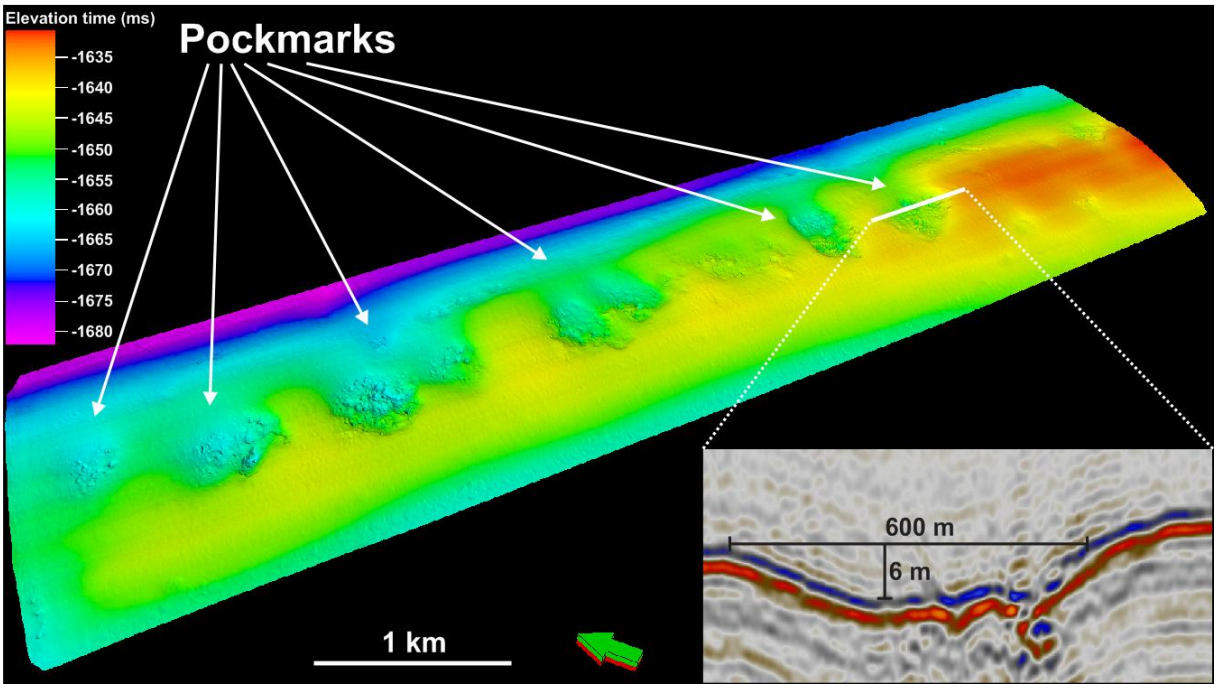

Fig. 4.1.1: Several large-scale pockmarks are visible on the seabed along the crest of the ridge; some are more obvious and rough-structured than others. A seismic line is taken over a pockmark of diameter ~600 m and depth ~6 m.

The reflectors R0, R1, R2 and R3 are interpreted, in addition to the seabed and the BSR (Ch. 4.2) in the study-area. Their positions are shown in **Fig 4.1.2** and **Fig. 4.1.3.** The R3-reflector lies below the BSR, whilst the three other additional reflectors are positioned in-between the SB and the BSR. A fault (Ch. 4.3) causes the reflectors R1, R2 and R3 to have a vertical throw, which has greatest impact on R3 and least impact on R1.

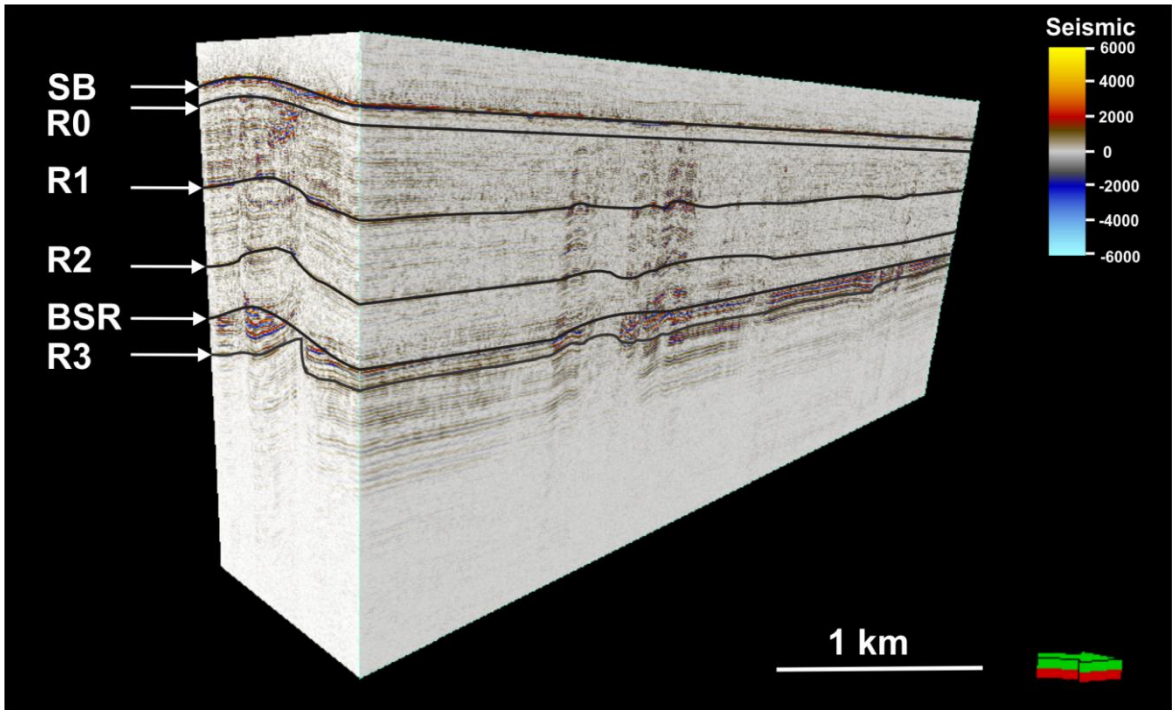

Fig. 4.1.2: The stratigraphical positions of the interpreted surfaces in the seismic cube; seabed denoted SB, R0, R1, R2, R3 and the BSR. Their surfaces are displayed in fig. 4.1.5.

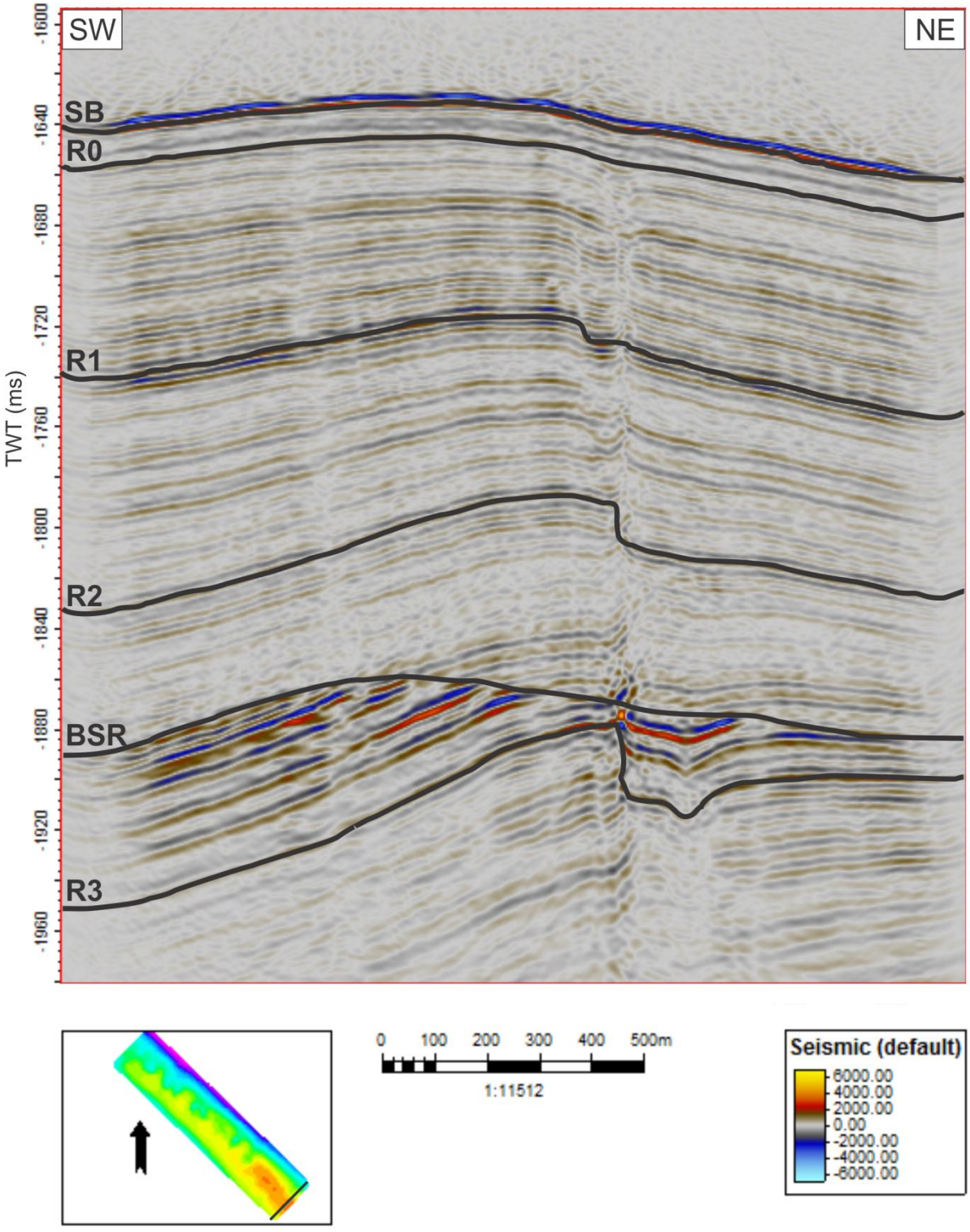

Fig. 4.1.3: The interpreted additional reflectors together with the SB and BSR viewed from SE. A fault is disturbing the reflectors R1, R2 and R3, causing them to have vertical throw. The throw is larger at the deeper-lying reflector R3 and smaller for the shallowest reflector R1 of these three. The BSR strongly stands out from the surrounding reflectors R2 and R3 regarding shape, and is obviously cross-cutting several reflectors.

This part of the Vestnesa Ridge is a slightly asymmetrical and disharmonic anticlinal fold with NW-SE fold-axis orientation. The axis-interpretation is done by establishing the contour-lines' position, where they would have propagated if they were undisturbed by chimney-structures. As the limbs are dipping with dissimilar steepness, the axis is placed by extending the limbs' surfaces based on their gradients - and establishing the points where they cross. Assuming seismic velocity for water at 1500 ms^{-1}; the steepest limb of the ridge is dipping with ~1.0° towards the NE in average, and the other limb has a dip of ~0.9° to the SW in average.

By objective assessment of the SB and the reflectors, R1, R2 and R3 (**Fig. 4.1.4**), it is observed that the axis of the Vestnesa Ridge at this location is migrating to the SW with time. The shape of the SB-axis is less curved than the axes of R1, R2 and R3. To the NW of the investigation area, the axis of the SB makes a crossover with the axes of the underlying reflectors. The underlying reflectors are however converging in a mutual point. The largest horizontal offset between the SB- and R3-axis is ~500 m from Ne to SW. The largest offset opposed to this is ~150 m from SW to NE. The axis of the BSR is least deviating from, and appears almost identical to the axis of R1.

The surfaces beneath the SB show both local depressions and highs related to the chimneys positions.

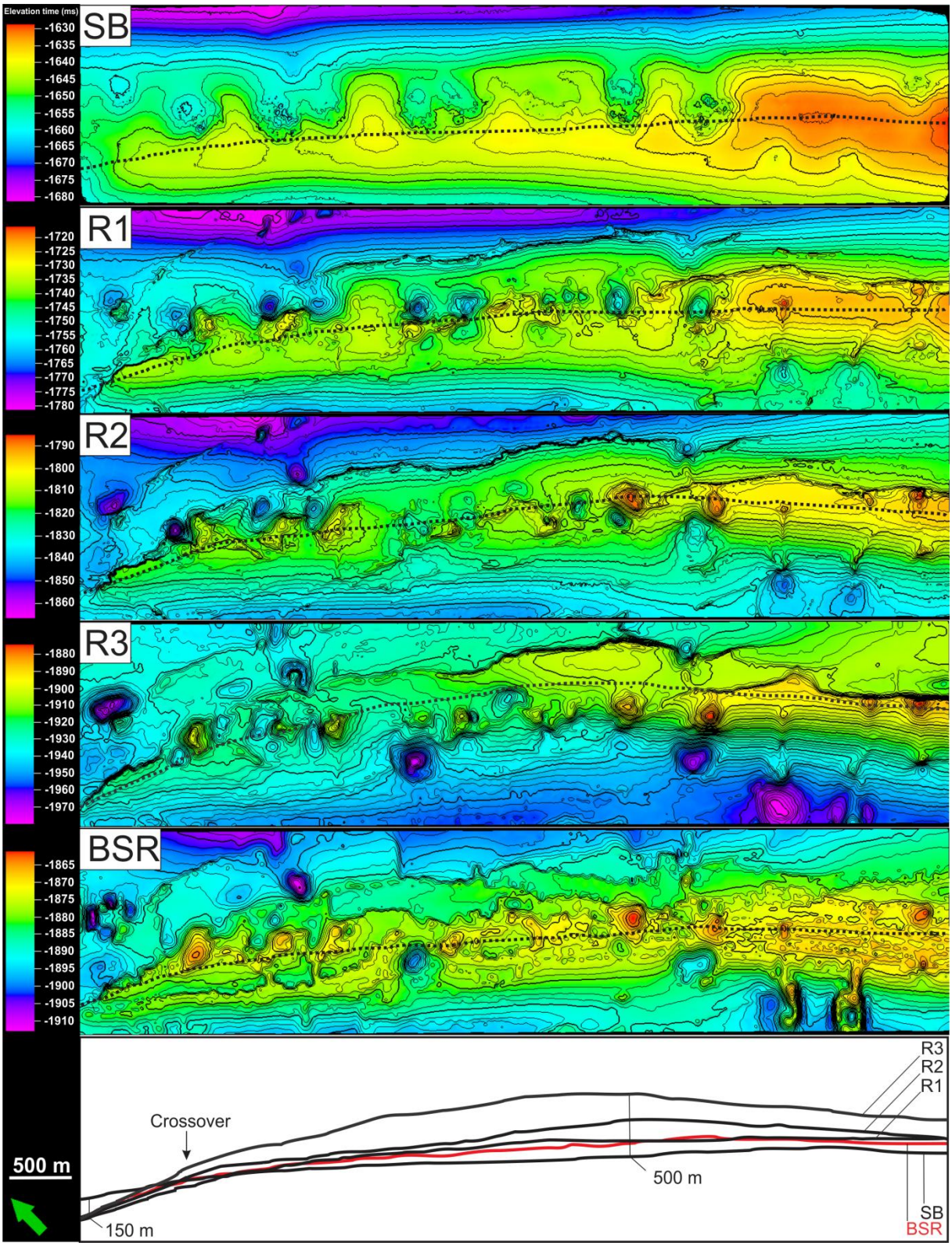

Fig. 4.1.4: The surfaces of the seabed, reflectors R1, R2, R3 and the BSR with their respective folding-axes shown as stippled lines. Including a comparison of them to show how the axis of the ridge has prograded in SW direction. NW in the investigation-area, all of the axes converge in a mutual point, except the SB-axis which makes a crossover to the other axes. The largest offset between the SB- and the R3-axis in SW-direction is 500 m, and the largest offset in NE-direction is 150 m. The BSR-axis (red color) is most similar to the axis of the R1-reflector. The contour lines are separated by 2.5 ms (TWT) vertical height and bold for every 10'Th ms (TWT).

The sedimentary layering are of conform boundaries. However the thickness of the layers is inconsistent throughout the area; they are thinning at the fold-axis and thickening at the folds limbs. **Fig. 4.1.5** shows thickness-maps generated between the SB and R1, between R1 and R2 and between R2 and R3. It shows for these intervals a thicker sedimentation at the folds limbs, and the thinnest sedimentation at the fold-axis. The sedimentation thickness between the reflectors; SB to R1 varies by ~55 ms, R1to R2 varies by ~65 ms and R2 to R3 varies by ~90 ms (TWT). Accordingly there is increasing topography-variations between the reflectors with depth.

The sedimentation between R2 and R3 differs from the other two. There is an apparent NW-SE-oriented boundary separating thinner sedimentation in the NE, and thicker sedimentation in the SW. This boundary is positioned adjacent to some striking faults (Ch. 4.2), which in the thickness-maps appears as thinner elongated lines from NW to SE.

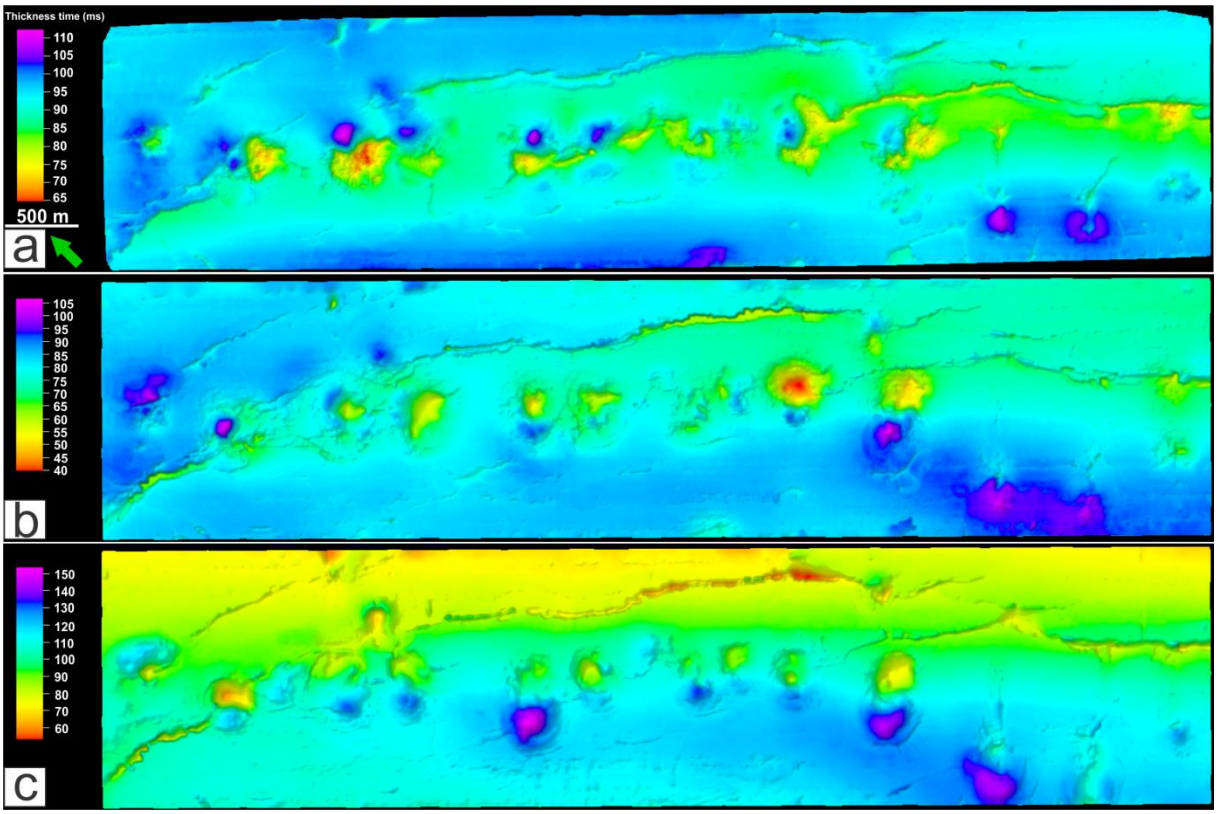

Fig. 4.1.5: Time-thickness maps generated between; a) Seabed and surface R1, b) Surfaces R1 and R2, c) Surfaces R2 and R3. a) and b) shows a thinning in sedimentation at the crest of the ridge, and thickening at the flanks. Also there are local prominent thinning and thickening at the chimneys location. NE-SW-reaching thin lines are found at some of the faults paths. c) Shows a thinning in sedimentation at the NE-side of the crest, and a thicker sedimentation at the SW-side of the crest. Local thinning and thickening at the chimneys location is also seen in this interval. In addition the same faults also result in thinner lines of sedimentation.

4.2 BSR

A distinguished BSR is present throughout the entire study area, between ~-1860 to -1905 ms (TWT) depth. The shape of the BSR parallels to the SB and separates from its nearest reflectors, which are of a significantly steeper inclination. In **fig. 4.1.3** it is clearly observed that the BSR crosscuts several reflectors. Especially the beneath-lying reflector R3 has a rough and uneven surface of very steep inclination, which is only remotely similar to the BSR. A bottom-simulating reflector caused by gas-hydrate cementation of the sediment, may appear as a bright spot which cross-cuts bedding-related reflectors (*Selley, 1998*).

The polarity-reversal of the BSR is manifested in **fig. 4.4.1**, where the polarity of the wiggle trace is shown for the SB and the BSR. Reversed polarity is typically seen at the boundary between sediments with- and without gas-filled pores, gas-containing sediments at the bottom (*Andreassen, 2007a*). The BSR provides indirect evidence for the occurrence of gas hydrates in this study area. Within the sediments, it often represents the boundary between free gas underneath gas hydrate (*Haacke et al. 2007*). Gas-hydrate within sediments has a sealing effect towards fluid-flow (*Andreassen, 2007a*).

Fig. 4.2.1 displays the BSR in raw-data where each single seismic line is thoroughly interpreted, hence displaying the BSR in great detail. There are several circular areas where the BSR is not observed in the seismic, these are caused by the interpreted gas chimneys (Ch. 4.4) which are piercing through the BSR. In the figure we can also observe how the BSR is inconsistent within stratigrafical layers throughout the entire study-area. Especially prominent is the cross-cutting of reflectors beneath the crest of the Vestnesa Ridge, which is caused by the iso-temperatural boundary of the GHSZ. A time-structure map of the BSR is displayed in **Fig. 4.1.4**. The BSR follows an elongated anticlinal shape, slightly dipping in NW-direction. The surface shows irregular depressions and peaks that are seen in relation to the locations of the chimneys.

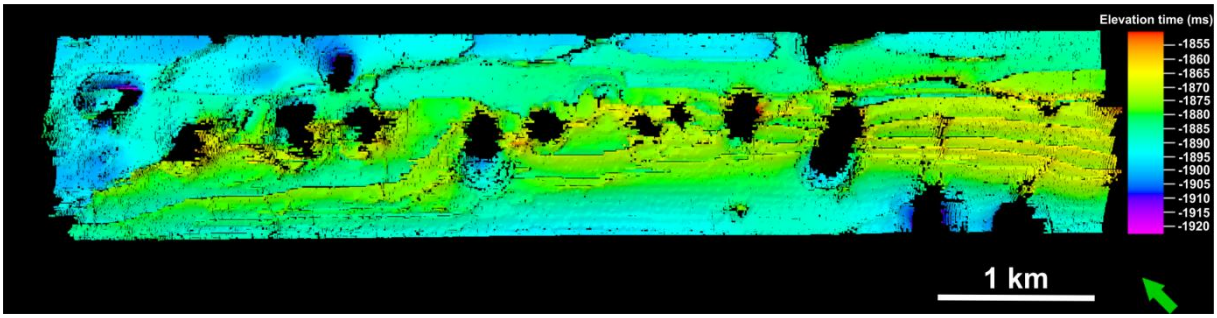

Fig. 4.2.1: Raw-data of the interpreted BSR made from the Vestnesa2012 dataset, allowing for comprehensive observation of the BSRs structure. Each line is thoroughly interpreted to show the BSR in its full detail. Chimneys are the reason for several holes piercing through the BSR. Breaches in the BSR are seen at faults, and where the BSR is shifting between reflectors.

From an instantaneous frequency attribute cube there was found a level of abrupt change in the frequency strength (**fig. 4.2.2**). At ~ -1860 to -1900 ms the frequency changes from generally high values up to 500 Hz, into generally low values mainly ~50 to 100 Hz. The lowest frequencies are seen between the BSR and down to ~-2000 ms (TWT). Low frequencies are often indicative of free gas accumulated beneath layers of high reflectivity, thus signifying a severe contrast in velocity (*Andreassen, K., 2009; Taylor et al., 2000*). These changes in frequency supports the establishment of the BSR as an indicator of the boundary between gas-hydrate bearing sediments above, and free gas in the sediments beneath. Below the BSR there is a ~100 ms (TWT) thick layer of assumed free gas. This layer appears thinning towards the flanks of the BSR, and its thickest column is found directly beneath the apex of the BSR.

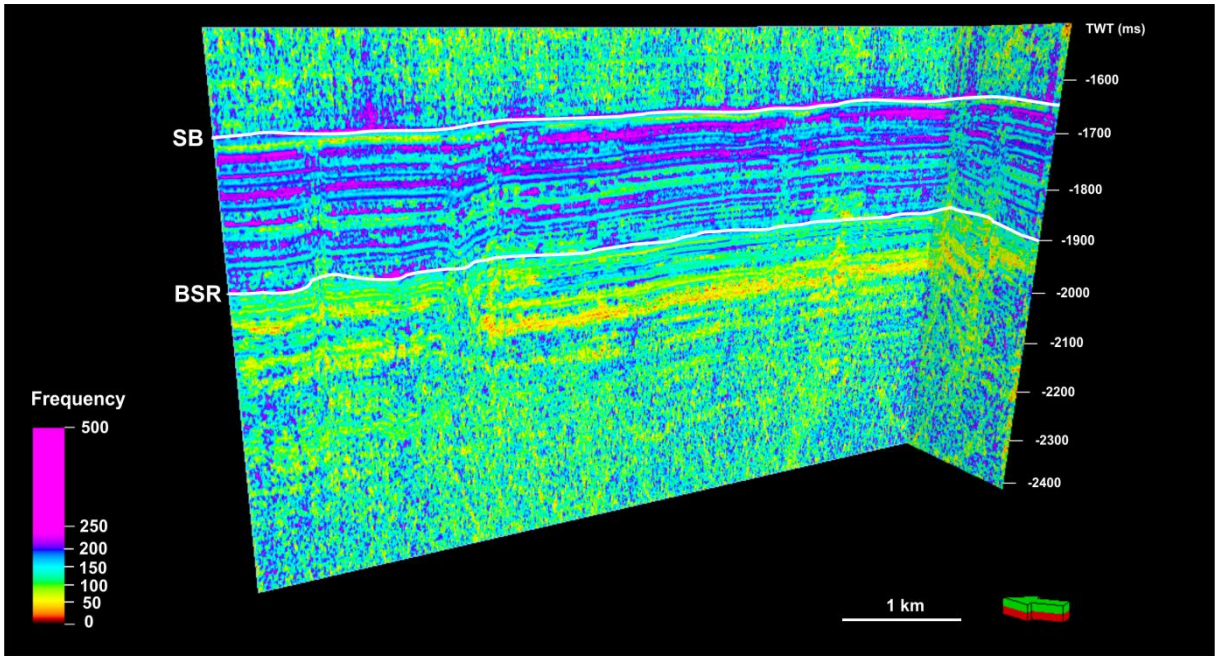

Fig. 4.2.2: Instantaneous frequency attribute cube showing higher frequencies above the BSR, and lower frequencies indicative of free gas beneath. The strongest low frequencies are found between the BSR and ~100 ms (TWT) below.

Fig. 4.2.3 shows the time thickness map generated between the SB and the BSR. The time-thickness varies with 60 ms (TWT). The lowest- and highest values however, are related to the chimneys that are piercing through this volume. This is an effect from the depressions in the SB by the pockmarks, and the BSRs elevation in some of the chimneys. Disregarding these irregularities, the time-thickness varies with not more than ~10 ms (TWT) throughout the investigation area. Thus, the thickness-map is demonstrating the evident parallelism between the BSR and the SB. A minor deviation is present by a slightly thinner separation at the NE than at the SW.

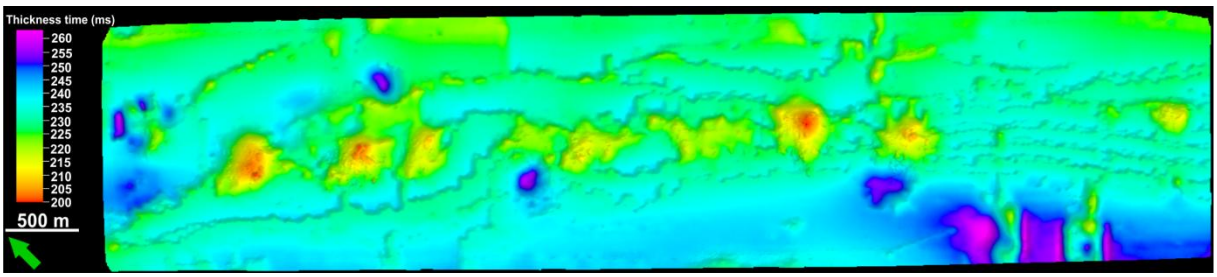

Fig. 4.2.3: Time-thickness map generated between the seabed and BSR. The thinnest- and thickest parts are related to the chimney-structures, where the SB is depressed and the BSR is elevated or depressed. Except for these irregularities, the sedimentation thickness varies from 225 to 235 ms (TWT) between the SB and the BSR.

4.3 Faults

The term fault covers fractures ranging from scales of meters to much larger extent (*Twiss & Moores, 2007).* Several faults extend from the reflector R0, just beneath the seafloor, and reach far below the BSR. Their depths are not seismically manifested due to the limitations of the seismic data, and in this project they are only interpreted down to -2175 ms (TWT). **Fig. 4.3.1** covers the faults upon two variance-attribute time-slices; at the BSR and ~35 ms (TWT) below the SB. On the variance-time-slice, the faults are represented by elongated red lines. The related red and circular areas are interpreted chimney-structures (Ch. 4.4). The faults are also presented together with the SB, visualized from below.

The faults are steeply inclined and appear vertical. Four larger NW-SE-oriented faults with slightly curved fault traces, spread throughout the investigation area. Two of them are each branched with two fault traces that are situated alongside the main branch, so called anastomosing faults (*Twiss & Moores, 2007*). In addition there are four smaller NE-SW-oriented faults, which merely reach over a short distance (0.5 - 1 km) perpendicularly between neighboring larger faults. These are interpreted as faulting caused by the large faults' movements.

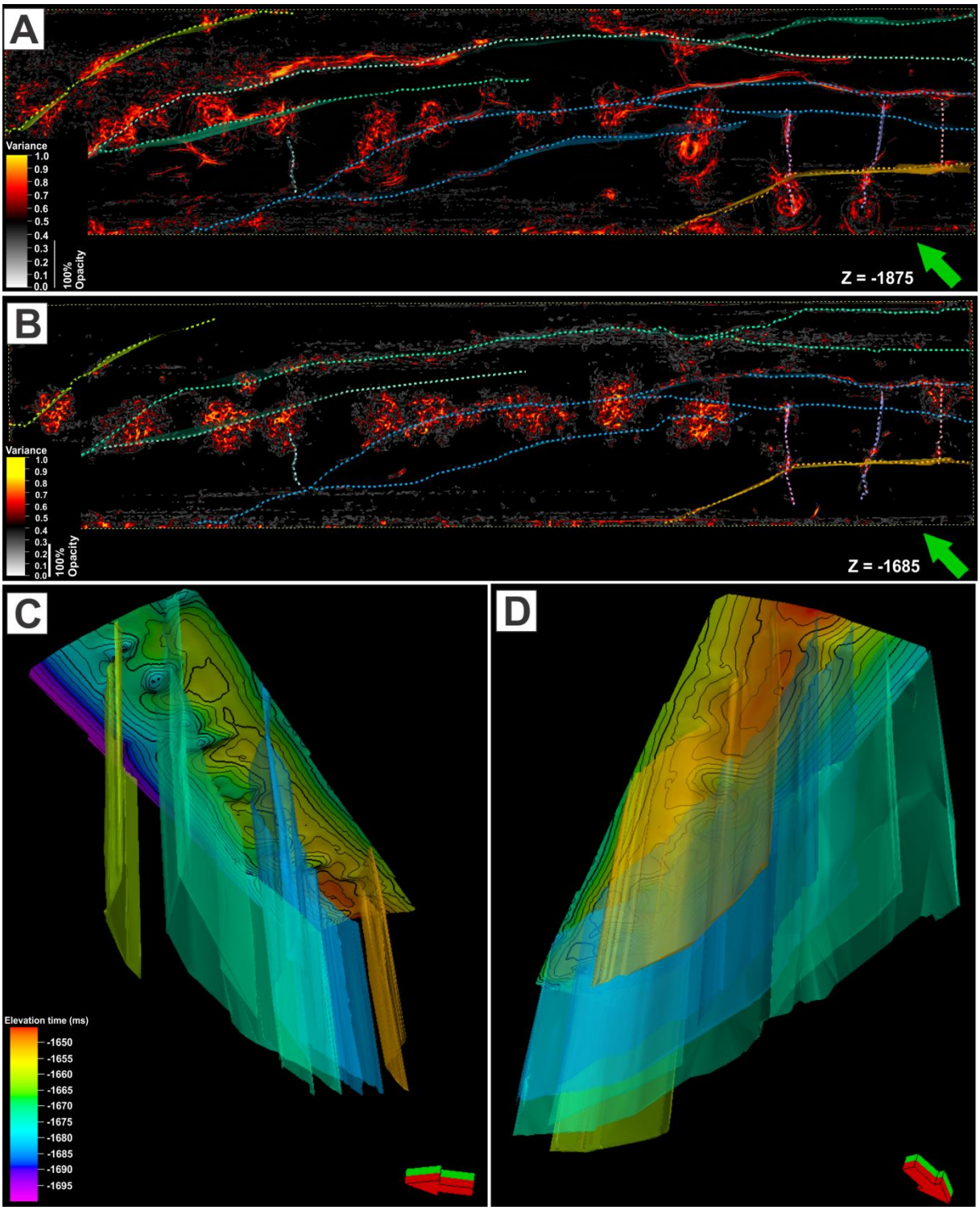

Fig. 4.3.1: A) displaying the large faults traces on a variance-attribute time-slice at -1875 ms (TWT), the depth of the BSR. The faults and the chimneys are seen in high variance values (red). 100% opacity is used on the variance values from 0 to 0.36 to emphasize the faults close relation to the chimneys. B) Displaying the fault traces on the variance-attribute time-slice at -1655 ms (TWT), ~30 ms (TWT) beneath the seabed. 100% opacity is used on the variance values from 0 to 0.27. C) and D) displaying the faults and the reflector R0 from beneath. C from west and D from southeast.

Fig. 4.3.2 shows some of the faults as observed in the seismic and their position at the SB. They are recognized as thin lines of acoustic blanking through the reflectors. At some occasions the reflectors have a vertical shift at the faults. All of the faults reach up to the reflector R0, which lies ~17 ms (TWT) below the seafloor. This shallowness indicates recent and related timing of the events.

The faults are generally of severely limited throw (vertical slip), which is not possible to determine in the seismic data. **Fig. 4.3.3** shows the throws that were measurable, as indicated in **fig. 4.3.2**. They are quantified on the R1-, R2- and R3-reflectors.
*(Note: the fault in **a1-3** and the NE-fault of **b1-3** is the same anastomosing fault).*

R1-reflector: The reflector show breaches by pull-up at the faults. For all of the faults in **a1** and **b1**, pull-up of the reflection SW of the faults is observed. However, the entire reflector remains at the same depth through the faults.

R2-reflector: At the fault in **a2**, the reflector has a throw of 3 ms (TWT). The SW-fault in **b2** has a true vertical throw of 5 ms (TWT). Pull-up is observed SW of this fault. The NE-fault in **b2** shows a breach by pull-up of the reflector SW of the fault. The reflector does not have vertical throw at this fault.

R3-reflector: The pull-up effect is seen both at the SW- and the NE-side of the faults in **a3** and **b3**. As the reflector also is affected by pull-down in **a3**, the true throw is uncertain at this point. The SW-fault in **b3** has a true throw of 8 ms (TWT), and the NE-fault has a throw of 6 ms (TWT). **a4** displays the only measurement on the northernmost fault of the investigation area, which has a throw of 3 ms (TWT).

For the faults with vertical throw, the throw-heights increase with depth. This is inferring that the faults have been continuously active through time.
(The heave/ horizontal slip cannot be established from the seismic data).

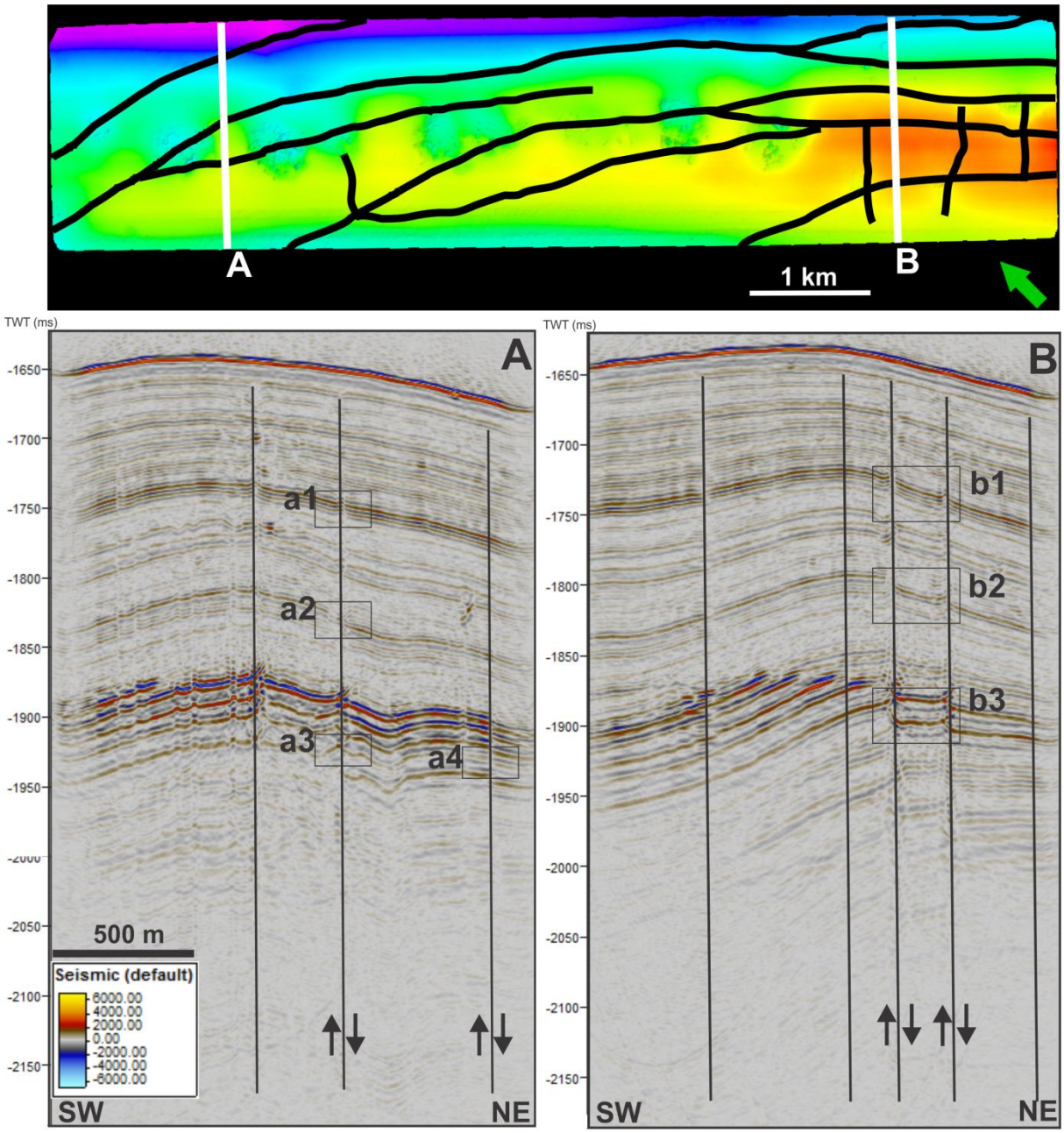

Fig. 4.3.2: Top: The SB with projected fault-traces, along with the seismic lines A and B of the Vestnesa 2013 seismic cube. A) Displaying the faults in the NW. B) displaying the faults in the SE. Arrows indicate the vertical throw-direction of the blocks. The black squares a1-a4 and b1-b3 are zoomed in on the seismic to measure the faults vertical throw of the reflectors R1, R2 and R3 in fig. 4.3.3.

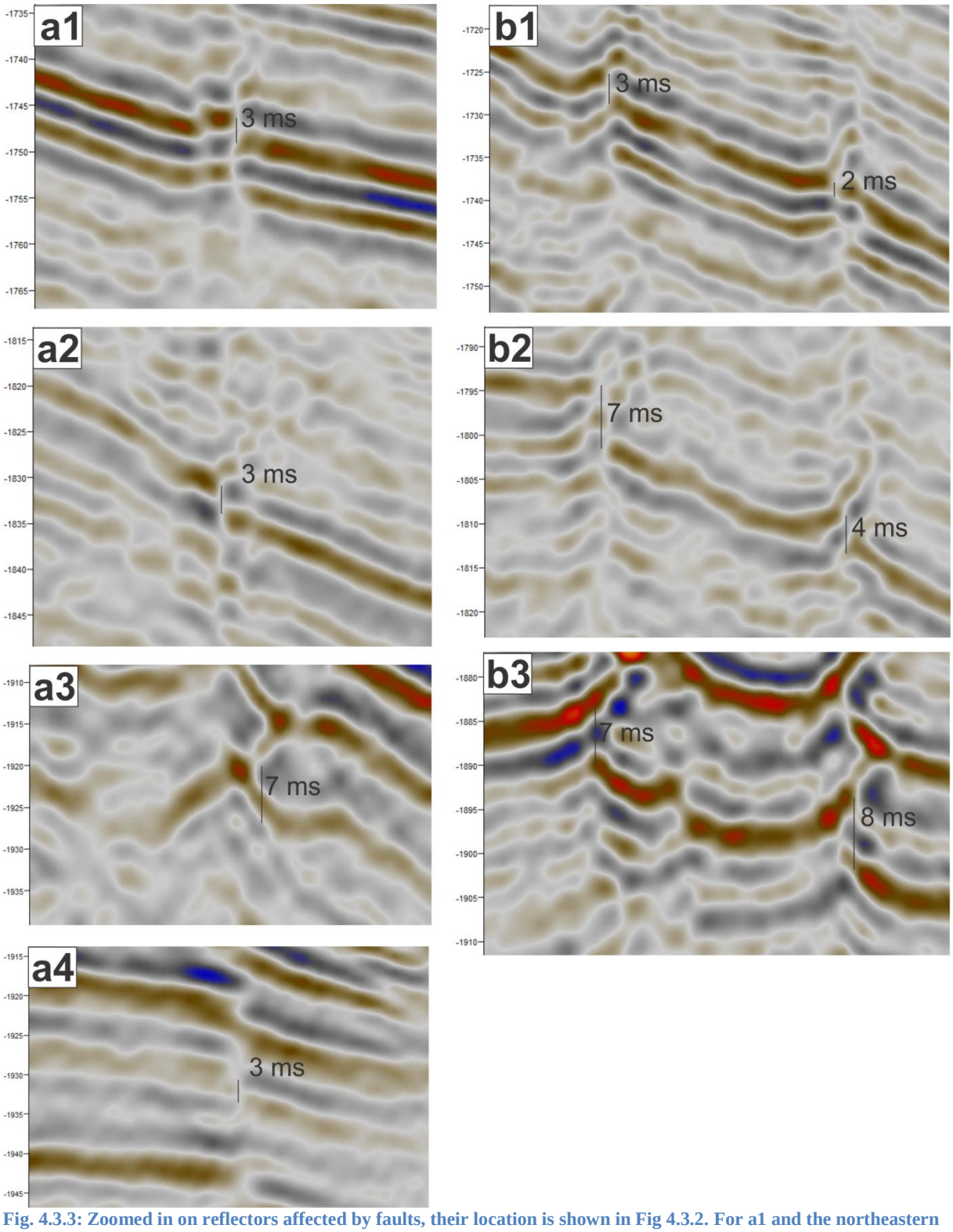

Fig. 4.3.3: Zoomed in on reflectors affected by faults, their location is shown in Fig 4.3.2. For a1 and the northeastern fault (to the right) in b1 and b2; the measurement does not involve the whole block, but only measuring a small fault-related bending of the reflectors. From a1 to a3 and b1 to b3, vertical-throw impact increases with depth. a4 is the only zoomed in part of its fault displaying a vertical throw that is not seen in the reflectors above from Fig. 4.3.2.

4.4 Chimneys

Chimneys are recognized by many features in the seismic. The most prominent observation is vertical sections of chaotic reflections that are cutting through the BSR and lead to the pockmarks at the SB (**Fig. 4.4.2** and **4.4.3**). Both pull-down and pull-up is seen on several reflectors and on the BSR at the chimneys outer rim. Within the upper parts of the chimney-structures, bright spots (Ch. 4.5) are observed.

A simple investigation of the sizes and shape of the chimneys cross-sections at the BSR and the SB is presented in **fig. 4.4.1**. It states that the elliptical shape is dominating both at the BSR and at the SB. However there is a slight tendency towards a more circular shape at the SB. All research on pockmarks suggests that they generally vary between circular to elliptical shape (*Cathles et al., 2010*), which is prominent at this site.

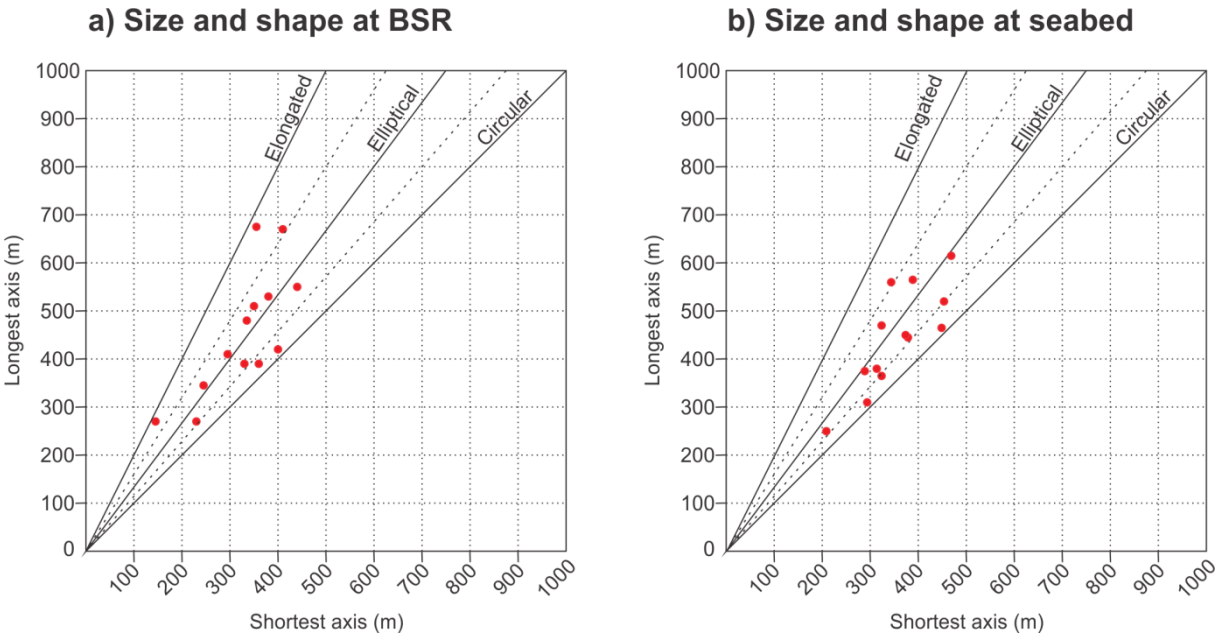

Fig. 4.4.1: The sizes of the chimneys in cross sections taken at a) the BSR, and b) the SB. The elliptical shape is dominant both at the BSR and at the seabed, but they are generally trending toward the circular shape with height.

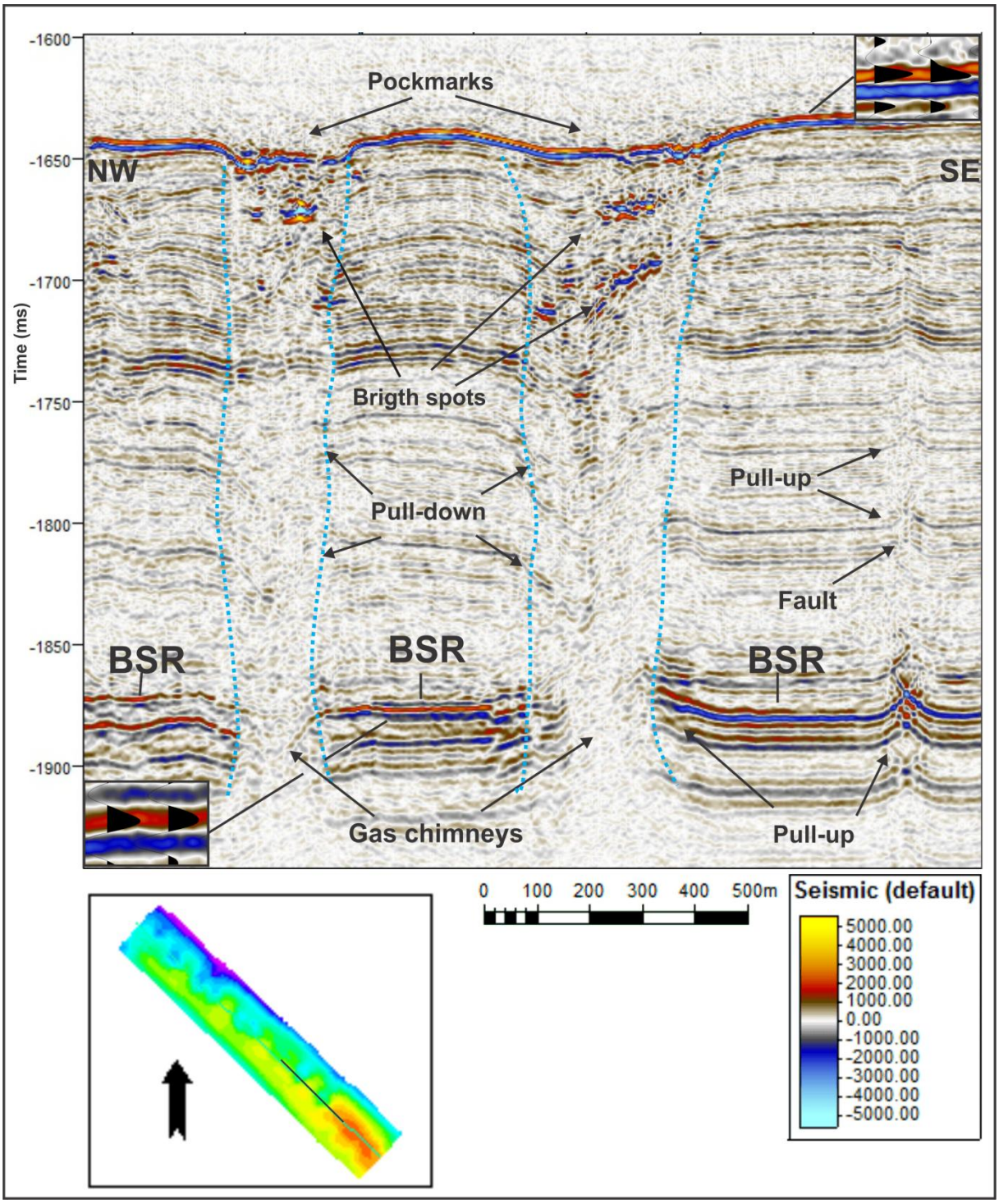

Fig. 4.4.2: From Vestnesa 2012. A seismic line through the two leaking chimneys that are investigated in this project. The Chimneys are recognized by vertical zones of seismic wipe-out that pierce through the BSR, and reach up to the pockmarks in the SB. Chimney-related features; pull-down and pull-up of seismic and bright spots (gas indicators) are pointed out in the figure. Seismic pull-up is also observed on the BSR and reflectors especially at the chimneys' base. Pull-up of the seismic is prominent at the fault, which also causes a limited breach in the seismic. The wiggle-traces for the SB and the BSR are also shown to visualize their opposite polarity.

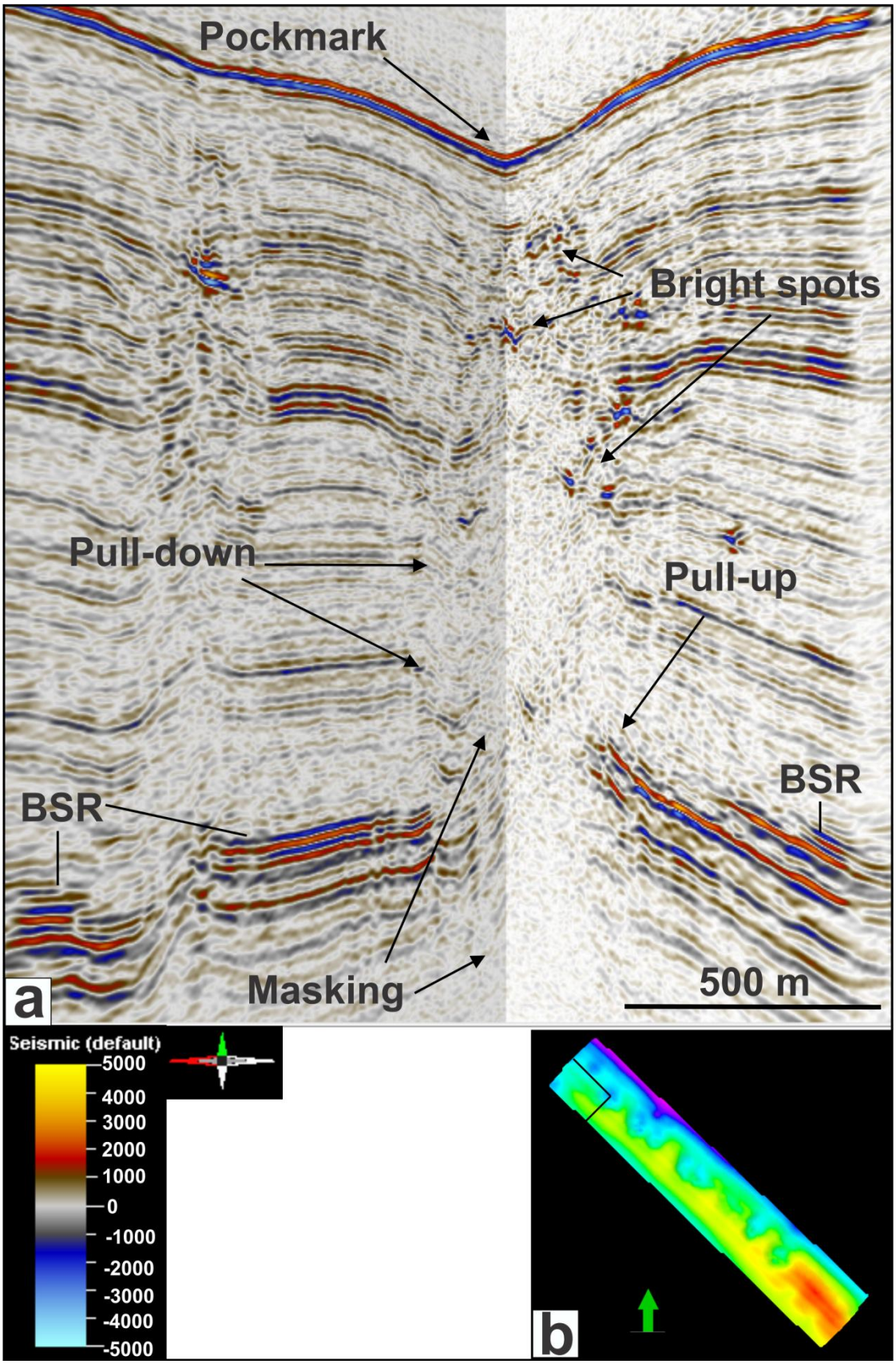

Fig. 4.4.3: From Vestnesa 2012. a) Two seismic lines enabling the examination of the non-leaking chimney investigated for this project in 3D. Less prominent bright spots are found here, than at the leaking chimneys in fig. 4.4.2. Also, this pockmark has a smoother surface. b) Location of the lines shown on the SB.

Fig. 4.4.4 displays a seismic line taken over the most striking pockmarks at the SB. The vertical zones of seismic wipe-out are clearly visible below each pockmark. A time-slice is taken through the strong reflections directly beneath the BSR. The wipe-out appears as elliptical zones on the time-slice. **Fig. B** displays the modeled chimneys on top of the same seismic, hence it is easily seen that the chimney-models fill in the wiped-out seismic sections. The chimneys are displayed with the aim of presenting their main characteristics. They are modeled by the chaos-attribute, which also strongly manifests faults. Locking each chimney into its own sub-cube was necessary due to severe disturbance from faults. The chimneys are cut off from the faults going into them. These boundaries are seen in bright yellow on the chimney-models surfaces. Generally the chimney-models have a red color that signifies the true outer boundaries of the structures. The chimneys appear as somewhat rough-edged pillars.

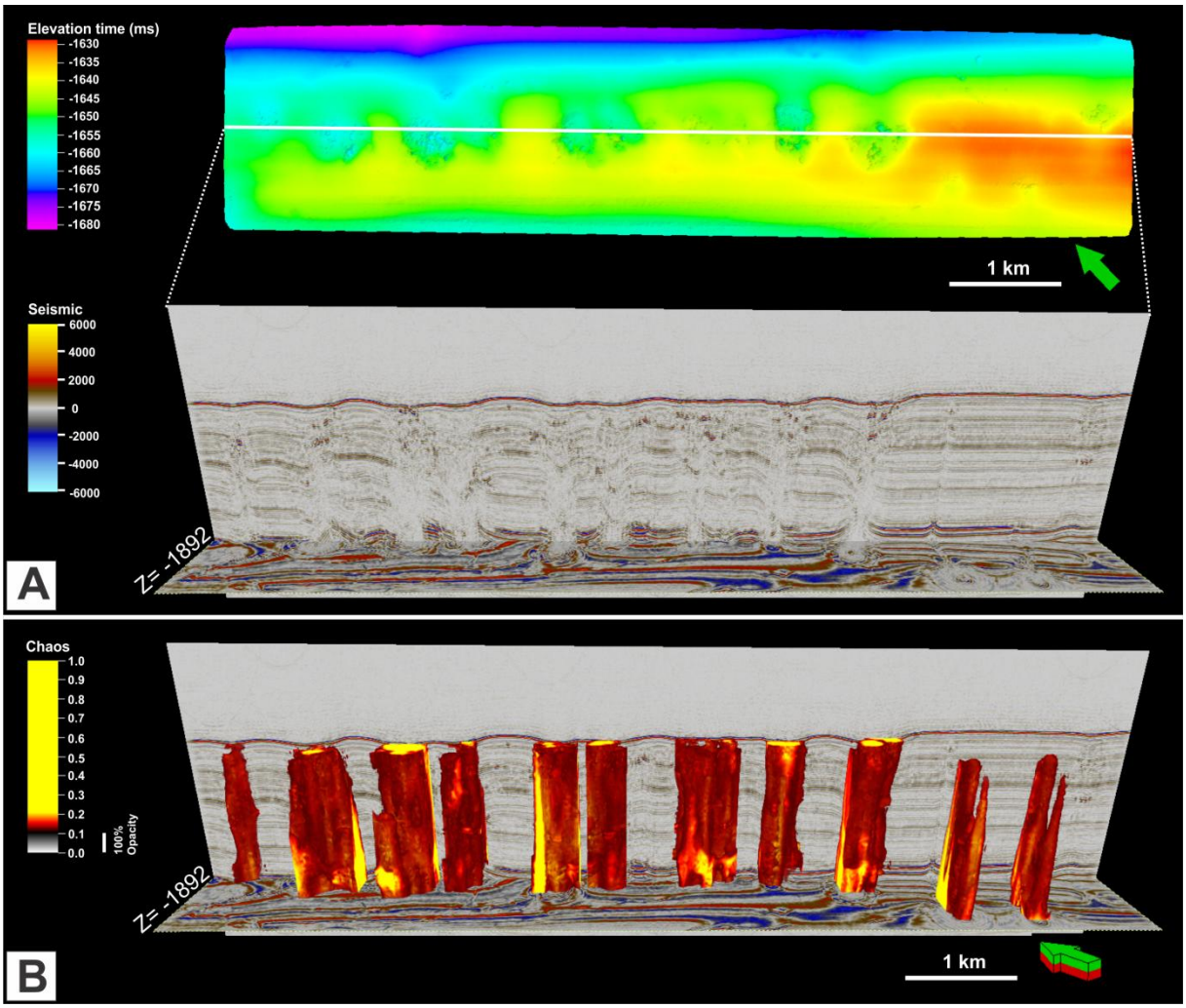

Fig. 4.4.4: A) A seismic line is taken over the main chimneys of interest, displayed together with a time-slice right below the BSR. The chimneys are observed as vertical zones of faded seismic signals from the BSR terminating the pockmarks in the SB. B) The chimney-structures made from the chaos-attribute, visualized together with the seismic. They are mainly observed in red which delimits their natural outer surface. Their cut-offs from faults going into them, appear in bright yellow.

In **fig. 4.4.5**, the SB is viewed from below both with and without the modeled chimneys. The chimney-models coincide with the pockmarks.

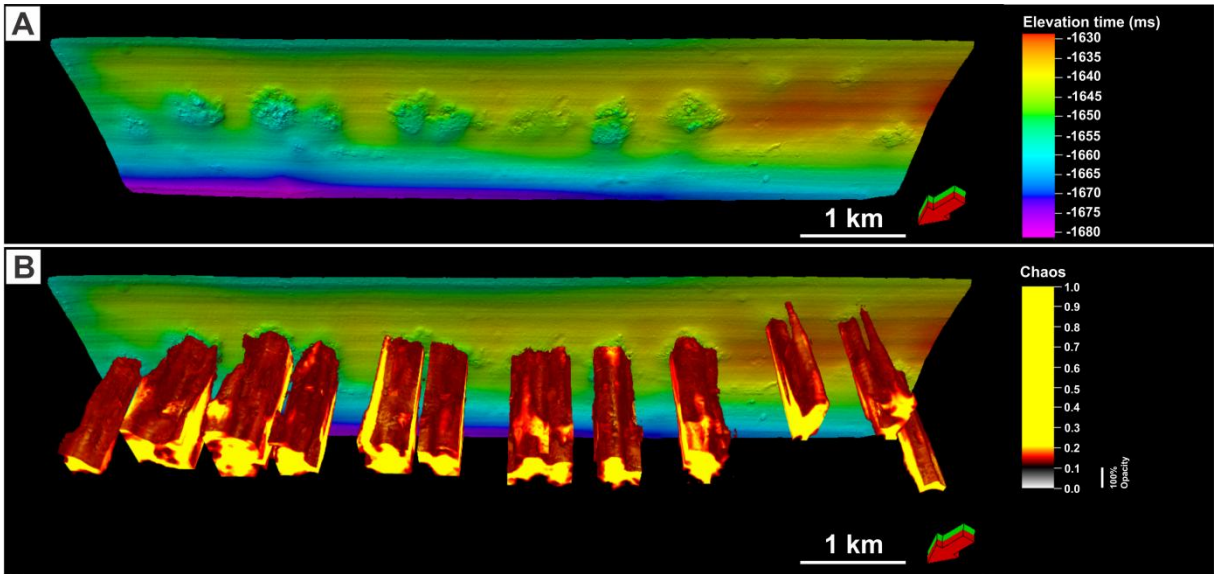

Fig. 4.4.5: A) Displaying the SB from below, with clearly visible pockmarks. B) Displaying the chimney-structures made with the chaos-attribute together with the SB. The chimneys are clearly linked to the pockmarks.

In **fig. 4.4.6**, the chimneys outline is mapped for three depths; ~25 ms (TWT) below the SB, at the BSR and directly between these two depths. Time-slices from the variance-attribute were used for this investigation. The outlines are given distinctive colors for each depth, and are gathered in an overlap to clearly visualize the bending effect.

Furthest to the SE of the investigation area, a smaller chimney-structure is found emanating from the branching point between two faults. This structure does not reach down to the BSR, but comes forth at ~-1775 ms (TWT).

It is found that the chimneys are slightly bending towards the apex of the Vestnesa Ridge with height. This tendency seems more prominent with the chimneys located furthest away from the apex, perpendicularly from the NE and the SW. At their base (-1875 ms), the chimneys are leaping out from faults. As they rise towards the seabed they continue to have a close relation to the faults, although slightly deviating around them.

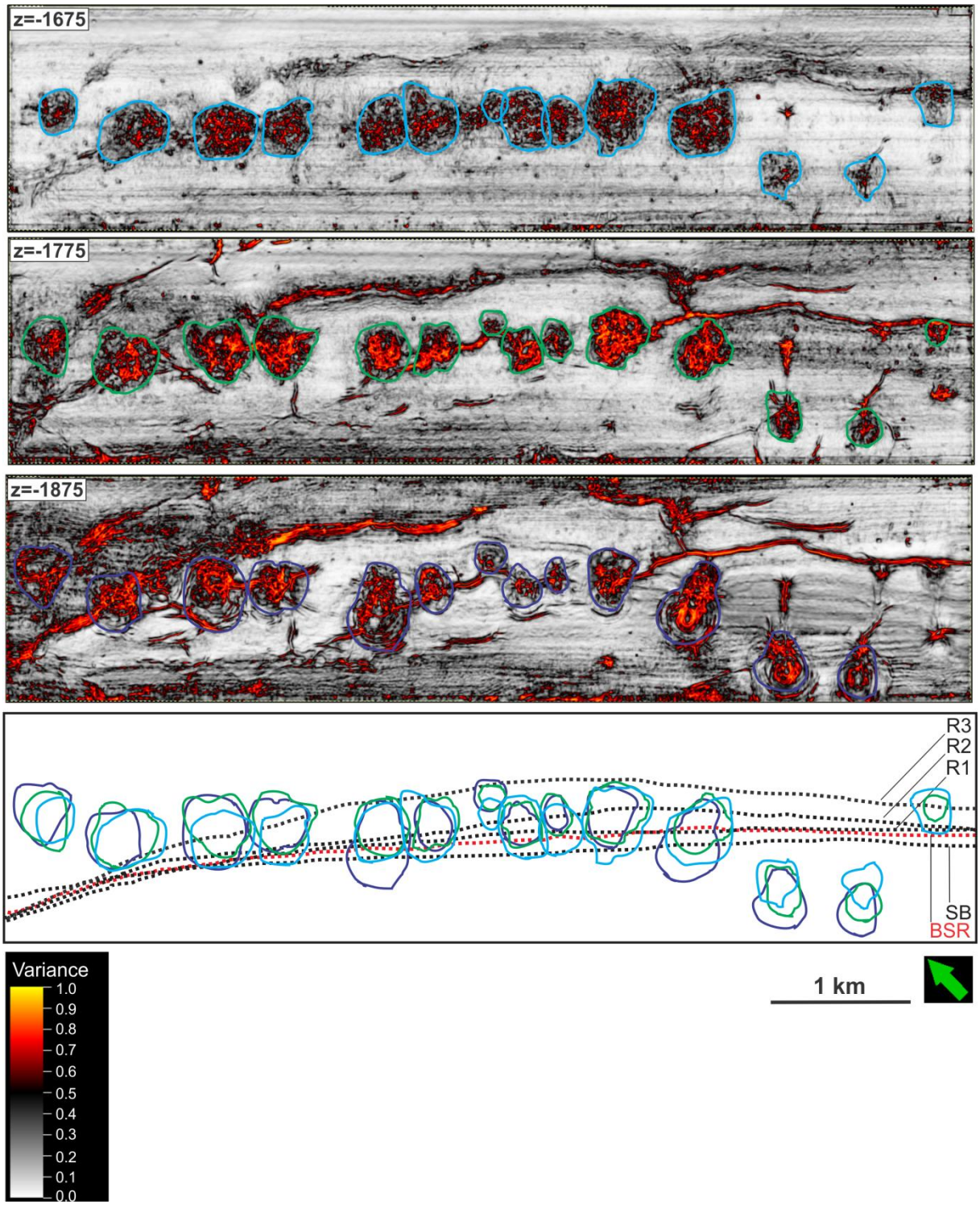

Fig. 4.4.6: Variance-attribute time-slice taken from directly beneath the SB, halfway between the SB and the BSR, and at the BSR. The Chimney-structures (red) are encircled for each time-slice, and displayed together with each other and the apex-distribution from fig. 4.1.4. The overlain figure presents their shape and general trend of bending towards the apex of the SB.

4.5 Fluid Flow

4.5.1 Bright Spots

Bright spots are generally indicators of gas (*Andreassen, 2007a*). In the seismic of **fig. 4.4.2** and **4.4.3**, these features are pointed out within the chimney-structures. Bright spots are found throughout the entire study area.

Fig. 4.5.1 displays the chimney-models together with the strongest amplitudes of the RMS-cube. In **fig. A**, the chimneys and amplitude-anomalies are viewed from the SW, together with the SB and BSR. In **fig. B**, they are displayed together with the faults from the top onto the BSR.

Fig. 4.5.2 is an RMS-amplitude mapping of the top 100 ms below the SB. The amplitudes are gathered into 20 ms intervals where the highest amplitudes are highlighted in red. The chimneys outline is made from time-slices at the midpoint of each 20 ms-interval, and displayed in yellow.

It is evident that most of the highest amplitudes are found within the chimney-structures, and mostly in the upper half of the space between the SB and the BSR. However, the different chimneys hold the amplitude-anomalies to a varying degree of quantity. There are smaller amounts of high amplitudes within the faults. Faults are well established conduits for fluid-flow (*Cartwright et al., 2007*).

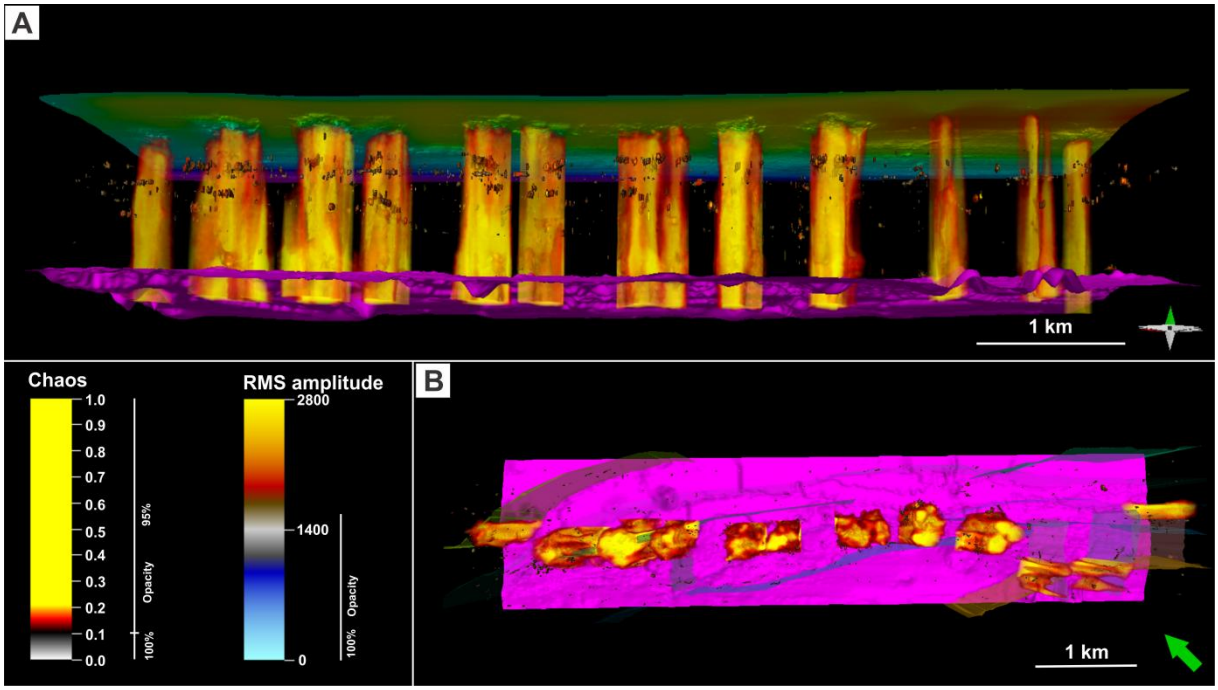

Fig. 4.5.1: A) Transparent chimneys and the strongest RMS-amplitudes displayed together showing that most of the highest amplitudes are found within the chimney structures upper half. From the SW the SB is seen in graded colors, and the BSR is seen as a pink surface. B) The chimneys and the RMS seen from above also displaying the faults through this area and the BSR. The highest amplitudes are seen within the chimneys and otherwise in the faults.

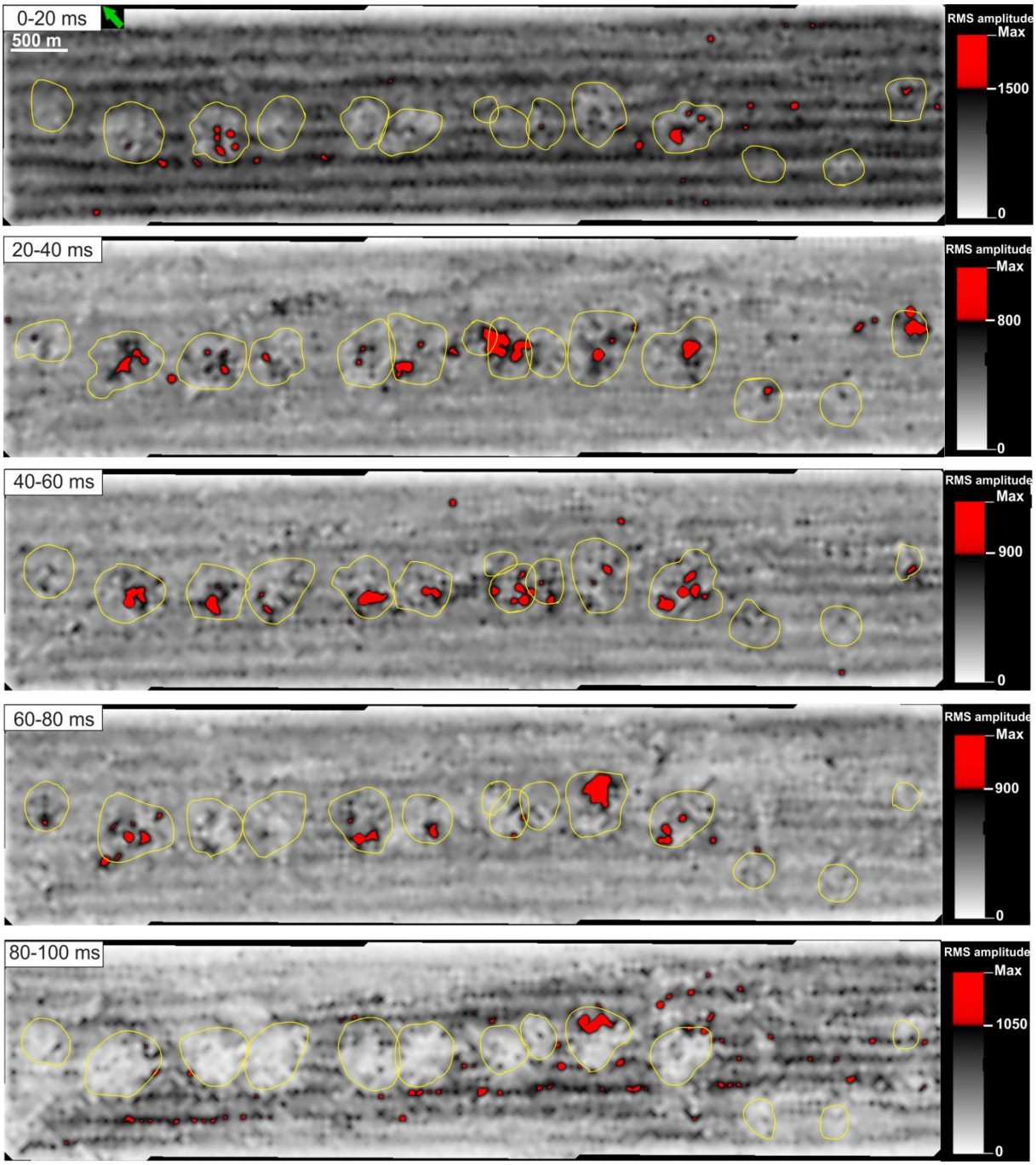

Fig. 4.5.2: RMS amplitude investigation of the first 100 ms (TWT) below the seabed. The surfaces are generated in 20 ms (TWT) intervals. The highest amplitudes are concentrated within chimney-structures (yellow outlines) in a varying degree. The RMS-values vary slightly between the surfaces.

4.5.2 Detailed Migration-Mapping

Three chimneys are more thoroughly investigated regarding fluid flow in this project; Two of them were recorded as leaking in both 2010 and 2012 by Smith et al. (2014) (**fig. 2.5.1**), and the last one has not been recorded as recently leaking.

By the chimney-models from the chaos-attribute and the seismic interpretation, it was chosen three independent chimneys that are isolated from the surrounding chimneys and their fluid flow. Within these there are found sections of high amplitudes, which are separated by vertical zones where the high amplitudes are absent. The sequences of related high amplitudes are interpreted to indicate gas, and are hereby referred to as plumes. These levels are thoroughly presented by time-slices of RMS-amplitude in **fig. 4.5.4, 4.5.7 and 4.5.10**. The slices are taken by 5 ms (TWT) equidistance. For this presentation it was chosen to use 100% opacity on the weakest amplitudes. The chimneys outline and through-going faults are highlighted. The outline is for each slice found from the variance-attribute. These time-slices are also gathered as overlaps for each level in **fig. 4.5.5, 4.5.8 and 4.5.11**. A black outline marks the chimneys widest outline for each section, and also for the gathered overlap. The levels are given different colors and are also displayed together in the same overlap to accentuate their relationship. Hereby follows the visualizations of the plumes positions within the chimney structures, and interpretations of their relation to the faults and each other.

i. Chimney 1: Leaking

Features: Pockmark depth is ~-1650 ms (TWT)
Size 450×450 m at the SB
Size 250×300 m at the BSR

Two seismic cross-lines through the chimney are given in **fig.4.5.3**, where its position at the SB is also displayed. Three faults are related to this chimney; one disseminates outside of the chimneys border to the NE, two are propagating throughout the chimney-structure. Beneath the roughest parts of the pockmark, there are found high amplitudes. These shallow amplitudes are omitted for the RMS-investigation. However they can be observed in the seismic as related to the top mapped sequence, especially in **fig. 4.5.3.B**.

There are found four levels containing high amplitudes (**fig 4.5.4)**.The observations are presented for each level, starting at the deepest.

-1760 to -1765: A small plume is centered on the middle fault, near the chimneys edge to the NE.

-1730 to -1750: Ne in the chimney a plume emerges between the middle fault and the NE-fault. The plume slightly exceeds the edge of the chimney. The faults appear sealing; the middle fault is sealing towards the SW and (the visible part of) the NE-fault is sealing towards the NE.

-1690 to -1715: Two plumes are observed in this section. In the middle of the chimney, a plume emerges centered on the SW-fault, with a slight connection to the middle fault. The W-plume also emerges from the SW-fault, from which it deviates to the chimneys W-edge with height.

-1665 to -1675: A small plume is centered on the SW-fault in the middle of the chimney.

In **fig. 4.5.5** these sections are displayed as gathered overlaps, by themselves and together. The high amplitudes are spread horizontally through almost the entire chimney. Their position above each other reveals a possible vertical connection between the plumes. The two deepest sequences and the E-plume of the sequence second from the top, are all fed by the NE-fault. They are slightly overlapping each other, indicating a migratory connection between theese. The E-plume is also fed by the SW-fault. It is the only plume in this chimney that is found connecting to two faults. The W-plume of this

sequence have no apparent connection to the other plumes. At the top the small plume is seen in connection to the underlying plume through the SW-fault. Thus, a probable migration-route that links all four sequences of high-amplitudes is found, starting through the NE-fault and ending through the SW-fault at the top.

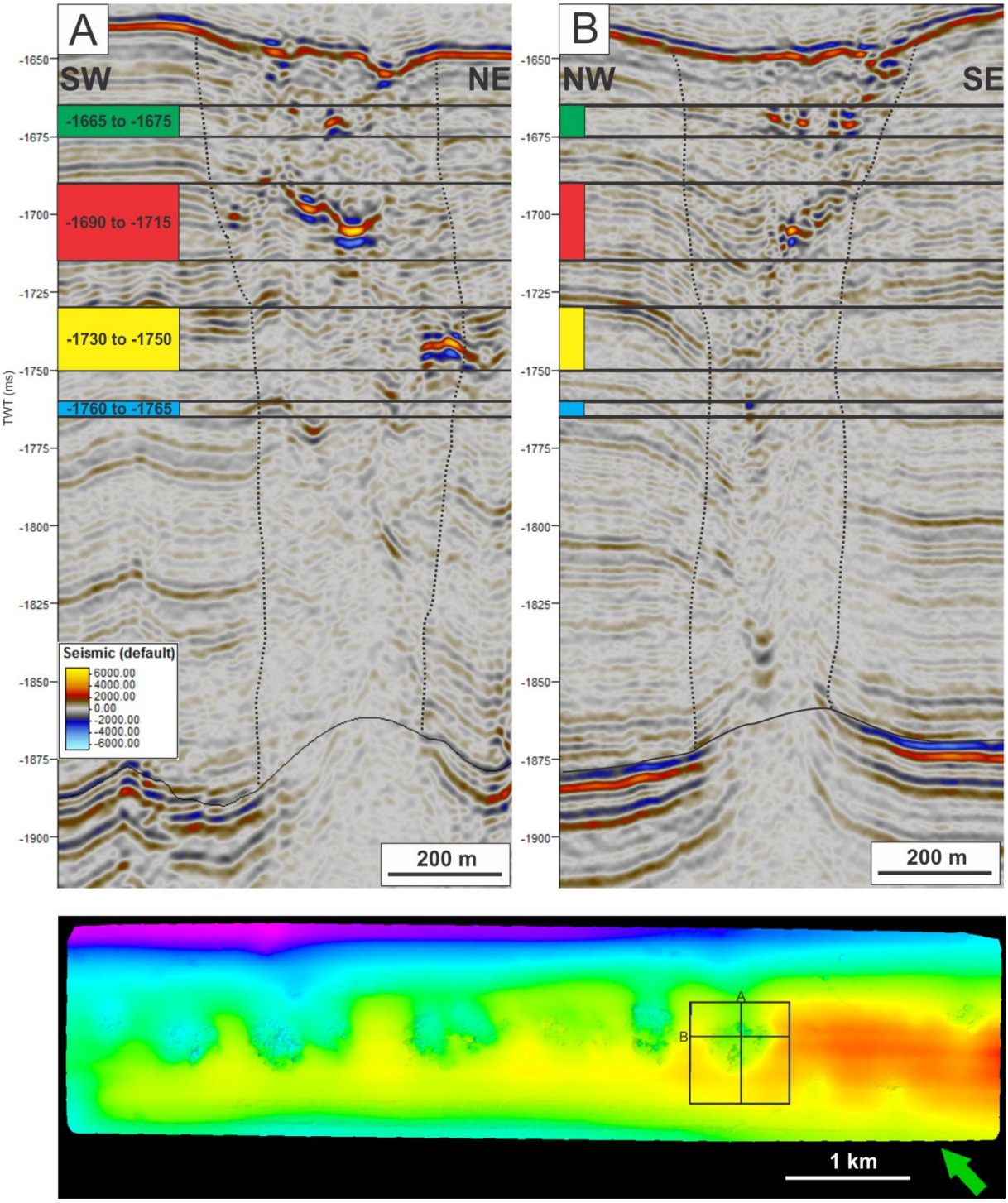

Fig. 4.5.3: Chimney 1, declared as recently leaking by Smith et al. (2014). The chimneys outline is shown by stippled black lines in the seismic profiles; A and B. There are four color-coded sections of high amplitudes within the chimney. These are displayed in fig. 4.5.4. The BSR-surface is seen as a black line at ~-1875 ms (TWT).

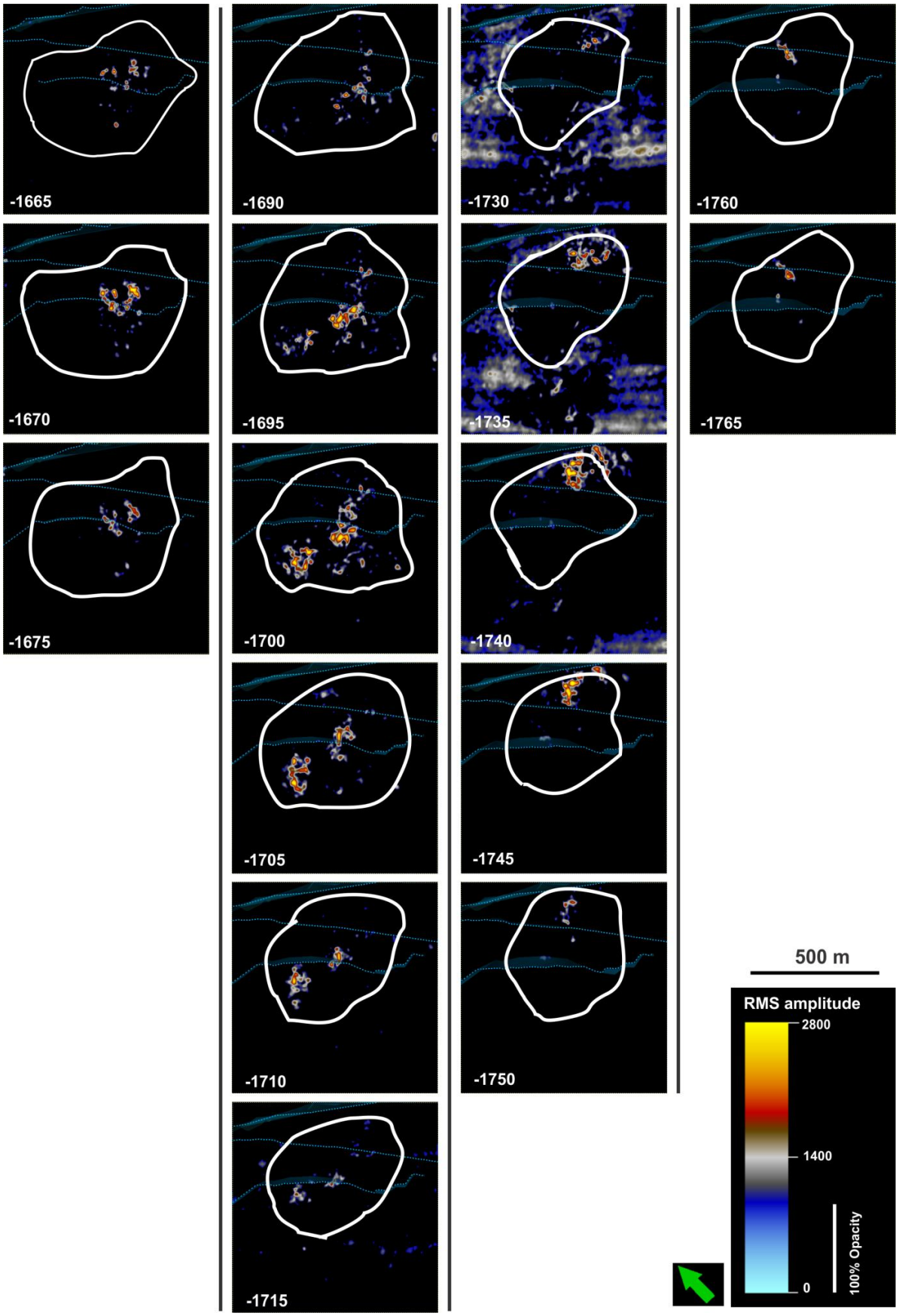

Fig. 4.5.4: RMS amplitude time-slices with vertical separation of 5 ms (TWT), through Chimney 1 showing the four separated "levels" of high amplitudes. 100% opacity is used on the weakest amplitudes. Chimney-related faults are shown in stippled lines. The chimneys outline (white) is found from the corresponding variance time-slice for each RMS time-slice. Fig. 4.5.5 shows the overlap of these high amplitudes.

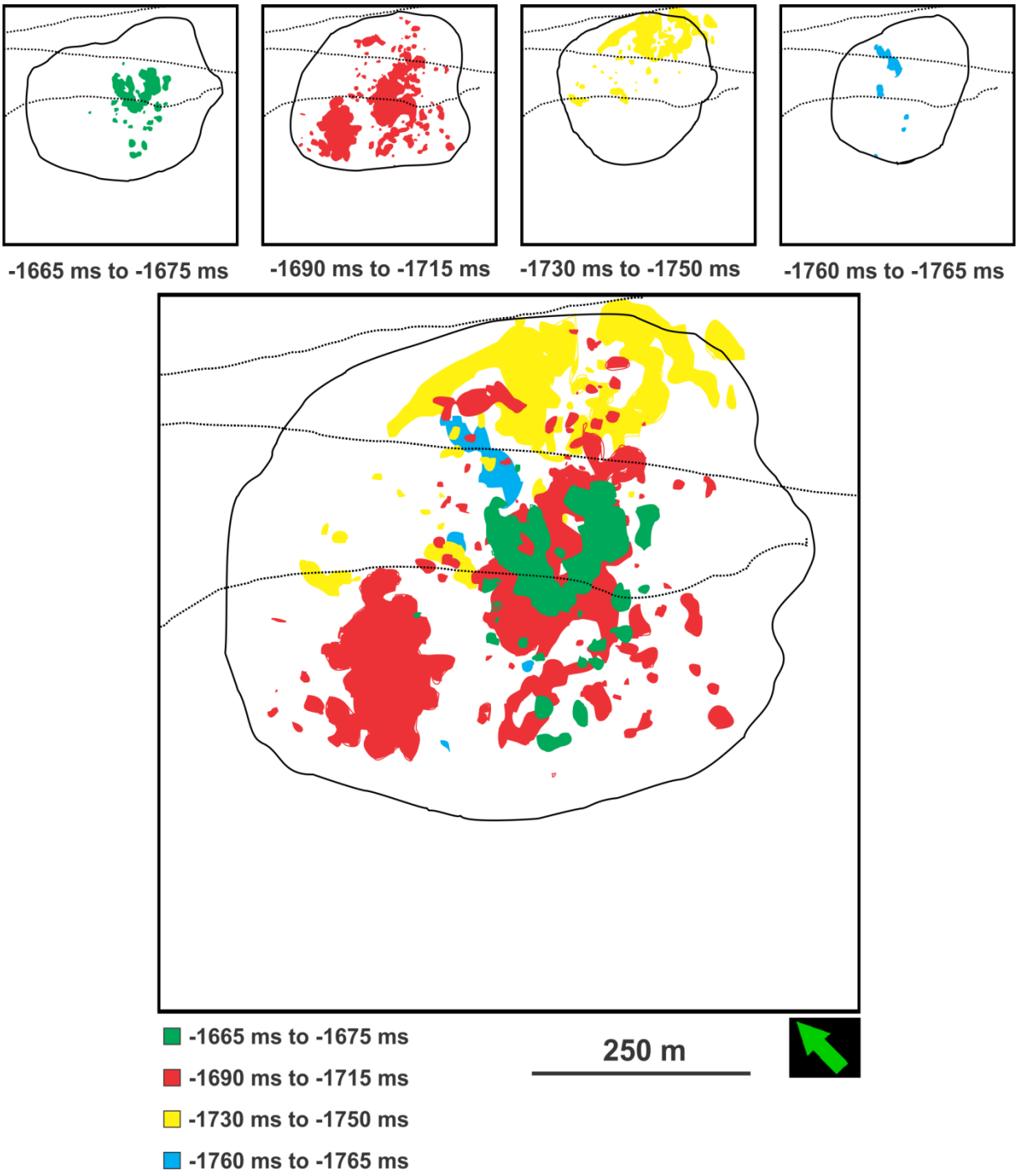

Fig. 4.5.5: Overlap-display of the four color-coded sections of high-amplitudes through chimney 1. The sections are displayed by themselves, and as a gathered overlap, together with the faults and the outermost chimney-outline.

ii. Chimney 2: Leaking

Features: Pockmark depth is ~-1650 ms (TWT)
Size 400×500 m at the SB
Size 350×400 m at the BSR

Two seismic cross-lines through the chimney are given in **fig.4.5.6**, where its position at the SB is also displayed. Two faults are related to this chimney; one propagates through the center of the structure, and branches to the SE within the chimney. The other one is positioned at the SW of the chimney barely within the structure, and at some occasions at the border.

There are found two levels containing high amplitudes (**fig 4.5.7)**. The observations are presented for both levels, starting at the deepest.

-1690 to -1765: One large distorted plume is emanating in close relation to the NE-fault. Up to -1720 ms (TWT), there is high concentration of high amplitudes between the NE-fault and the NE-border of the chimney, and the fault appears as sealing towards the SW. The plume fades out above this depth. It is found centered within the chimney and also to the SW of the NE-fault. A few spots of high amplitudes are seen in the SW-fault.

-1660 to -1685: A small plume of high amplitudes is situated between the two faults. It originates from the NE-fault and propagates towards the SW-fault. The SW-fault is closely related to most of the amplitudes, and seals the plume off from the further SW.

In **fig. 4.5.8** these sections are displayed as gathered overlaps, by themselves and together. The deepest section is divided into three overlaps to give a clearer overview of the amplitudes' distribution. High amplitudes are found mainly in the NE-half of the chimney. At the shallowest part, the amplitudes are in the central and SW-half of the chimney. It is observed a clear link between the high-amplitudes, through a migration route from the NE-fault shifting towards the SW-fault at the top. It is uncertain how much of the amplitudes that have migrated through the SW-fault over the entire distance.

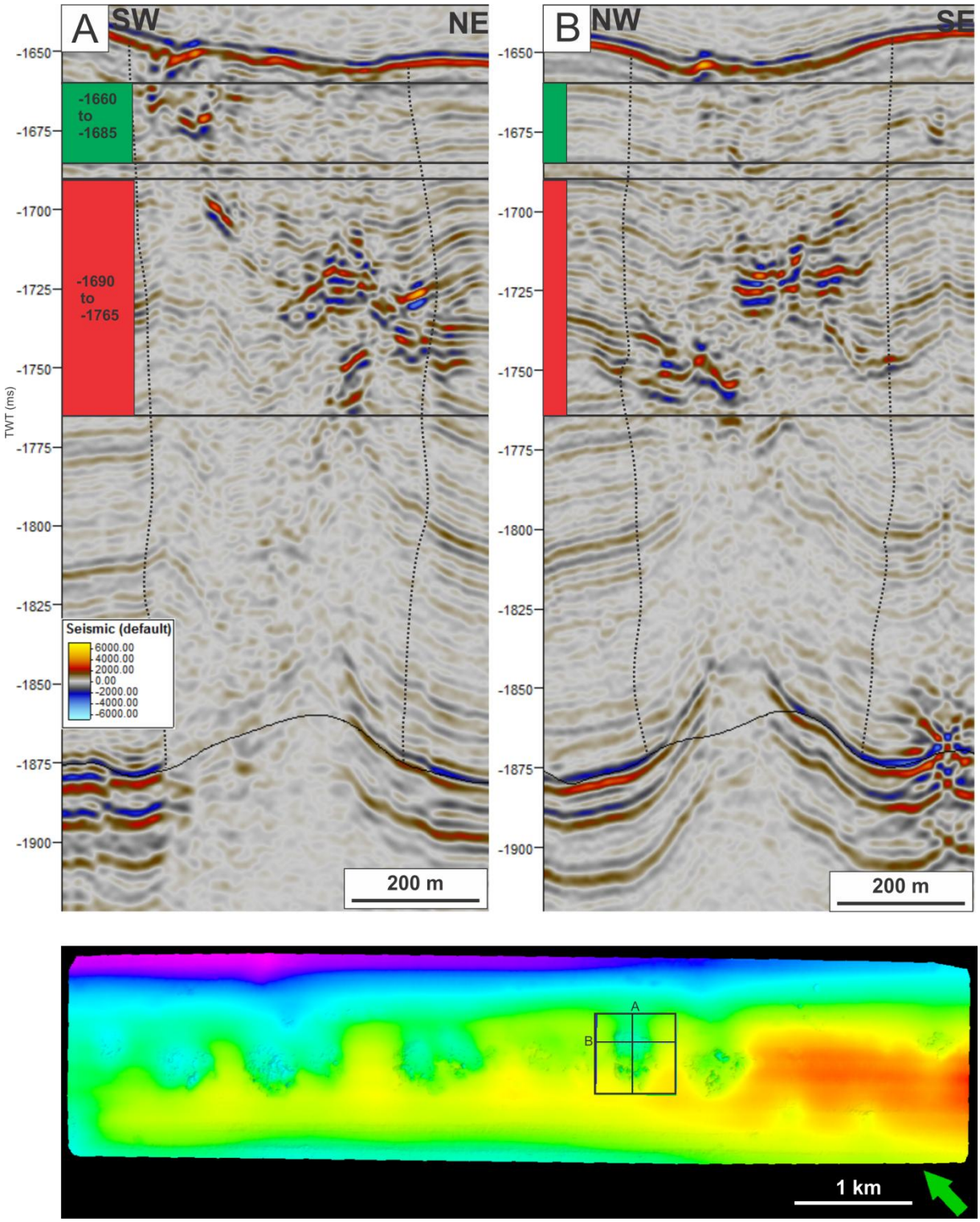

Fig. 4.5.6: Chimney 2, declared as recently leaking by Smith et al. (2014). The chimneys outline is shown by stippled black lines in the seismic profiles; A and B. There are two color-coded sections of high amplitudes within the chimney. These are displayed in fig. 4.5.7. The BSR-surface is seen as a black line at ~-1875 ms (TWT).

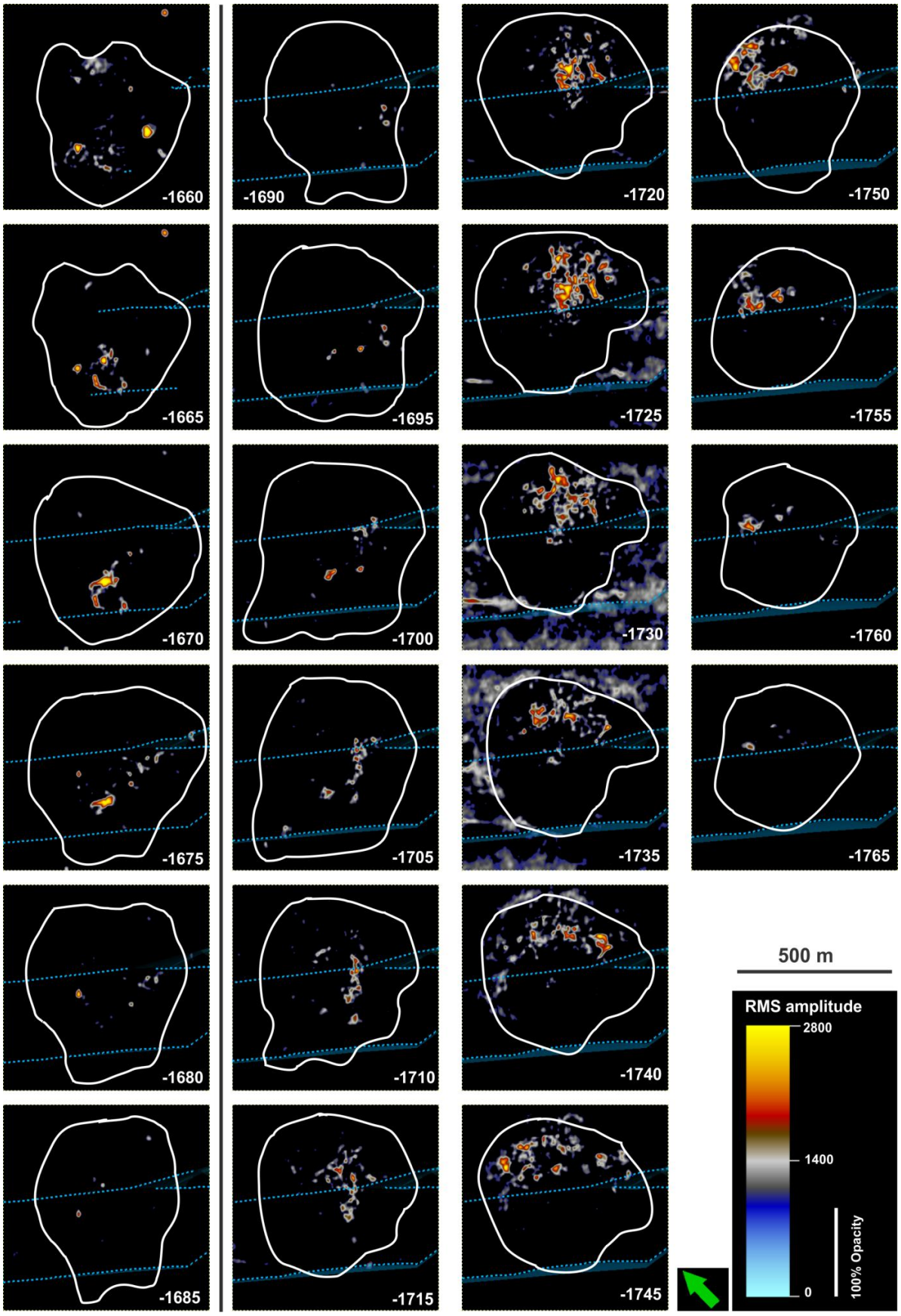

Fig. 4.5.7: RMS amplitude time-slices with vertical separation of 5 ms (TWT), through Chimney 2 showing the two separated "levels" of high amplitudes. 100% opacity is used on the weakest amplitudes. Chimney-related faults are shown in stippled lines. The chimneys outline (white) is found from the corresponding variance time-slice for each RMS time-slice. Fig. 4.5.8 shows the overlap of these high amplitudes.

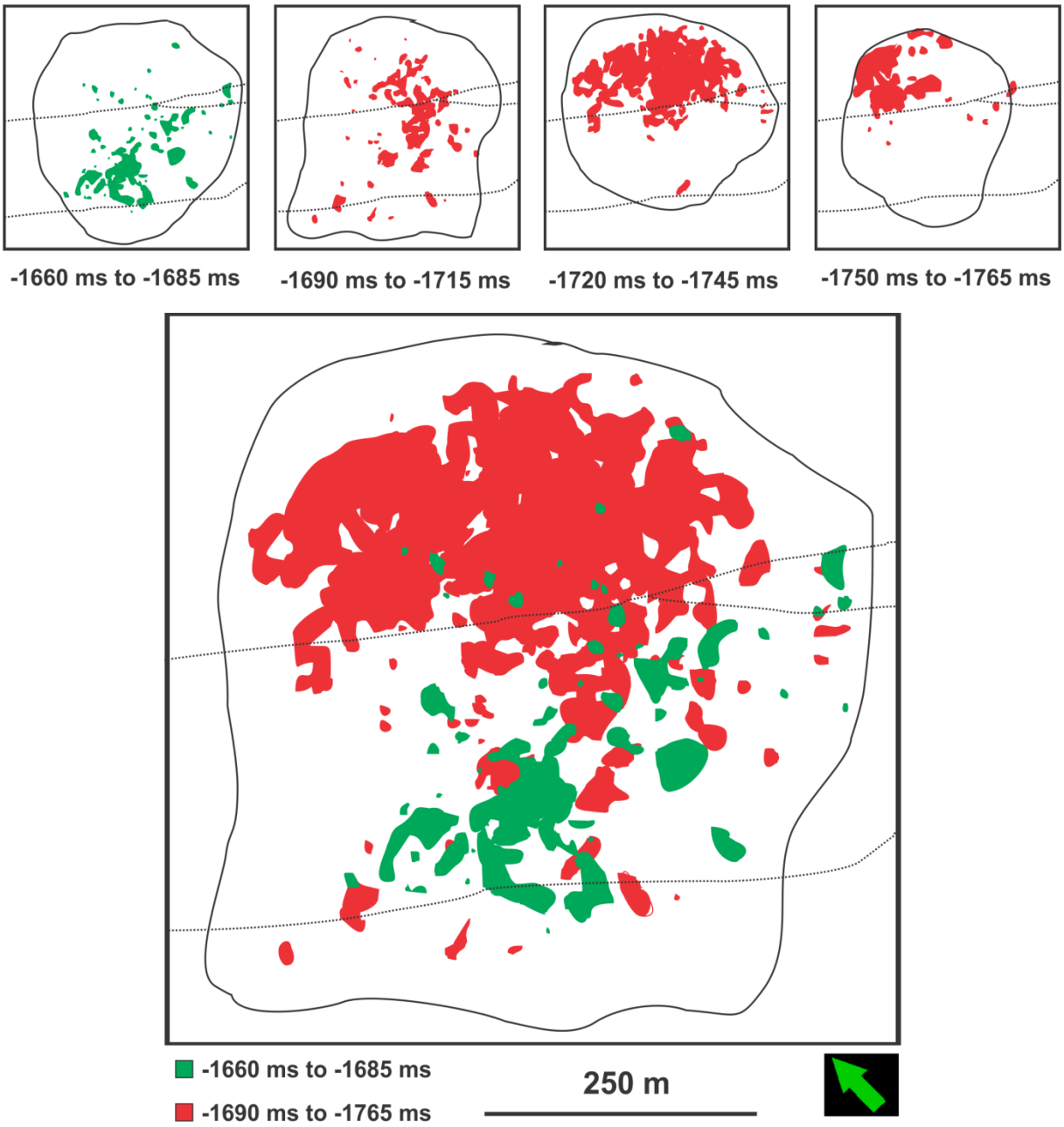

Fig. 4.5.8: Overlap-display of the two color-coded sections of high-amplitudes through chimney 2. The sections are displayed by themselves, and as a gathered overlap, together with the faults and the outermost chimney-outline.

iii. Chimney 3: Non-leaking

Features: Pockmark depth is ~-1650 ms (TWT)
Size 500×600 m at the SB
Size 400×500 m at the BSR

Two seismic cross-lines through the chimney are given in **fig.4.5.9**, where its position at the SB is also displayed. Two faults are related to this chimney; they both propagate within the structure and also meet in a branching-point at the chimneys border to the W. The most striking feature about this chimney is the lack of high amplitudes near the SB. There are no amplitude-anomalies above -1680 ms (TWT). In addition, the pockmark has a smoother surface than the pockmarks of the leaking chimneys.

There are found four levels containing high amplitudes (**fig 4.5.10)**. The observations are presented for each level, starting at the deepest.

-1770 to -1780: A very small plume is situated between the two fault-branches, close to their branching point. The plume is closely related to the SW-fault.

-1750 to -1760: A slight accumulation of high amplitudes is found SW of the SW-fault. It reaches towards the chimneys boundary to the SW. The SW-fault is sealing towards the NE.

-1705 to -1730: Two plumes are found in this sequence. The E-plume propagates from the NE-fault and mostly spread out between the two faults. The SW-fault seals this plume off from the SW of the chimney. The W-plume is found emanating closely to the SW-fault to its SW. The SW-fault is sealing towards the NE except at the branching point, where the plume slightly makes contact with the NE-fault.

-1680 to -1690: A weak accumulation of high amplitudes is centered in the chimney between the two faults. A slight connection is seen to the NE-fault, whilst the SW-fault is found sealing towards the SW. The plume stretches nearly all the way between the chimneys E- and W-border.

In **fig. 4.5.11** these sections are displayed as gathered overlaps, by themselves and together. Within the chimney there are less high amplitudes than for the two leaking chimneys. The plumes are generally

smaller and less concentrated. The plumes are well centered within the chimneys centre, and are distanced at least 100 m from the chimneys borders. The amplitudes in the two deepest sequences are following the SW-fault, and appears related to each other and to the E-plume of the sequence second from the top. There might be a further connection between these connected sequences and the top sequence, although this is not obvious from the results. The E-plume of the second shallowest sequence appears separated from the said connection. A migratory route through the NE-fault joins this plume to the top-plume.

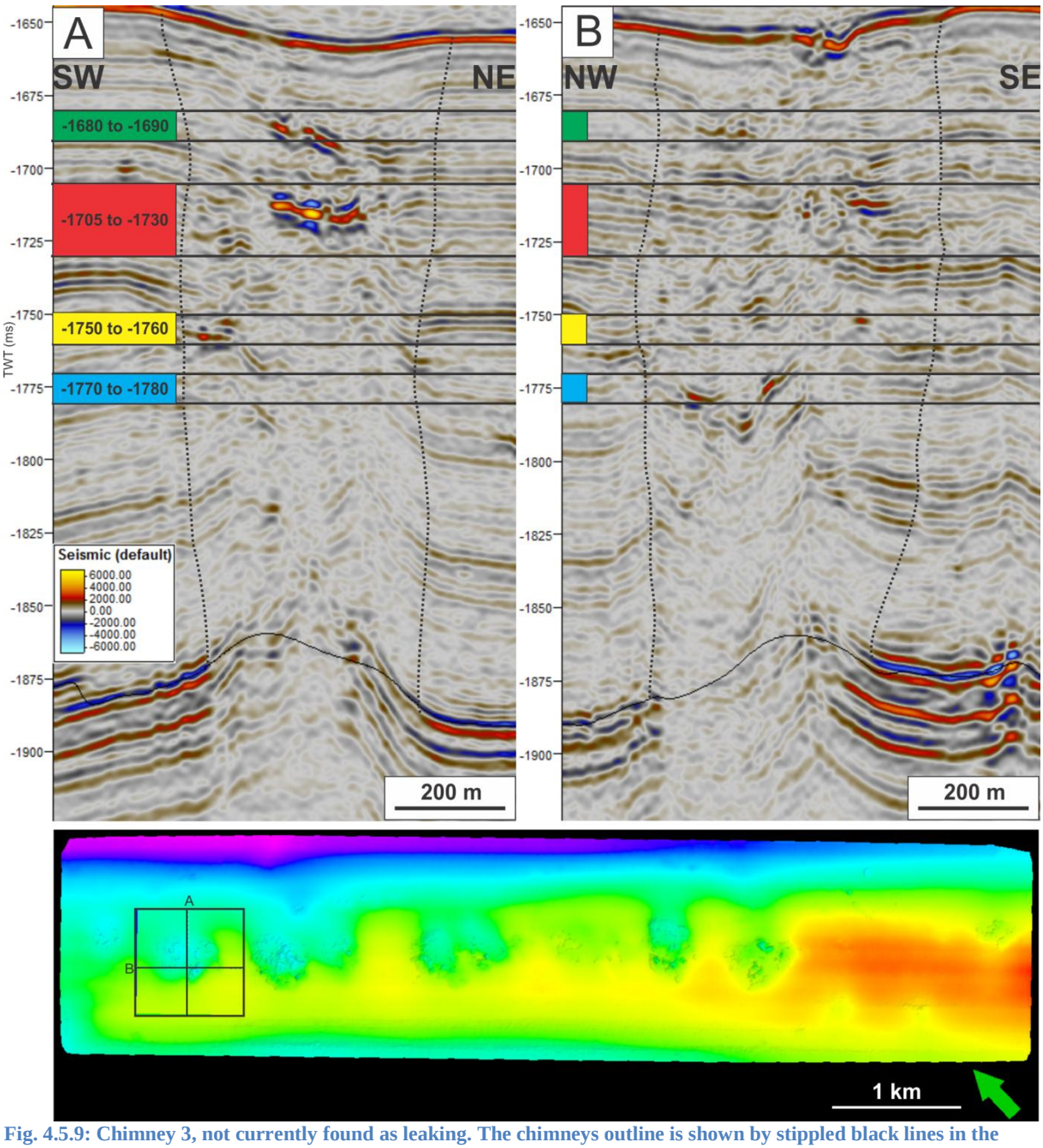

Fig. 4.5.9: Chimney 3, not currently found as leaking. The chimneys outline is shown by stippled black lines in the seismic profiles; A and B. There are four color-coded sections of high amplitudes within the chimney. These are displayed in fig. 4.5.10. The BSR-surface is seen as a black line at ~-1875 ms (TWT).

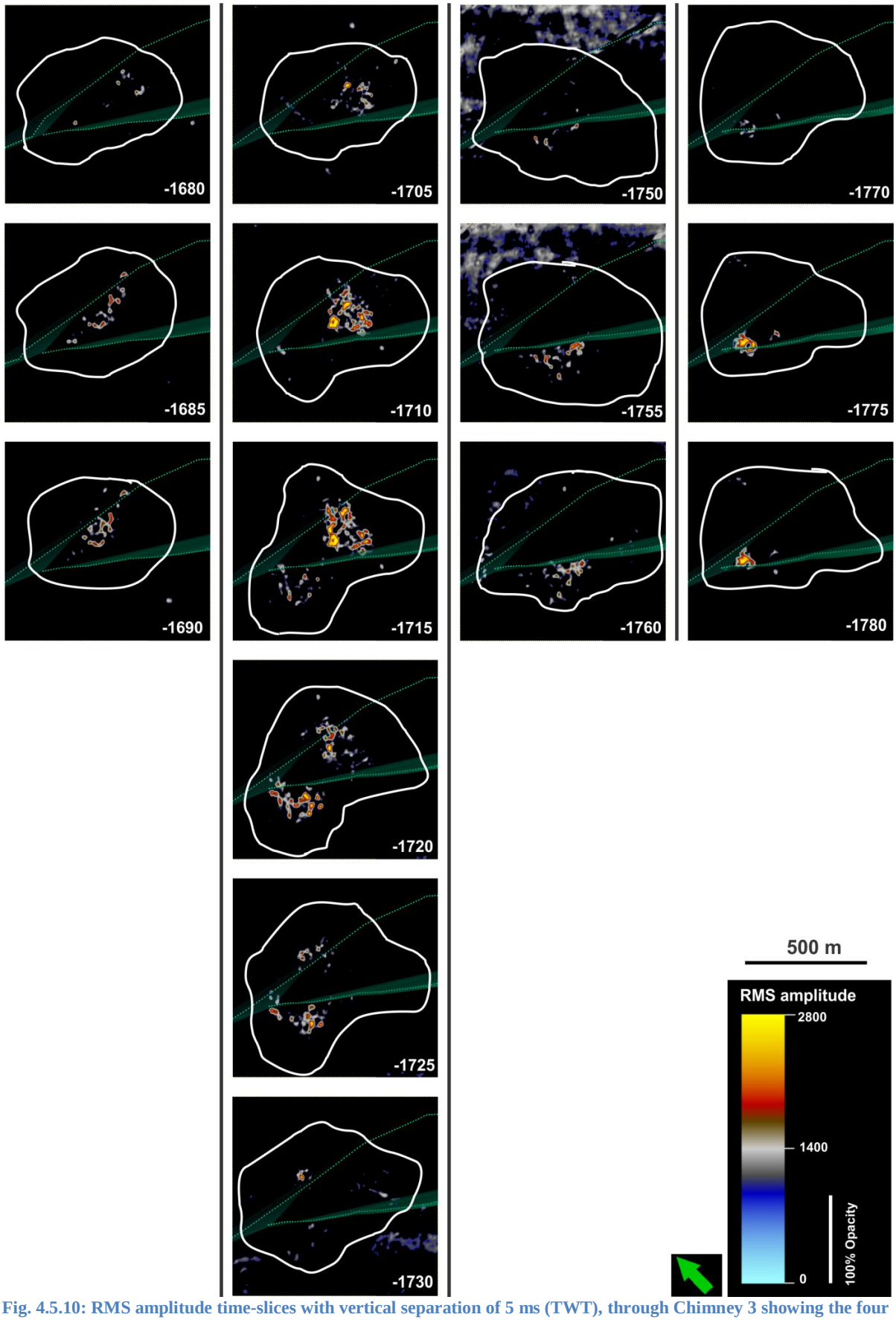

Fig. 4.5.10: RMS amplitude time-slices with vertical separation of 5 ms (TWT), through Chimney 3 showing the four separated "levels" of high amplitudes. 100% opacity is used on the weakest amplitudes. Chimney-related faults are shown in stippled lines. The chimneys outline (white) is found from the corresponding variance time-slice for each RMS time-slice. Fig. 4.5.11 shows the overlap of these high amplitudes.

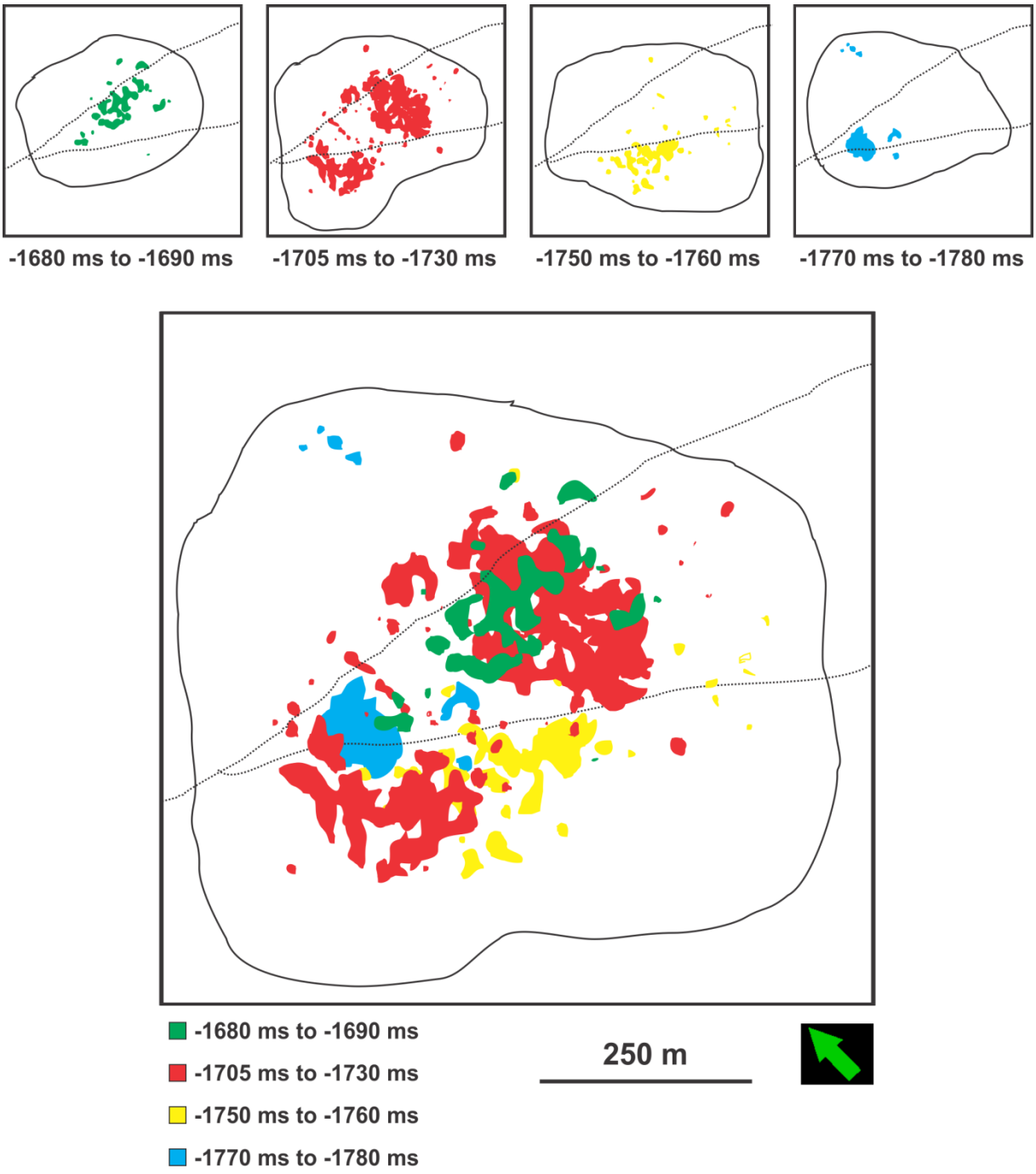

Fig. 4.5.11: Overlap-display of the four color-coded sections of high-amplitudes through chimney 3. The sections are displayed by themselves, and as a gathered overlap, together with the faults and the outermost chimney-outline.

5 DISCUSSION

The Vestnesa Ridge is situated upon young (<20 Ma) and hot oceanic crust at the western Svalbard margin. Properties which make this a remarkable location to study fluid flow. Gas hydrates are able to prevent vertical fluid flow, by reducing the porosity and permeability of its host-rock. This circumstance causes potentially free gas to accumulate beneath the anticlinal trapping mechanism that forms corresponding to the topography of Vestnesa Ridge. A thick layer of free gas is observed by high-amplitude negative reflections beneath the BSR, throughout the study-area. An observation which is also documented by Bünz et al. (2012) and Hustoft et al. (2009)

The seismic data reach down to -2400 ms (TWT), covering the YP3-unit and the upper part of the YP2-unit. Hustoft et al. (2009) interpreted the BSR directly at- and just beneath the YP2-YP3-boundary. It is expected that one of the uppermost reflectors incorporated in the BSR at the site, represents the boundary between the YP2- and YP3-unit. This reflector lies ~40 ms (TWT) perpendicularly above the R3-reflector and clearly stands out by strong reflectivity, together with its nearest beneath-lying reflectors. The seismic resolution becomes very poor beneath ~-1950 ms (TWT), thus making interpretation difficult and unreliable. The R3-reflector is the deepest that was possible to interpret from the seismic data. By applying attributes, it was possible to achieve some information from depths beneath this limit.

5.1 Sedimentation and Axis-Migration

The sedimentary thickness between the interpreted reflectors in the YP3-unit appears as a continuously smooth draping over the ridge, with thinning at the crest and thickening at the flanks of the ridge. The sedimentary thickness between the R3 reflector and the R2 reflector stand out a bit from the above intervals; it is thinner on the NE-side and thicker on the SW-side, separated by an almost straight NW-SE oriented boundary. This is seen in relations with the two different sedimentary units that these two reflectors are affiliated to. It is a possibility that the large throws of blocks in the YP2-unit are causing a depositional lee of suspended sediments in the N-oriented ocean-current, an enhanced deposition "in front" of the blocks. The result is a thinning of the sedimentary column on the down-faulted NE-block, and a thickening of the up-lifted SW-block. This might be how the ridge originated; the positions of build-up anticlinal ridges might be related to horst and graben structures in addition to the prevailing ocean current (*Mattingsdal et al. 2013*).

For this part of the ridge, the fold-axis is generally found migrating towards the SW, semi-opposite of the ocean-currents direction. The displacement varies from 150 m NE-direction to 500 m SW-direction. The axes of the subsurface-reflectors in addition to the BSR, gather in a mutual point to the NW of the investigation area. The SB-axis stands out by making a crossover to the underlying reflectors, as it propagates NE of the gathering point of the other reflectors. These results are interesting as they contradict the general trend in the area; Mattingsdal et al. (2013) found a system of buried anticlinal ridges of continuous seismic reflections that were migrating towards the E at a rate of ~2.5 m/ka, within the upper part of the YP2-unit. They also found that the deposition rates were higher at the crests and the eastern sides of the ridges than at the western sides. The eastern branch of the Western Spitsbergen Current (WSC) is suggested as driving force in this migration, as well as determining the deposition rate over the ridges with the highest rate at the lee-side. However, this investigation covers only a minor part of the whole ridge and does not give the full picture of how the Vestnesa Ridge has developed. This may be an indication of the ridges' out-straightening or torsion about the area where the SB crosses and the subsurface reflectors gather.

5.2 Gas Hydrates and Free Gas

At the SE part of the investigation area, the BSR is crosscutting several reflectors. Thus, strongly displaying its independence of the sedimentary strata, this is typical for a BSR. The BSR is not observed at the base of the chimneys, thus it is unsure whether there are gas-hydrates at their position or not, as the BSR is only indicative of gas hydrates. However, gas hydrates were sampled by both piston coring and gravity coring within 2 – 4 m bsf at this site, proving their presence (*Smith et al., 2014*). Smith et al. (2014) argued for a thermogenic generation of the gas, however the origin is unclear. Early Miocene source rocks at the eastern basin margin are seen as a possible origin (*Knies and Mann, 2002*). Accumulation of free gas beneath the crests of local anticlinal ridges was suggested by Mattingsdal et al. (2013). Additionally, ODP sites at the Yermak Plateau proved the occurrence of free gas in high amounts (*Myhre et al. 1995*). Vanneste (2005) found the highest thickness of the gas-column beneath Vestnesa Ridge to be ~150 ms (TWT), which is also observed on the frequency-attribute from the site.

The thickness map reveals a minor deviation by a slightly thinner separation at the NE than at the SW, between the BSR and the SB. Additionally, the axis of the BSR is almost identical to the R1-reflectors' axis, rather than that of the SB. It is evident that the BSR-surface has strong similarities to the SB, but is not perfectly identical. The temperature has a strong influence in the formation of hydrates, and the deviation might be a consequence of the time consuming adaption of the iso-boundary, to a continuously changing stratigraphy. The iso-boundary may not have "caught up" with the present sedimentary build-up at Vestnesa Ridge. Vanneste et al., (2005) found the increase of the geothermal gradient towards the MTF, by using the BSR as an in-situ temperature proxy. As the SW-flank of the BSR is situated closer to the MTF than the NE-flank is; warming might cause the deviation of the BSR.

The BSR is situated at a depth of ~225-235 ms (TWT) bsf at the Vestnesa Ridge. Mattingsdal et al. (2013) calculated the velocities down to ~600 ms (TWT) bsf from three ODP sites at the S Yermak Plateau, and found velocities varying between 1565 – 2000 ms^{-1}. By evaluating the velocities found for the three sites; the upper 235 ms (TWT) bsf the average velocity is ~1700 ms^{-1}. By using this estimation together with the TWT-depth of the BSR at Vestnesa Ridge; the BSR-depth is hereby proposed to range between 191-200 m bsf. Hence, the BSR is situated within a reasonable window considering gas-hydrate formation. Haacke et al. (2008) established the same depth of ~200 m bsf for the BSR on the W Svalbard margin. Smith et al. (2014) predicted a depth of 155 m bsf for the base of the hydrate stability zone (BHSZ). By using the interval velocity of 1620 ms^{-1}, Petersen et al. (2010) proposed a depth of ~162 m bsf. Hence, the most recent estimates of the BSR-depth range in-between 155-200 m bsf at Vestnesa Ridge. Vanneste et al. (2005) established a BSR at ~250 ms (TWT) bsf, between the oceanic ridge and

the upper continental slope in this area. They argued that the sub-bottom depth of the hydrate stability limit varies laterally and is mainly controlled by the bottom-water temperature and the geothermal trend connected with lithospheric cooling in distance from the Molloy spreading Ridge. The top of the hydrate stability zone is proposed at 860 m above the SB, at 340 m water depth, by Smith et al., (2014). The gas hydrates' dependency of pressure and temperature gives rise to the assumption that they are not present at the chimneys due to lower pressure caused by faults, or by higher temperatures due to fluid flow through the faults (*Smith et al., 2014*).

5.3 Faults

Fault-interpretation is simplified by the variance attribute, compared to the regular seismic in which they are less prominent beneath ~-1950 ms (TWT) depth. The variance-attribute enabled a secure interpretation of faults to the depth -2175 ms (TWT). However, it is expected that the faults reach to a much greater depth. Hustoft et al. (2009) interpreted several faults beneath the Vestnesa Ridge, and found their depth extent down to the YP1-unit, which lies at ~-3500 ms (TWT) beneath this part of the ridge. Because of their steep-inclination, limited throw, anastomosing and curved propagation; these faults are interpreted as of transform strike-slip type (*Selley, 1998*). These faults are seen in relations to the nearby Knipovich Ridge and the Molloy Transform Fault Zone; major contributors to the forces affecting this area, which provides a force directed towards the SE. The throw-increase with depth shows that the faulting here is a dynamic process, probably due to the constant movements of the MTF. Throw-increase downwards demonstrates the faults synchronous movement to the deposition. Faults that behave like this are termed growth faults. They often have curved fault traces, with the down-thrown block on the inside of the curve (*Selley, 1998*). At this site the down-thrown blocks are on the outside of the curve, and the faulted blocks make out a positive flower structure (*Twiss and Moores, 2007*). The faults terminate the R0-reflector, at ~17 ms (TWT) bsf. By the interval velocity of 1565 ms^{-1} for the upper part of the Yermak Plateau, by Mattingsdal et al. (2013), it corresponds to a depth of ~13.3 m bsf.

5.4 Chimneys

Chimneys are recognized by acoustic masking in the seismic, and pockmarks at the SB. Acoustic masking-zones that are more or less vertical extending might represent conduits for high fluid-flux caused by overpressure (*Wiprut and Zoback 2000*). Løseth et al. (2001) proposed that chimneys terminating pockmarks at the SB, are created by fast-flowing gas-charged pore fluids ascending from an underlying reservoir. The chimneys align at the crest of the ridge, but are also severely affected by the faults locations. Fractures often occur adjacent to faults and they enhance the permeability and the storage-capacity of fluids of their host-rock (*Selley, 1998; Twiss and Moores, 2007*). Pockmarks seem to form at the SB over a limited amount of time, and the initial fluid migration appears to be conducted by small cracks. The cracks are gradually enlarged by the fluid flow, and eventually pockmarks appear (**fig. 5.4.1**) (*Cathles et al., 2010*). A critically pressured column of free gas beneath the BSR at Vestnesa Ridge is assumed to feed the chimneys (*Bünz et al.,2012; Hustoft et al., 2009*). Cartwright et al., (2007) proposed that fracturing of the sedimentary strata was performed by the high pore pressure at the crest of the gas column. Consequently, free gas is able to penetrate the hydrate stability zone. The buoyancy of the gas will increase with vertical height in the sediments, hence the pipes and chimneys' formation escalates as the structures approach the SB (*Cathles et al., 2010*). The result is that the last stage of formation is dramatic, and this might be the reason why the chimneys at the site are off-bending towards the apex at the top. Their propagation might be somewhat topographically controlled. From the thickness maps in **fig.4.1.5** it was found that the sedimentary column was thinning towards the axis of Vestnesa Ridge. This gives reason to believe that the sedimentary layering nearby the axis is of higher porosity than the sedimentary layering at the flanks where it might be a stronger degree of compaction. Thus it is easier for fluid-flow to migrate towards the axis, than the opposite way.

The BSR have a controlling factor regarding the positions of the leakage structures, which are for this survey along the crest of the Vestnesa Ridge. The flanks of the ridge show no indication of leakage. Interpreted sub-surface reflectors both above and beneath the BSR indicate that the structures originate at or below the BSR; a conclusion that is also drawn from the interpretation of seismic profiles of the structures. The interpreted BSR have several circular gaps corresponding to the rooting-zones of the leakage-structures, and is more evenly distributed along the flanks. Thus it is a fact that vertical fluid migration occurs where the BSR is absent in this study area. Bünz et al. (2012) suggest that continued gas flow through stratal boundaries would cause an overpressure that would lead to the gas release through the existing leakage-structures.

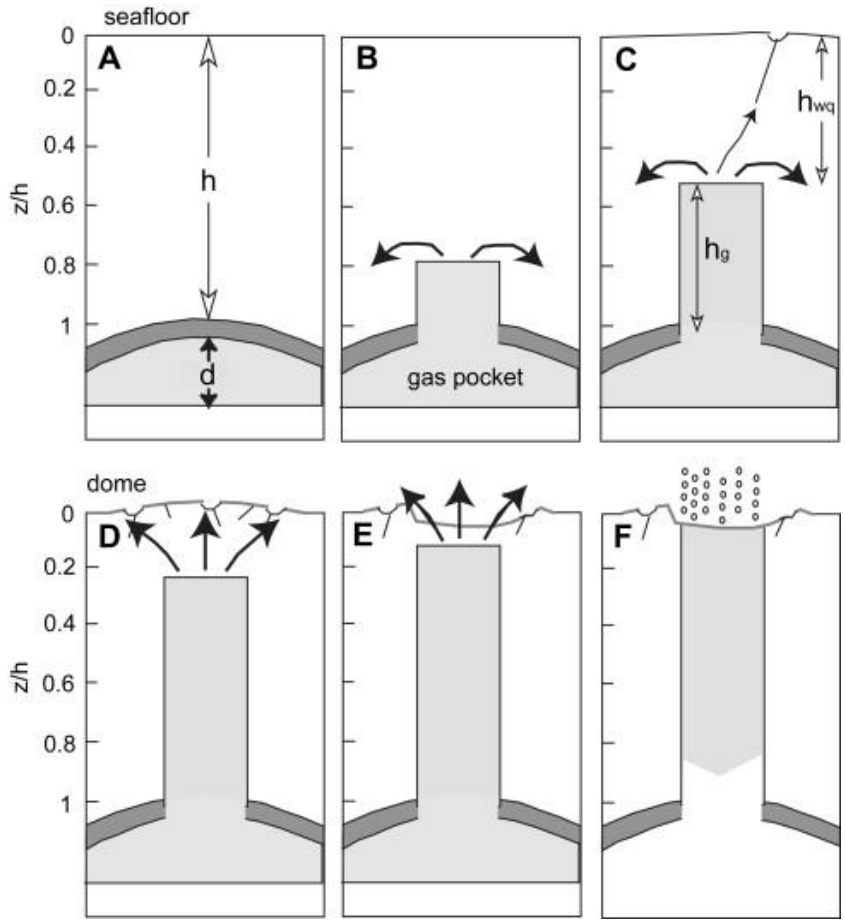

Fig. 5.4.1: Illustration of the formation of a pipe or chimney, by the push-through of gas within an originally impermeable layer A) Free gas is initially trapped below an impermeable anticline. B) The seal fails under the high pressure from the thick gas column, and the gas starts to migrate upwards while water in the sediments is displaced (black arrows). C) The first signs of pockmark-formation occur at the SB when the chimney has developed about half way to the SB. D) Deformation of SB-sediments increases and several small pockmarks appear at the SB. E) The scattered small pockmarks above the chimney merge into one large pockmark, with dimensions similar to the chimney. F) The complete chimney is formed, and the free gas may escape from the subsurface (From *Cathles et al., 2010*).

5.5 Gas-Migration

Mapping of high RMS amplitude was chosen for the study of fluid flow, as they may be indicative of gas (*Andreassen et al. 2007a*). Amplitude-mapping proved that most of the bright spots are found within chimney-structures, and some are found scattered within faults. The bright spots are mainly situated within the upper ~100 ms (TWT) bsf. It is a question why there are almost no bright spots beneath this level and down towards the BSR. It might be attenuation of the seismic signal, prohibiting the detection of gas-presence at this interval. It is also possible that the permeability of the sedimentary layers in this interval is poor and that the fluids have easier flow-path vertically through the faults, until a height where the permeability of the layers facilitates the lateral fluid flow. Therefore the fluids rapidly bypass this distance, whilst the migration is more time-consuming and involving plume build-ups in the upper part of the chimneys.

Methane has a viscosity ~60 times less than water in the shallow subsurface, hence a resistance to upwards migration is the required displacement of water (*Cathles et al., 2010*). Cathles et al., (2010) proposed that a gas pipe which is not situated within a gas hydrate regimen has a piston-like behavior; by internal pores saturated with water until a gas build-up beneath is able to displace the water and emerge to the SB. Hence, a repeated sequence of seal failure, water and gas venting and pockmark formation will occur periodically. However, Vestnesa Ridge is situated within a gas hydrate regimen, thus it is possible that gas hydrates have formed within the chimney structures that have not recently showed sign of leakage e.g. chimney 3. Due to these special conditions, it might be that neither water nor hydrates refill the pores.

As previously discussed, the chimneys are strongly related to faults. The faults represent a weakening of the local pressure, possibly lowering it to a value that is not preferably for the formation of hydrates. Additionally, the chimneys are made of a high-fracture zone that also deteriorate the local pressure, and allows warm fluid flow from the deep. Beneath the crest of the ridge, the accumulated gas-column is at its thickest. Due to buoyancy, a high pressure is directed upwards from the gas-column, especially at the crest. The shape of reflector R3 is seen as to represent several of its nearest reflectors. These steeply inclined surfaces are seen as possible gas-"feeders" to the BSR (which crosscuts several of them) leading gas from deeper reservoirs (*Hustoft et al., 2009*). However, it remains uncertain if the present-day gas-expulsions at the site emanates as free gas from below the BSR, or if it is from dissolved gas hydrates. It might be a combination of the two processes. By the lack of gas flares from the pockmarks during cruises in both 2006 and 2007 (*Bünz et al., 2012; Hustoft et al., 2009*), a recent increase in gas-expulsion is indicated (*Smith et al., 2014*).

5.6 Analogies of Fluid Flow

The two leaking chimneys (1, 2) display obvious similarities in fluid flow. They contain large plumes, which spread out laterally through most of the chimneys' structure. The accumulations of bright spots correspond to the same sedimentary layering; the three lowest sequences of amplitude-anomalies within chimney are spread out in the same TWT-interval as the lower plume of chimney 2 (between -1690 to -1765 ms). Additionally, the top sequences of both chimneys are found at a similar depth. Migration-traces by smaller bright spots, allows for an understanding of the last flow-path until the gas reaches the surface of the SB. In both chimneys, a clear link between the top-plume and the SB is seen by this occurrence. It is also possible to determine possible migration-routes from the bottommost anomaly, through the plumes and onto the SB. Chimney 1 was the most active regarding fluid expulsion during the cruise in 2010, and its highest gas-flare was 930 m above the SB. During the cruises in 2010 and 2012, the gas-venting from the leaking chimneys appeared continuous (*Smith et al., 2014*), which is considered common (*Cathles et al., 2010*).

With the non-leaking chimney 3 the most striking difference from the leaking chimneys, is that accumulated gas within is much lesser than for the leaking chimneys. The small plumes are centered within the chimney, with a good lateral clearing from the chimneys borders. The top plume is situated 30 ms beneath the SB, and this interval shows no enhanced amplitudes. This is very different from the leaking chimneys (1, 2), which hold high amplitudes also in this shallow area. The plumes are distanced further away from the chimneys borders, than they are in the leaking chimneys. It was surprising that there were small amounts of amplitudes centered at the branching point between the two faults. This area probably consists of highly fractured strata, and was expected to lead a large amount of fluids. However, it is possible that such an event has occurred, and that a highly fractured zone did not permit the accumulation of gas-plumes.

The most compelling observation is of the clear link between the plumes and the faults within the chimneys. The migration-study within the three chimneys strongly suggests a clear relationship between the faults that propagate through the chimneys, and the fluid flow within them. Phase-reversed, strong amplitude seismic reflection segments that are situated at various stratigraphic levels along a fault, is indicative of fluid flow through the fault. It is reasonable to assume that the upward migration of gases or pore fluids have occurred through a fault-pathway, and accumulated in porous traps along the fault (*Wiprut and Zoback, 2000*).The mapped plumes are generally connected to at least one fault, by spreading laterally out from them to either both or only one side. It is expected that the fluid emerge through the chimneys' internal fracture-structure, where the faults does not appear dominating for this purpose.

Where the vertically stacked plumes are fed by different faults, there is a possibility that the fluids have migrated laterally from one fault to another through chimney-fractures. The plumes within the three chimneys appear somewhat governed by the same reflectors. This indicates that there are specific sedimentary layers that are of preferred properties, when it comes to lateral fluid-migration from the faults. They are most likely of higher permeability, although varying fracture-zones within the chimney may also affect the flow.

It is unclear how gas is able to by-pass the GHSZ (*Smith et al., 2014*). Hereby, it is proposed that the gas-migration within the chimney-structures at this site is mainly conducted by through-going faults. Continuous free migration of gas through chimneys might be sustained by inadequate access to water which is necessary in the hydrate-formation, high salinities of enhanced temperatures caused by the fluid flow from warmer depths (*Tréhu et al., 2004*).

6 CONCLUSIONS

High-resolution 3D-seismic data has enabled detailed interpretation of a BSR and fluid flow structures at the eastern Vestnesa Ridge on the W-Svalbard margin. By its phase-reversed reflection, the BSR is an indicator of free gas accumulated beneath gas hydrates, within the sediments at this location. Gas hydrates work as a permeability-barrier for the flow of gas, by clogging the pores of the hosting sediments. Free gas is indicated both by strong, reversed seismic reflection amplitudes, and outstanding low frequency below the BSR. The BSR is observed cross-cutting several reflectors, as its shape rather resemblances the seabed than the nearest sedimentary strata at 200-260 ms (TWT) bsf. Vestnesa Ridge is one of the northernmost (79°N) documented sites where gas-hydrates are occurring in oceanic sediments.

Axis-mapping of several reflectors, including the SB, proved continuous axis-migration to the SW. The distributions of pockmarks at the seabed are restricted to the crest of the anticlinal axis of the ridge. These pockmarks are the termination of acoustic chimneys which are piercing through the BSR, and together they indicate the emergence of focused fluid flow. Fluid flow into the water-column through several of the pockmarks has been recently documented. Combined with the lack of these features at the flanks of the ridge, it is implied that vertical migration of fluids is topographically determined by the sealing gas-hydrates.

Transform faults reaching far below the BSR are propagating through the ridge. Strong relations are established between the chimneys and the faults, by that each chimney is connected to at least one fault. Amplitude anomaly mapping manifested that bright spots indicative of gas, were mainly found within the chimney-structures. Thorough inspection of the relation between these bright spots and the faults cutting through three separate chimneys showed that their internal fluid flows are strongly conducted by faults.

The chimneys show a slight off-bending towards the axis of the ridge with height, this trend is increasing with the chimneys distance from the crest. Thickness-maps between several reflectors showed a thinning sedimentary column at the crest of the ridge, and thicker columns at the flanks. Although the chimneys are emanating around faults, it is expected that their propagation has been slightly affected by the faint resistance through thinner sedimentary layers at the crest.

7 REFERENCES

Aagaard, K., Foldvik, A., Hillmann, S. R., (1987). The West Spitsbergen Current: disposition and water mass transformation. J. Geophys. Res. 92, 3778-3784

Andreassen K., 2009, MARINE GEOPHYSICS, Lecture Notes for Geo-3123, UIT, 105 p.

Andreassen, K., Glad Nilsen, E. and Ødegard, C. 2007a. Analysis of shallow gas and fluid migration within the Plio-Pleistocene sedimentary sucession of the SW Barents Sea using 3D-seismic data. *Geomarine Letters*, *27*, 155-171.

Andreassen, K., Ødegaard, C. M., Rafaelsen, B.(2007b) Imprints of former ice streams, imaged and interpreted using industry three-dimensional seismic data from the south-western Barents Sea. In: Davies, R. J., Posamentier, H. W., Wood, L. J. & Cartwright, J. A. (eds) Seismic Geomorphology: Applications to Hydrocarbon Exploration and Production. Geological Society, London, Special Publications, 277, 151–169.

Badley, ME. 1985. Practical Seismic Interpretation. International Human Resources Development Corporation (IHRDC), Boston.

Bacon, M., Simm, R. and Redshaw, T. 2003. 3-D Seismic Interpretation, p. 17-26. Cambridge University Press

Bartoli, G., Sarnthein, M., Weinelt, M., Erlenkeuser, H., Garbe-Schonberg, D., Lea,D.W., 2005. Final closure of Panama and the onset of northern hemisphere glaciation. Earth Planet. Sci. Lett. 237, 33–44.

Birchwood, R., Dai, J., Shelander, D., Boswell, R., Collett,T., Cook, A., Dallimore, S., Fujii, K., Imasato, Y., Fukuhara, M., Kusaka, K, Murray, D., Saeki, T. (2010) Developments in Gas Hydrates.Schlumberger, Oilfield Review Spring 2010: 22, no.1.

Bünz, S., Petersen, J., Hustoft, S., and Mienert, J., 2008, Environmentally – sensitive gas hydrates on the W-Svalbard margin at the gateway to the Arctic ocean: Proceedings of the 6th International Conference on Gas Hydrates, Vancouver, British Colombia, Canada, July 6-10, 6 p.

Bünz, S., Polyanov, S., Vadakkepuliyambatta, S., Consolaro, C., Mienert, J., 2012, Active gas venting through hydrate-bearing sediments on the Vestnesa Ridge, offshore W-Svalbard. Marine Geology 2012.p. 189 – 197.

Butt, F.A., Elverhøi, A., Solheim, A., Forsberg, C.F., 2000. Deciphering Late Cenozoic development of the western Svalbard Margin from ODP Site 986 results. Mar.Geol. 169, 373–390.

Cartwright, J. A., Huuse, M. (2005) 3D seismic technology: the geological 'Hubble'. Basin Res. 17:1–20

Cartwright, J., Huuse, M., Aplin, A., (2007). Seal bypass systems. AAPG Bulletin, v. 91, no. 8, p. 1141-1166. DOI:10.1306/04090705181.

Cathles, L. M., Su, Z., Chen, D., (2010). The physics of gas chimney and pockmark formation, with implications for assessment of seafloor hazards and gas sequestration. Mar. Pet. Geol. 27(1), p. 82-91. DOI:10.1016/j.marpetgeo.2009.09.010.

Dahlgren, K.I.T., Vorren, T.O., Stoker, M.S., Nielsen, T., Nygård, A., Sejrup, H.P., 2005.Late Cenozoic prograding wedges on the NW European continental margin: their formation and relationship to tectonics and climate. Mar. Pet. Geol. 22, 1089–1110.

De Schepper, S., Groeneveld, J., Naafs, B.D.A., Van Renterghem, C., Hennissen, J., Head, M.J., Louwye, S., Fabian, K., 2013. Northern Hemisphere glaciation during the globally warm early Late Miocene. PLoS ONE. http://dx.doi.org/10.1371/journal.pone.0081508.

Dörr, N., Clift, P.D., Lisker, F., Spiegel, C., 2013. Why is Svalbard an island? Evidence for two-stage uplift, magmatic underplating and mantle thermal anomalies. Tectonics 32, 1-14. http://dx.doi.org/10.1002/tect.20039.

Eiken, O., and Hinz, K., 1993, Contourites in the Fram Strait: Sedimentary Geology, v. 82, p. 15-32.

Fohrmann, H., Backhaus, j.0., Blaume, F., Haupt, B.j., Kampf, j., Michels, K.,Mienert,j., Posewang,j., Ritzrau, W., Rumohr,j.,Weber, M., Woodgate, R, 2001.Modern Ocean current-controlled sediment transport in the Green-land—Iceland—Norwegian (GIN) seas. In: Schafer, P., Riizau, W., Schluter, M.,Thiede, j. (Eds), The Northern North Atlantic: A Changing Environment.Springer-Verlag, Berlin, pp. 135—154.

Forsberg, C.F., Solheim, A., Elverhoi, A., Jansen, E., Channell, J.E.T., Andersen, E.S., 1999. The depositional environment of the western Svalbard margin during the late Pliocene and the Pleistocene: Sedimentary facies changes at Site 986. In: Raymo, M., Jansen, E., Blum, P., Herbert, T.D. (Eds.), Proc. ODP, Sci. Results 162. Ocean Drilling Program, College Station, TX, pp. 233–246.

Geissler, W., Jokat, W., 2004. A geophysical study of the northern Svalbard continental margin. Geophys. J. Int. 158, 50-66.

Graversen, R. G., Mauritsen, T., Tjernstrom, M., Kallen, E., Svensson, G., (2008). Vertical structure of recent Arctic warming, Nature, 451(7174), 53-56.

Haacke, R. R., Westbrook, G K, Hyndman, R. D. (2007) Gas hydrate, fluid flow and free gas: Formation of the bottom-simulating reflector. Earth and Planetary Science Letters, v. 261, p. 407-420.

Haacke, R.R., Westbrook, G.K., Riley, M., (2008). Controls on the formation and stability of gas hydrate-related bottom-simulating reflectors (BSRs): a case study from the west Svalbard continental slope. Journal of Geophysical Research 113. doi:10.1029/2007JB005200 B05104

Hansen, B., Osterhus, S., 2000. North Atlantic—Nordic Seas exchanges. Progress in Oceanography 45, 109—208.

Harland, W. B., Geddes, I., Doubleday, P. A., 1997. Central western Spitsbergen. In: Harland, W. B., Anderson, L. M., Manasrah, D. (Eds), The Geology of Svalbard. Memoirs of the Geological Society of London, pp. 154-178.

Hegewald, A., Jokat, W., 2013. Relative sea level variations in the Chukchi region – Arctic Ocean – since the Late Eocene. Geophys. Res. Lett. 40, 1–5. http://dx.doi.org/10.1002/GRL.50182.

Houghton, J. T. (2009) Global Warming; The complete briefing. 4th Ed. Cambridge University Press, New York.

Hovland, M., (1989). Modern analogues to middle Ordovician sedimentary mounds and washout depressions. Journal of Sedimentary Petrology, 59 (1989), pp. 585–589

Howe, j.A., Shimmield, T.M., Harland, R., 2008. late Quaternary contourites and glaciomarine sedimentation in the Fram Strait. Sedimentology 55, 179—200.

Hustoft, S., Bünz, S., Mienert, J., and Chand, S., 2009, Gas hydrate reservoir and active methane-venting province in sediments on <20 Ma young oceanic crust in the Fram Strait, offshore NW-Svalbard: Earth and Planetary Science Letters, v. 284, p. 12-24.

Jakobsson, M., Backman, J., Rudels, B., Nycander, J., Frank, M., Mayer, L., Jokat, W., Sangiorgi, F., O'Regan, M., Brinkhuis, H., King, J., Moran, K., 2007. The early Miocene onset of a ventilated circulation regime in the Arctic Ocean. Nature 447, 986–990.

Jokat, W., Geissler, W., Voss, M., 2008. Basement structure of the north–western Yermak Plateau. Geophys. Res. Lett. 35. http://dx.doi.org/10.1029/2007GL032892. L05309

Knies, J. and Mann, U., (2002). Depositional environment and source rock potential of Miocene strata from the central Fram Strait: introduction of a new computing tool for simulating organic facies variations, Marine and Petroleum Geology, 19(7), 811-828.

Knies, J., Matthiessen, J., Vogt, C., Laberg, J. S., Hjelstuen, B. O., Smelror, M., Larsen, E., Andreassen, K., Eidvin, T., Vorren, T. O., 2009. The Plio-Pleistocene glaciation of the Barents Sea – Svalbard region: a new model based on revised chronostratigraphy. Quat. Sci. Rev. 28, 812-829.

Laberg, J.S., Andreassen, K., Knies, J., Vorren, T.O., Winsborrow, M., 2010. Late Pliocene–Pleistocene development of the Barents Sea Ice Sheet. Geology 38, 107–110

Løseth, H.,Wensaas,L.,Arntsen, B., Hanken, N., Basire, C. & Graue, K. (2001) 1000 m long gas blow-out pipes. 63rd EAGE Conference & Exhibition, Amsterdam, Extended Abstracts, P524.

Løseth, H., Gading, M., and Wensaas, L., 2009, Hydrocarbon leakage interpreted on seismic data: Marine and Petroleum Geology, v. 26, p. 1304-1319.

Matthiessen, J., Knies, J., Vogt, C., Stein, R., 2009a. Pliocene palaeoceanography of theArctic Ocean and subarctic seas. Philos. Trans. R. Soc. Lond. A 367, 21–48.

Matthiessen, J., Brinkhuis, H., Poulsen, N., Smelror, M., 2009b. Decahedrella martinheadii Manum 1997 – a stratigraphically and paleoenvironmentally usefull Miocene acritarch of the high northern latitudes. Micropaleontology 55, 171-186

Mattingsdal, R., Knies, J., Andreassen, K., Fabian, K., Husum, K., Grøsfjeld, K., de Schepper, S. (2013) A new 6 Myr stratigraphic framework for the Atlantic-Arctic Gateway. Quat. Sci. Rev. http://dx.doi.org/10.1016/j.quascirev.2013.08.022

Mudelsee, M., Raymo, M.E., 2005. Slow dynamics of the Northern Hemisphere glaciation. Paleoceanography 20. http://dx.doi.org/10.1029/2005pa001153. Pa4022.

Myhre, A., Thiede, J., Firth, J. A., 1995. Proceedings of the Ocean Drilling Program. Initial Reports, Leg 151. Ocean Drilling Program, College Station, Texas, USA, p. 951.

Petersen, C.J., Bünz, S., Hustoft, S., and Mienert, J., 2008, 3D seismic imaging of marine gas hydrates in arctic sediments of the Vestnesa Ridge off the W-Svalbard margin: Proceedings of the 6th International Conference on Gas Hydrates, Vancouver, British Colombia, Canada, July 6-10, 8 p.

Petersen, C.J., Bünz, S., Hustoft, S., and Mienert, J., Klaeschen, D., 2010, High- resolution P-Cable 3D seismic imaging of gas chimney structures in gas hydrated sediments of an Arctic sediment drift, Marine and Petroleum Geology 2010, 14 p.

Poore, H.R., Samworth, R., White, N.J., Jones, S.M., McCave, I.N., 2006. Neogene over- flow of Northern Component Water at the Greenland–Scotland Ridge. Geochem. Geophys. Geosyst. 7. http://dx.doi.org/10.1029/2005gc001085. Q06010.

Reagan, M. T. and Moridis, G. J., (2007). Oceanic gas hydrate instability and dissociation under climate change scenarios, Geophysical Research Letters, 34(22), L22709.

Ritzmann, O., Jokat, W., 2003.Crustal structure of northwestern Svalbard and the adjacent Yermak Plateau: evidence for Oligocene detatchment tectonics and non-volcanic breakup. Geophysical Journal International 152, 139-159.

Ritzmann, O., Jokat, W., Czuba, W., Guterch, A., Mjelde, R., Nishimura, Y., 2004. A deep seismic transect from Hovgård Ridge to northwestern Svalbard across the continental-ocean transition: a sheared margin study. Geophysical Journal International 157, 683-702.

Ruddiman, W.F., 2010. A Paleoclimatic Enigma?. Science 328, 838–839.

Rudels, B., Björk, G., Nilsson, J., Winsor, P., Lake, I., Nohr, C., (2004). The interaction between waters from the Arctic Ocean and the Nordic Seas north of Fram Strait and along the East Greenland Current: results from the Arctic Ocean-02 Oden expedition. Jour. Mar. Sys. doi:10.1016/j.jmarsys.2004.06.008

Ryseth, A., Augustson, J.H., Charnock, M., Haugerud, O., Knutsen, S.-M., Midbøe, P.S., Opsal, J.G., Sundsbø, G., 2003. Cenozoic stratigraphy and evolution of the Sørvestnaget Basin, southwestern Barents Sea. Nor. J. Geol. 83, 107-130.

Sarkar, S., Berndt, C., Chabert, A., Masson, D. G., Minshull, T. A., Westbrook, G. K., 2011. Swithching of a paleo-ice stream in northwest Svalbard. Quat. Sci. Rev. 30, 1710-1725.

Sarnthein, M., Bartoli, G., Prange, M., Schmittner, A., Schneider, B., Weinelt, M., Andersen, N., Garbe-Schönberg, D., 2009. Mid-Pliocene shifts in ocean overturning circulation and the onset of Quaternary-style climates. Clim. Past 5, 269–283.

Selley, R. C (1998). Elements of Petroleum Geology, 2nd. Ed. Academic Press, San Diego.

Sheriff , RE. 2006. Encyclopedic Dictionary of Exploration Geophysics, 5th. Ed. Tulsa: Society of Exploration Geophysics.

Sloan, E. D. (1990) Clathrathe Hydrates of Natural Gases. Marcel Decker, New York.

Smith, A. J., Mienert, J., Bünz, S., Greinert, J., (2014). Thermogenic methane via bubble transport into the upper Arctic Ocean from the hydrate-charged Vestnesa Ridge, Svalbard. Geochemistry, geophysics, geosystems, Vol.15, no.5 p.,1945 -1959. Doi: 10.1003/2013GC005179.

Taylor, M.H., Dillon, W.P., and Pecher, I.A., (2000). Trapping and migration of methane associated with the gas hydrate stability zone at the Blake Ridge diapir: new insights from seismic data: Marine Geology, v. 164, p. 79-89.

Tréhu, A. M., Flemings, P. B., Bangs, N. L., Chevallier, J., Gràcia, E.,Johnson, J. E., Liu, C. S., Liu, X., Riedel, M., Torres, M. E., (2004). Feeding methane vents and gas hydrate deposits at south Hydrate Ridge. Geophys. Res. Lett. 31(23), L23310.

Twiss, R. J., Moores, E. M. (2007) Structural Geology 2nd Ed. W. H. Freeman and Company, New York.

Vanneste, M., Guidard, S., and Mienert, J., 2005, Bottom-simulating reflections and geothermal gradients across the Svalbard margin: Terra Nova, v. 17, p. 510-516.

Vogt, P.R., Crane, K., Sundvor, E., Max, M.D., and Pfirman, S.L., 1994, Methane-generated(?) pockmarks on young, thickly sedimented oceanic crust in the Arctic: Vestnesa Ridge, Fram Strait: Geology, v. 22, p. 255-258.

Vorren, T.O., Laberg, j.5., 1997. Trough mouth fans — Palaeoclimate and ice-sheet monitors. Quaternary Science Reviews 16, 865—881.

Vorren, T.O., laberg, j.S., Blaume, F., Dowdeswell, j.A., Kenyon, N.H., Mienert, j., Rumohr, j., Werner, E, 1998. The Norwegian Greenland Sea continentalmargins: morphology and late Quaternary sedimentary procesSes and envi- ronment. Quaternary Science Reviews 17, 273—302.

Vågnes, E., Faleide, J.I., Gudlaugsson, S.T., 1992. Glacial erosion and tectonic uplift in the Barents Sea. Nor. Geol. Tidsskr. 72, 333–338

Wiprut D, Zoback MD (2000) Fault reactivation and fluid flow alonga previously dormant normal fault in the northern North Sea. Geology 28(7):595–598

---

http://peer.tamu.edu/curriculum_modules/ecosystems/module_3/whatweknow2.htm